AN ABSTRACT OF THE DISSERTATION OF

Ellen Grace Lauchnor for the degree of Doctor of Philosophy in Chemical
Engineering presented on February 28, 2011.

Title: Inhibition, Gene Expression and Modeling of Ammonia Oxidation in Biofilms
of *Nitrosomonas europaea*

Abstract approved:

_____

Lewis Semprini   Brian Wood

This dissertation explores the physiology and gene expression of the ammonia-oxidizing bacterium *Nitrosomonas europaea* in surface-associated bacterial communities, or biofilms. Biofilms of *N. europaea* were cultivated in drip flow reactors for several weeks and gene expression microarrays were used to detect 240 genes differentially expressed between the mature biofilms and exponential batch cells. Using RT-qPCR, genes up-regulated in the biofilm microarray were detected in continuous cultures of suspended cells, and were increasingly up-regulated with decreasing dilution rates. The observations suggest a correlation between the biofilm-related gene expression and slow growth rates of the cells.

N. europaea cells in the biofilms upon exposure to the aromatic hydrocarbons phenol and toluene were more resistant to inhibition of ammonia oxidation than suspended cells. 50% inhibition was observed upon exposure of mature biofilms to 60 μM phenol and 100 μM toluene, compared to 10 μM phenol and 20 μM toluene with exponential batch (suspended) cells. However, the transcriptional response to the hydrocarbons was similar between suspended cells and biofilms, with two genes up-regulated in both growth states in response to phenol (NE1545-NE1546) while no transcriptional response was observed during toluene exposure.

To further explore the response to phenol exposure, cells were cultivated in continuous reactors at various growth rates and NH_3 oxidation rates and exposed to phenol. The inhibition of ammonia oxidation by 20 μM phenol decreased with slower

growth rates and NH_3 oxidation rates and approached the inhibition level of the biofilms. Increasing the dissolved oxygen (DO) concentration in the biofilms resulted in higher NH_3 oxidation rates and greater phenol inhibition, leading to the conclusion that the tolerance of biofilms is likely related to O_2 limitation causing slow NH_3 oxidation rates and slower growth rates.

DO and pH were measured in the biofilms with microsensors and the concentration profiles were simulated with 2-D reactive transport that combined advective and diffusive transport. The half-saturation coefficient for suspended cells fit the biofilm profiles, indicating that the kinetics of NH_3 oxidation between the biofilm and suspended cells were the same. The model was also able to simultaneously predict the observed pH and DO biofilm profiles for tests conducted with limited buffering capacity, where pH was lowered by the cells, which resulted in NH_3 limitations and reduced O_2 consumption.

Inhibition, Gene Expression and Modeling of Ammonia Oxidation in Biofilms of
Nitrosomonas europaea

by
Ellen Grace Lauchnor

A DISSERTATION

submitted to

Oregon State University

in partial fulfillment of
the requirements for the
degree of

Doctor of Philosophy

Presented February 28, 2011
Commencement June 2011

Doctor of Philosophy dissertation of Ellen Grace Lauchnor presented on February 28, 2011

APPROVED:

_____

Co-Major Professor, representing Chemical Engineering

_____

Co-Major Professor, representing Chemical Engineering

_____

Head of the School of Chemical, Biological and Environmental Engineering

_____

Dean of the Graduate School

I understand that my dissertation will become part of the permanent collection of Oregon State University libraries. My signature below authorizes release of my dissertation to any reader upon request.

_____

Ellen Grace Lauchnor, Author

ACKNOWLEDGEMENTS

CONTRIBUTION OF AUTHORS

TABLE OF CONTENTS

LIST OF FIGURES

LIST OF FIGURES (Continued)

LIST OF TABLES

LIST OF APPENDIX FIGURES

LIST OF APPENDIX TABLES

Inhibition, Gene Expression and Modeling of Ammonia Oxidation in Biofilms of
Nitrosomonas europaea

Chapter 1

General Introduction

A rising global population is exerting pressure on drinking water sources in areas around the world. This higher demand and depletion of groundwater is resulting in increasing use of surface waters as municipal drinking water sources. Therefore, the remediation of wastewater is extremely important for preservation of surface water quality. The biological removal of nutrients, such as nitrogen, is necessary during wastewater treatment, as waterways with high nutrient loadings have adverse effects on aquatic life and water quality due to eutrophication (28).

Ammonia (NH_3) is a ubiquitous contaminant in wastewater and high concentrations of NH_3 in treated wastewater effluent can lead to negative ecological impacts such as eutrophication of receiving waters. The U.S. Environmental Protection Agency (EPA) has established limits for the discharge of nitrogen from wastewater treatment plants (29). Biological nitrogen removal processes in wastewater treatment plants (WWTP) are increasingly being used for the treatment of wastewater containing NH_3.

The process of biological nitrogen removal consists of nitrification, the oxidation of ammonia (NH_3) to nitrate (NO_3^-), and subsequent denitrification of NO_3^- to dinitrogen gas (N_2). Nitrification is accomplished in two stages consisting of NH_3 oxidation to nitrite (NO_2^-), and further oxidation of NO_2^- to NO_3^- (89). The critical step of nitrogen removal is the initial oxidation of NH_3 performed by ammonia-oxidizing bacteria (AOB).

Nitrosomonas europaea is a species of AOB that performs the first step of nitrogen removal in WWTP. The AOB are aerobic chemoautotrophs, which makes them slow growing and typically a small percentage of the microbial population in WWTP (78). Additionally, AOB are sensitive to many organic compounds including

aromatic hydrocarbons (41, 44, 79, 83). Sensitivity of AOB to a range of contaminants and environmental perturbations such as changes in temperature and pH (101), can also reduce ammonia oxidation activity. These factors make them some of the most sensitive organisms in WWTP, which is problematic for establishing reliable nitrification processes.

In natural and engineered systems, microorganisms tend to grow in biofilms, which often consist of multiple microbial species. Biofilms are aggregates of microbial cells that are attached to a surface and typically held together by an extracellular poly-saccharide (EPS) matrix secreted by the microorganisms (22). Bacteria in biofilms can exhibit a range of metabolisms and physiological characteristics due to microenvironments created by diffusion limitation of soluble substrates and products within the biofilm (30, 113). To improve the efficiency of nitrogen removal, fixed film bioreactors are used in WWTP. While biofilm reactors have demonstrated benefits over conventional reactors, the physiological and transcriptional behavior of AOB biofilms has not been well studied. Therefore, the investigation of AOB responses in biofilms is important for understanding the activity and inhibition of the organisms in nitrification processes. The research presented here extends the knowledge of physiology and gene expression in *N. europaea* biofilms and investigates reasons for *N. europaea* biofilm resistance to environmental contaminants.

Ammonia Oxidation

The ammonia oxidizing bacteria (AOB) are obligate aerobic chemoautotrophs that use ammonia as a sole electron donor for metabolism and growth (112). The most well characterized AOB that is found in WWTP is *Nitrosomonas europaea.* In *N. europaea* and other AOB, the oxidation of NH_3 to NO_2^- is a two-step process, involving the two enzymes ammonia monooxygenase (AMO) and hydroxylamine oxidoreductase (HAO) (4). The AMO enzyme oxidizes NH_3 to the intermediate product hydroxylamine (NH_2OH), which is then oxidized to NO_2^- by HAO (4). The entire process yields four electrons and during steady-state two electrons are supplied

back to AMO, and two proceed down the electron transport chain to provide energy and reductant for cell growth and maintenance (112). The stoichiometric equation for ammonia oxidation in AOB is as follows:

$$NH_3 + O_2 + 2H^+ + 2e^- \rightarrow NH_2OH + H_2O \rightarrow NO_2^- + 5H^+ + 4e^-$$

NH_3 is the growth substrate for AMO and the enzyme is unable to oxidize the ionic form ammonium (NH_4^+), which is in acid-base equilibrium with NH_3. The protonated form NH_4^+ is favored in the equilibrium at low pH, making the substrate for AMO less accessible under acidic conditions (102). The NH_3 oxidation reactions carried out by AOB produce hydrogen ions (H^+) as well as NO_2^-, as shown in the above chemical equation. Consequently, AOB cause a reduction of pH in their environment, which then results in NH_3 oxidation inhibition partially due to the low availability of substrate.

AMO has a broad substrate range and can oxidize a number of low molecular weight compounds by co-metabolism, including aliphatic hydrocarbons (44), aromatic hydrocarbons (19, 41, 45) and chlorinated compounds (40, 83). The process of co-metabolism by AMO competes with oxidation of the growth substrate and can adversely affect cell metabolism (27). Cellular energy drain can result from AMO co-metabolism due to consumption of reductant by the monooxygenase, with no subsequent electron generation by HAO (27). Additionally, co-metabolism in *N. europaea* by some substrates has been shown to cause inactivation of AMO (83) or inhibition due to daughter product formation, as is the case with oxidation of benzene to its inhibitory product phenol (79).

Because AOB are autotrophic they must use inorganic carbon for synthesis of organic molecules used in cell growth (112). This is an energy intensive process which requires high turnover of ammonia and results in slow growth of AOB in comparison with heterotrophic bacteria (78). Although this slow growth makes AOB such as *N. europaea* sensitive to environmental perturbations, it also allows for activity tests of ammonia oxidation rates without growth of biomass (27).

N. europaea is a widely studied AOB in laboratory experiments and its biochemistry and physiology are well-characterized (4, 78). It is the first AOB to have a completely sequenced genome (17). As a result, numerous whole-genome transcriptional studies using microarray technology have been performed on *N. europaea* (36, 68, 79). Due to the wide use of this organism in laboratory experiments and the availability of molecular tools for transcriptional analysis, *N. europaea* is an ideal AOB to study in biofilms.

Nitrification in WWTP

During nitrification in WWTP, NH_3 oxidation is followed by a second oxidation of NO_2^- to NO_3^-, performed by nitrite-oxidizing bacteria (NOB), which are also autotrophic bacteria. The two-step process traditionally occurs in activated sludge of a WWTP or an aerobic fixed film process such as a trickling filter (89). The resulting NO_3^- is then reduced to N_2 gas under anoxic conditions, by heterotrophic organisms that perform denitrification. Nitrification by AOB occurs simultaneously with organic carbon degradation by hetertrophic bacteria in systems such as activated sludge (89).

Due to their slow growth rates, AOB comprise a small fraction of the microbial population in WWTP and are prone to wash-out during periods of perturbation such as shifts in temperature or influx of inhibitory species (88). Wash-out of AOB in suspended WWTP reactors, such as activated sludge, causes the incomplete removal of nitrogen. Attached growth reactors which retain biomass are therefore advantageous in WWTP for nitrification processes involving sensitive AOB.

The application of biofilms in wastewater treatment technologies has been established in trickling filters for over a century and other types of biofilm reactors have been more recently developed (62). Biofilm reactors are beneficial for biological nitrogen removal because slow growing organisms such as nitrifiers are retained in the attached biomass and are not as easily washed out of the system (88). Additionally, in a biofilm reactor higher rates of nutrient removal can be achieved in a comparatively small reactor volume due to high biomass concentration and no need for solids

separation processes (89). Evidence that slow-growing AOB are protected in the deeper layers of biofilm and encased by heterotrophic bacteria provides evidence supporting the use of biofilm reactors for protection of AOB (65).

In addition to the above benefits of biofilms, fixed-film reactors in WWTP help to avoid inhibition of nitrification during exposure to contaminants such as aromatic hydrocarbons. Inhibition of nitrification and in particular ammonia oxidation inhibition by aromatic hydrocarbons has been examined in mixed nitrifying biofilms (5, 93). In a study by Morita et al., NH_3 oxidation occurred in gel immobilized cells of *N. europaea* exposed to inhibitory concentrations of phenol, presumably due to transport limitation of the phenol and consumption by heterotrophic bacteria in the gel (61). The inhibition of *N. europaea* biofilms by the ammonia oxidation inhibitor, nitrapyrin, was investigated by Powell and Prosser, who reported that established biofilms were protected from inhibition in comparison to suspended cells (77).

Biosensors for monitoring biological nitrogen removal

Due to the sensitivity of nitrifying bacteria in wastewater treatment, there is a need for process monitoring of biological nitrogen removal. Specifically, the early detection of ammonia oxidation inhibition is necessary to prevent long term failure of nitrogen removal (32). For this purpose, monitoring systems can be developed to detect conditions in a WWTP which will cause inhibition of ammonia oxidizing bacteria such as *N. europaea*. An ideal monitoring system needs to give real-time results and be sensitive and specific enough to identify the contaminant or type of contaminant causing inhibition. A biosensor is a type of monitoring system that may be used for this purpose, which uses the response of the organisms themselves to determine when inhibitory or undesired conditions are present.

Types of biosensors that have been developed for monitoring the health of nitrifying bacteria include titrimetric methods to monitor the rate of acidification (5), respirometers to measure oxygen uptake rates (46), and a bioluminescence assay of recombinant *N. europaea* (42). While all of these methods are effective in evaluating changes in activity of nitrifying bacteria, they do not identify the inhibitor causing the

reduction in nitrification. In contrast, the transcriptional response of bacteria has the potential to indicate conditions of stress in the organism and can be specific enough to identify the inhibitor or class of inhibitor.

In microorganisms, the response to an environmental stress or inhibitory condition begins as gene expression, which leads to protein production. The response at the transcriptional level is fast and often specific genes are expressed during exposure to a chemical or class of chemicals, which are known as sentinel genes (35). The potential for fast signal detection and identification of the contaminant causing the response makes sentinel gene expression a candidate for biosensor technology. Using molecular techniques and genetic markers, transcriptional changes can be monitored in real time, for instance linking GFP production to the transcriptional stress response. Additionally, attached bacteria, such as those in biofilms, are beneficial for the development of biosensor technology, as they can be fixed on a surface of a flow-through system.

Contaminants of interest

The contaminants of interest in this research are the aromatic hydrocarbons toluene and phenol. These aromatics have all been shown to inhibit nitrification in wastewater (117) and are co-metabolic substrates of AMO in *N. europaea* (45, 79). Toluene is a component of petroleum and its products (7). It can be found in many industrial wastewaters and is considered a common groundwater contaminant. Phenol is used in many industries such as herbicides, plastics and petrochemicals manufacturing, and is commonly found in industrial wastes, sometimes co-occurring with ammonia (61).

In batch assays with sludge from industrial WWTP, the presence of high phenol concentrations caused reduction in the extent of nitrification (2). Although heterotrophic bacteria in activated sludge have been shown to degrade phenol, ammonia oxidation is stalled while phenol is still present in the wastewater (61), which can cause low efficiency of nitrogen removal.

Phenol and toluene are inhibitory to ammonia oxidation in pure cultures of *N. europaea*, due to their co-metabolic interaction with the AMO enzyme. Toluene is a cometabolic substrate of AMO and is oxidized by *N. europaea* to benzyl alcohol and benzaldehyde (45). While toluene cometabolism by *N. europaea* is somewhat inhibitory to ammonia oxidation, it causes no enzyme inactivation or daughter product inhibition. In contrast, phenol is a product of benzene co-metabolism by AMO which is inhibitory to cells of *N. europaea* and induces a transcriptional response (79). Radniecki et al. used microarrays to detect a cluster of genes, NE1545 – NE1551, which are all up-regulated during phenol exposure. The genes identified in the microarray study may be used as sentinel genes to signal the presence of phenol in engineered systems.

Microsensors and nitrifying biofilms

Microsensors are important tools for measuring *in situ* activity and determining localized rates of consumption and production in biofilms (86). Microsensors are devices that consist of needle-like electrodes with a tip diameter of 1-20 μm that measure the concentration of a specific chemical species, such as O_2, NH_4^+, NO_3^- or NO_2^- (34). Oxygen microsensors typically consist of a Clark-type O_2 electrode (85), while ion-based sensors measure electrical potential due to charge separation across an ion-selective membrane at the sensor tip (34). The small sensor tip allows concentration measurements to be taken in small spatial increments with depth in a biofilm. At steady state, the resulting concentration profiles can be used to calculate the flux of the species into the biofilm and the rates of activity at each depth interval within the biofilm (34).

Previous research on nitrifying biofilms has combined microelectrode measurements for nitrifying rate determination with molecular techniques for the identification of bacterial species (97). Studies on nitrifying biofilms have found that *in situ* ammonia oxidation rates determined with microsensors correlate with the location of AOB species identified by 16S rRNA hybridization (33, 94). *N. europaea*-like species have been identified as some of the predominant AOB in wastewater

nitrifying biofilms by linking microsensor rates with molecular identification techniques (97). Microelectrode measurements have also been used to explore the kinetic properties and rates of nitrification within WWTP biofilms (98).

Microsensor profiling can also be used during exposure to inhibitory or toxic compounds to investigate spatial shifts in microbial activity and overall changes in substrate consumption do to inhibition. Satoh, et al. performed microsensor measurements on wastewater biofilms exposed to 2-chlorophenol (93). The authors calculated rates of O_2 and NH_4^+ consumption based on profiles and determined that exposure to 2-chlorophenol caused greater inhibition of ammonia oxidation than oxygen uptake due to heterotrophic bacteria (93). Li and Bishop also used microelectrodes to study azo dye inhibition of nitrifying biofilms, showing that concentrations of substrates inside biofilms increased with higher dye concentration, which indicated that cells were being increasingly inhibited (54). The application of microsensors is ideal for examining the ammonia oxidation activity in biofilms of *N. europaea*.

Biofilm modeling

Kinetics in biofilm systems are heavily influenced by the diffusion of substrates within the biofilm, which adds spatial gradients that are not present in suspended microbial systems. To address this complexity, biofilm modeling can be useful for comparing biofilm kinetics with those of suspended cell systems. Mathematical simulations of bacterial biofilms typically incorporate both diffusive mass transport of soluble chemical species and kinetic relationships describing rates of substrate transformation and cell growth (107).

Nitrifying biofilm models have been used to determine kinetic models or parameters of nitrifying bacteria (16, 25), predict performance of nitrifying reactors (11), and determine the dynamics between different microbial processes or reactions in a complex system (67, 72). Steady-state models can be used to simulate concentration gradients and fluxes of solutes inside biofilms and fit to experimental data from microsensors (25). Experimental data from microsensor measurements can

be simulated and used to determine model parameters such as kinetic coefficients that are otherwise difficult to determine in biofilms (116).

In the research presented here, biofilms of *N. europaea* were grown in drip flow reactors. *N. europaea* biofilm inhibition by phenol and toluene exposure was tested with a focus on the physiological and transcriptional responses of the cells to the inhibitors. Microsensor measurements coupled with biofilm modeling were used to evaluate rates of ammonia oxidation in biofilms and examine the kinetic parameters of the biofilms. The overarching goal of this research was to determine the differences between biofilm and suspended cell behavior of *N. europaea*, and determine the major factors that control ammonia oxidation activity and inhibition by phenol and toluene in *N. europaea* biofilms.

Objectives

(1) Expose *N. europaea* biofilms to phenol and toluene to compare inhibition and transcriptional changes with suspended cells response

Chapter 2 of this dissertation examines the physiological and transcriptional response of *N. europaea* biofilms to phenol and toluene exposure. In a previous study, suspended cells of *N. europaea* exhibited ammonia oxidation inhibition during exposure to phenol and toluene (79). The study also identified a gene cluster that was up-regulated during phenol exposure (NE1545-NE1551) of which NE1545 was the highest fold up-regulated and is a potential sentinel gene for phenol exposure. Considering the existing paradigm that biofilms provide protection to bacterial cells (22), it was hypothesized that *N. europaea* biofilms would be more resistant to ammonia oxidation inhibition that those in suspended batch culture. Possible mechanisms for resistance include mass transfer limitations which create gradients in cell activity, and differential gene expression, which provides biofilm cells with innate tolerance to inhibitory compounds (31).

The research presented in Chapter 2 accomplished the first objective by examining the ammonia oxidation and gene expression in *N. europaea* biofilms during phenol and toluene exposure. A Drip Flow Biofilm Reactor was used to cultivate the

biofilms and to expose the mature biofilms to phenol and toluene during continuous flow of liquid medium through the reactor. To evaluate the inhibitory effects, nitrite production by biofilms during exposure was monitored and compared to results of inhibition in batch cultures. The possibility that biofilm resistance is due to transcriptional response was explored by determining whole-genome transcriptional changes in the biofilms through microarray analysis after biofilm exposure to both phenol and toluene.

(2) Determine differential gene expression between biofilms and suspended cells of *N. europaea* and explore the relationship between transcription and growth rate

Biofilm formation and growth is considered to be a result of transcriptional changes in bacterial cells brought on by environmental conditions or signaling mechanisms. Numerous studies comparing whole-genome transcription between biofilms and suspended cells have been implemented in well-studied heterotrophic bacterial species (8, 10, 105); however no such study has been previously completed with an AOB. Not only is the transcriptional profile in biofilms of interest, but the expression of genes under different growth conditions in suspended cells is also important. If genes expressed in biofilms of *N. europaea* are also up-regulated under certain conditions in suspended cultures, it may suggest that biofilm formation is likely to be induced under those culture conditions.

In Chapter 3, it is hypothesized that biofilms of *N. europaea* up-regulate different genes than exponential batch cells, and that biofilm genes are up-regulated in suspended cells under slow growth conditions. Suspended cells grown in batch culture were harvested in mid- to late-exponential phase and transcript levels were compared to those of the biofilms using microarrays. Selected genes up-regulated by the biofilms were tracked in continuous reactors under slow dilution rates.

(3) Determine if a correlation exists between rate of ammonia oxidation by *N. europaea* cells and the extent of inhibition during phenol exposure

The first objective summarized above examined the effect of phenol on biofilms of *N. europaea* and compared inhibition to that of suspended cells. In the objective presented in Chapter 4, further steps were taken to determine the cause of increased resistance to phenol in biofilms. The biofilm cells exhibited a depth-averaged rate of ammonia oxidation which was an order of magnitude lower than in suspended cells during batch tests in substrate-replete medium. To further examine differences in ammonia oxidation activity, continuous cultures of suspended *N. europaea* cells were maintained at different dilution rates to achieve various levels of activity. During phenol exposure of the continuous cultures, the level of inhibition was measured by reduction in oxygen uptake rates and was related to dilution rate of the culture. The cultures at faster dilution rates had higher rates of oxygen uptake and greater inhibition due to phenol exposure.

In chapter 4 of this dissertation, a hypothesis is presented that the inhibition of *N. europaea* during phenol exposure is related to the activity level of the cells. Evidence for this is shown in both suspended cell reactors with continuous cultures of *N. europaea*, as well as attached growth reactors with biofilms. Phenol exposure to biofilms was also examined under different conditions of O_2 availability that resulted in different rates of NH_3 oxidation and affected the biofilm inhibition.

(4) Evaluate reactive transport processes in *N. europaea* biofilms by microelectrode measurements and 2-D biofilm modeling

In the previous chapters, the differences in transcription and inhibition between biofilms and suspended cells were examined. Observed differences between cells in different growth rates may also be linked to kinetics in the respective growth states, such as attached and suspended. In Chapter 5, the kinetics of ammonia oxidation in *N. europaea* biofilms are explored using microsensor measurements and a biofilm model.

Numerical biofilm modeling is a beneficial tool for spatial evaluation of the influence of mass transport limitations on microbial kinetics. Models can be used to

simulate the chemical gradients in biofilms by estimation of microbial kinetic parameters. In this work, a reactive transport model is fitted to experimental data of dissolved oxygen gradients in a pure culture biofilm of *N. europaea*.

Chapter 5 examined the hypothesis that the kinetics of ammonia oxidation in *N. europaea* biofilms are equal to those in batch suspended cells and the observed differences are due to mass transfer limitations. This hypothesis is evaluated by using microsensors for DO and pH measurements in the biofilms coupled with a reactive transport model of the biofilm. The model was used to predict ammonia oxidation kinetics in biofilms, while accounting for mass transport. The simulated results of concentration profiles in the biofilms were compared to experimental data from microsensor profiles. The kinetic parameters derived from the model were compared to experimentally determined parameters of batch systems to determine if there was a difference in NH_3 oxidation kinetics between biofilms and suspended cells of *N. europaea.*

Chapter 2

Inhibition and gene expression of *Nitrosomonas europaea* biofilms exposed to phenol and toluene

Ellen G. Lauchnor, Tyler S. Radniecki, and Lewis Semprini

ABSTRACT

Pure culture biofilms of the ammonia-oxidizing bacterium *Nitrosomonas europaea* were grown in a Drip Flow Biofilm Reactor and exposed to the aromatic hydrocarbons phenol and toluene. Ammonia oxidation rates, as measured by nitrite production in the biofilms, were inhibited 50% when exposed to 56 μM phenol or 100 μM toluene, while 50% inhibition of suspended cells occurred at 8 μM phenol or 20 μM toluene. Biofilm-grown cells dispersed into liquid medium and immediately exposed to phenol or toluene experienced similar inhibition levels as batch grown cells, indicating that mass transfer may be a factor in *N. europaea* biofilm resistance. Whole genome microarray analysis of gene expression was used to detect genes up-regulated in biofilms during toluene and phenol exposure. Two genes, a putative pirin protein (NE1545) and a putative inner membrane protein (NE1546) were up-regulated during phenol exposure, but no genes were up-regulated during toluene exposure. Using qRT-PCR, up-regulation of NE1545 was detected in biofilms and suspended cells exposed to a range of phenol concentrations and levels of inhibition. In the biofilms, NE1545 expression was up-regulated an average of 13-fold over the range of phenol concentrations tested, and was essentially independent of phenol concentration. However, the expression of NE1545 in suspended cells increased from 20-fold at 7 μM phenol up to 80-fold at 30 μM phenol. This study demonstrates that biofilms of *N. europaea* are more resistant than suspended cells to inhibition of ammonia oxidation by phenol and toluene, even though the global transcriptional responses to the inhibitors do not differ in *N. europaea* between the suspended and attached growth states.

INTRODUCTION

Biological treatment strategies in wastewater treatment plants (WWTP) often utilize biofilms for the removal of nitrogen via nitrification and denitrification (91). Biofilms provide advantages over suspended cell processes in WWTP, including higher nutrient removal rates and the reduced wash out of slow growing organisms such as ammonia-oxidizing bacteria (AOB). AOB, such as *Nitrosomonas europaea*, carry out the first step in nitrification, the oxidation of ammonia (NH_3) to nitrite (NO_2^-) and are essential for nitrogen removal in WWTP (78). Ammonia oxidation by *N. europaea* can be inhibited by a range of organic compounds including aromatic hydrocarbons (45). Phenol and toluene are two aromatic hydrocarbons that can be present simultaneously with NH_3 in industrial wastewater streams, such as those from petrochemical industries (61), and can cause the incomplete removal of nitrogen from wastewater (117).

In *N. europaea*, NH_3, the sole growth substrate, is oxidized to NO_2^- in a two-step process yielding a net gain of two electron equivalents (4). The first oxidation step from NH_3 to hydroxylamine (NH_2OH) is catalyzed by the ammonia monooxygenase enzyme (AMO). AMO is capable of oxidizing a broad range of substrates co-metabolically, including aromatics, chlorinated compounds and polyaromatic hydrocarbons (19, 45, 82). The hydroxylamine oxidoreductase enzyme (HAO) further oxidizes NH_2OH to NO_2^- and yields four electrons, two of which provide the reducing power for the oxidation of NH_3 by AMO and two of which are used for cell growth.

Co-metabolism by *N. europaea* can inhibit NH_3 oxidation through competition for the active site of AMO and consumption of reducing power (19, 44). Phenol can be formed by co-metabolic oxidation of benzene by *N. europaea* and is further oxidized to hydroquinone (41, 45), while toluene is oxidized to benzyl alcohol and benzaldehyde by AMO (45).

Biofilms tend to be more resistant than suspended cells to inhibitory compounds and antimicrobials (5, 22). Some potential causes of increased biofilm

tolerance to inhibitory compounds are mass transfer limitation due to diffusion of the inhibitor, stratified growth conditions, and biofilm specific gene expression (31). Although numerous studies have reported the effect of inhibitory compounds on NH_3 oxidation by *N. europaea*, few have examined inhibition of pure culture biofilms of *N. europaea* (1, 77). This work explores the activity of *N. europaea* biofilms as a strategy to promote efficient NH_3 oxidation in the presence of phenol and toluene.

Previous studies have successfully used whole-genome microarrays to study gene expression associated with attached growth in model, single species biofilms (52). Recently, microarrays have been used to determine transcriptional responses of suspended *N. europaea* cells to heavy metals (69), chlorinated aliphatics (36), and aromatic hydrocarbons (79). A previous microarray study of suspended cells of *N. europaea* during phenol exposure detected a cluster of up-regulated genes, although no genes were up-regulated by toluene exposure (79). This study expands upon that work and is the first to examine both the physiological responses and the gene expression of *N. europaea* biofilms during nitrification inhibition by phenol and toluene.

MATERIALS AND METHODS

N. europaea batch cell cultivation

Nitrosomonas europaea (ATCC 19718) was cultured using methods previously described (79). Cells were grown for inoculation of biofilm reactors and suspended cell batch tests in AOB media (pH 7.8) defined as the following: 25 mM $(NH_4)_2SO_4$, 40 mM KH_2PO_4, 3.77 mM Na_2CO_3, 750 µM $MgSO_4$, 270 µM $CaCl_2$, 18 µM $FeSO_4$, 17 µM EDTA free acid, and 1 µM $CuSO_4$.

Drip Flow Biofilm Reactor

Biofilms of *N. europaea* were grown in four-channel Drip Flow Biofilm Reactors (DFR) (BioSurface Technologies, Inc., Bozeman, MT) for at least 4 weeks prior to inhibition studies. For the toluene inhibition studies, a stainless steel version of the DFR was constructed to minimize toluene sorption and volatilization. The DFR

was operated similar to methods described previously (14, 113) with modifications described here. Frosted glass microscope slides were used in the 4 DFR channels as biofilm growth surfaces. *N. europaea* batch grown cells described above were harvested in late exponential phase and concentrated by centrifugation to 20 mg protein L^{-1}. The concentrated cell cultures (15 mL) were aseptically added to each channel and the DFR was incubated in batch mode at 30ºC for 2-3 d. Subsequently, HEPES medium, defined as AOB medium with 20 mM HEPES buffer and 10 µM KH_2PO_4, instead of 40 mM KH_2PO_4 buffer, was fed to the DFR with a Masterflex peristaltic pump (Cole Parmer, Vernon Hills, IL) at a rate of 15 mL h^{-1} to each channel. Oxygen was supplied by mass transfer from the headspace of the DFR channels, which were connected to the room air through sterile 0.45 µm filters. The flow rate, NO_2^- and pH were monitored daily by sampling the effluent medium via quick-disconnect tubing fittings, using aseptic techniques and ethanol (70%) disinfection to prevent contamination. Liquid samples were spread plated on LB agar plates periodically to check for heterotrophic contamination.

Continuous Flow Inhibition Studies

Upon achieving steady-state NO_2^- production rates in the biofilms (4-6 weeks), continuous flow inhibition experiments were performed with phenol or toluene. Prior to inhibition tests, the concentration of $(NH_4)_2SO_4$ in the HEPES medium was adjusted to 2.5 mM. During each inhibition experiment, phenol (10-120 µM) or toluene (40-120 µM) was added via a syringe pump to the influent media of two of the biofilm channels for a period of 2-3 h, with the other two channels remaining as controls. Samples were collected from the effluent at 20 min intervals to monitor NO_2^- and the concentrations of phenol or toluene and their transformation products. Following phenol or toluene addition, biofilms were allowed to recover for at least 2 d, and subsequent inhibition tests were performed following a return to steady-state NO_2^- production. Tests were performed at multiple concentrations for each inhibitor (phenol or toluene). Extent of inhibition was determined by comparing the NH_3 oxidation rates of biofilms before and after phenol or toluene exposure.

Suspended and Resuspended Cell Batch Tests

Suspended cell batch tests were performed on cells in exponential growth and resuspended biofilm cells. For resuspended cell tests, slides with 4-6 week-old biofilms were removed from the DFR, rinsed twice and suspended in 1 mL 30 mM HEPES buffer (pH 7.8). For exponential cell tests, *N. europaea* cultures were harvested in late exponential phase (OD_{600}~0.07), centrifuged at 9000 RPM and suspended in 30 mM HEPES buffer (pH 7.8). Cells were added to bottles containing HEPES medium with 2.5 mM $(NH_4)_2SO_4$ to a final concentration of 6 mg protein L^{-1}. Treatment bottles contained phenol or toluene, while control bottles contained only HEPES medium. The bottles were shaken (200-250 RPM) for 3 h at 30ºC and NO_2^- production and aromatic hydrocarbon concentrations were monitored by extracting and analyzing headspace and liquid samples at 30-minute intervals.

Analytical Methods

Samples of DFR effluent liquid were taken daily during biofilm growth for pH and NO_2^- measurement via colorimetric assay (39). Flow rate was checked by weighing effluent liquid samples collected from the DFR over 10 min periods. The biuret assay was used to determine protein concentration in biofilms, after digestion of cell material in 3M NaOH (30 min at 60ºC) (39).

Phenol, hydroquinone, benzyl alcohol and benzaldehyde were measured with a Dionex-500 HPLC chromatograph with an Alltech Platinum C18 column (Alltech Associates, Deerfield, IL). The UV detector was operated at 275 nm for phenol and hydroquinone, and 254 nm for benzyl alcohol and benzaldehyde. The eluent composition was 25 mM KH_2PO_4 (pH 2.5) with 20% acetonitrile and was pumped through the column at 2 mL min^{-1}. The method was calibrated using external standards.

A gas phase headspace method of analysis was used for toluene. Liquid aliquots (0.5 mL) were added to sealed crimp top vials (1.8 mL) and 3.33 mM allylthiourea was added to halt cell activity and toluene cometabolism prior to shaking the vials at 250 RPM for 1 h. Headspace samples were taken for GC analysis, which

was performed according to methods described previously (79). The liquid concentrations of toluene were determined by mass balance using Henry's Law and a dimensionless Henry's constant of 0.271 at 25°C (55).

Biofilm depth was quantified by microscopic imaging with a Leica Z16 APO stereomicroscope (Leica Microsystems, Inc., Bannockburn, IL) equipped with a Qimaging MicroPublisher 3.3 digital camera (Qimaging, Surrey, BC). Qcapture Pro software was used to calibrate images and measure distances from the biofilm surface to the coupon interface.

Oxygen Concentration Profiles

Clark-type oxygen microelectrodes with tip diameters of 8-12 μm (Unisense Inc., Denmark) were used to determine oxygen concentration with biofilm depth, according to methods described previously (33). The oxygen microelectrode design is described in detail elsewhere (85). A micromanipulator with motor controller and SensorTrace Pro software (Unisense) were used to position the electrodes and record sensor output.

Cell Harvesting and RNA Extraction

For transcriptional analyses, biofilm cells were harvested from the DFR following phenol or toluene exposure, and suspended cells were harvested at the end of batch tests. Biofilm cells were scraped from each slide with a razor blade and rinsed in 1 mL HEPES buffer (30 mM, pH 7.8). Biofilm and suspended cells were pelleted by centrifugation, suspended in 500 μL Trizol reagent (Invitrogen, Carlsbad, CA), and immediately frozen and stored at -80ºC. For total RNA extraction, samples were thawed, an additional 500 μL Trizol was added, and the cells were lysed by syringing through a 21 gauge needle. Total RNA was isolated through a phenol-chloroform extraction (20), and further purified using the RNeasy Mini Kit (Qiagen Inc., Valencia CA).

Microarray Analysis

Roche NimbleGen gene expression chips in four-plex format (Roche NimbleGen, Inc., Madison, WI) containing all annotated *N. europaea* genes were used

to compare global gene expression between experimental triplicates of control, phenol and toluene treated biofilms. The concentration and purity of extracted Total RNA was measured via spectrophotometric quantification using a NanoDrop ND-1000 UV-Vis Spectrophotometer (Thermo Scientific, Wilmington, DE), and RNA quality was analyzed with an Agilent Bioanalyzer 2100 (Agilent Technologies, Santa Clara, CA). Synthesis of cDNA, labeling with Cy3 primers, and hybridization on a 4-bay NimbleGen Hybridization Station were performed as per NimbleGen instructions. Microarrays were scanned at 532 nm with an Axon GenePix 4200A scanner according to manufacturer specifications (Molecular Devices, Sunnyvale, CA).

Expression data were normalized through quantile normalization (12) and gene calls were generated using a Robust Multichip Average (RMA) algorithm (43). ArrayStar software (DNAStar, Inc., Madison, WI) was used to generate gene expression results and calculate p-values using the Modified t-test. Microarray data is available on the NCBI Gene Expression Omnibus (GEO) database, with the accession GSE22646.

Quantitative Reverse Transcriptase PCR (qRT-PCR)

The expression of *amoA* (ammonia monooxygenase)*, hao* (hydroxylamine oxidoreductase) and the seven genes NE1545-NE1551 were measured via qRT-PCR using oligonucleotide primers (Table 2.1) and according to methods described previously (79).

Analysis of qRT-PCR was performed with Data Analysis for Real-Time PCR (DART-PCR) (71). Gene expression was calculated by normalizing the target gene to the 16S rRNA and dividing expression of the treatments by the controls. Values of 95% confidence were determined from standard deviations of triplicates.

RESULTS AND DISCUSSION

Physiological Responses of Biofilms to Phenol and Toluene

After 4-5 weeks of DFR operation, the channels approached constant NO_2^- production rates and the biofilms were assessed to be at steady-state with respect to

NH_3 oxidation. The NO_2^- production rates of the control biofilms remained constant throughout the duration of each 3 h inhibition experiment, although rates varied between the reactor channels. Biofilm depth was evaluated by taking microscopic images of various locations on a single DFR coupon (n=13) and measuring depth by image analysis, which ranged from 86 − 326 µm. Biofilm coverage of the coupon surface was heterogeneous, resulting from the fluid flow in the DFR.

When 70 µM phenol was added to 2 DFR channels, the rate of NO_2^- production decreased by 68 ± 1% in the treated biofilms during the 3 h exposure (Fig. 2.1A). Phenol co-metabolism resulted in the production of 7.1 ± 0.2 µM hydroquinone (Fig. 2.1B), similar to previously reported results (41). Interestingly, regardless of the phenol concentration in the DFR, the hydroquinone concentration in the effluent was 6-11 µM. Addition of 10 µM hydroquinone did not inhibit NH_3 oxidation in suspended cells of *N. europaea* (data not shown). Therefore, the observed inhibition was due to phenol rather than its co-metabolic product, hydroquinone.

In a representative toluene exposure test, the addition of 97 µM toluene resulted in 53 ± 5% reduction in NH_3 oxidation by exposed biofilms (Fig. 2.1C). Toluene was co-metabolized to 53 ± 0.5 µM benzyl alcohol and 11 ± 0.5 µM benzaldehyde (Fig. 2.1D), which agrees with previous reports of toluene transformation products by suspended cells of *N. europaea* (45, 79). In batch tests with suspended cells, 15 µM benzyl alcohol and 5 µM benzaldehyde did not inhibit NH_3 oxidation (data not shown), suggesting that the observed inhibition was due to toluene and not the presence of transformation products.

The recovery of NO_2^- production was monitored after phenol or toluene addition was terminated (data not shown). During the first 2 h after stopping phenol addition, NO_2^- production rapidly recovered as phenol was washed out of the treated DFR channels. Twenty-four hours after stopping phenol addition, NO_2^- production rates in inhibited biofilms returned to 89% ± 6% of previous rates, which did not significantly differ from control biofilms at 96% ± 13% of pre-test NO_2^- production

rates. Biofilms inhibited by toluene returned to 109% $\pm$ 5% of previous NO_2^- production rates within 24 h of stopping toluene addition. The recovery of NH_3 oxidation indicates that toluene and phenol inhibition in biofilms are reversible, which is consistent with previously reported results with suspended cells (79).

Inhibition Comparison Between Growth Conditions

Nitrification inhibition tests were conducted on biofilms over a range of phenol (10-80 µM) and toluene (46-120 µM) concentrations (Fig. 2.2). For comparison with biofilm results, batch inhibition tests with suspended cells of *N. europaea* and resuspended biofilm cells were performed with phenol (10-80 µM) and toluene (20-115 µM).

In biofilms, 50% reduction in NO_2^- production was caused by exposure to 56 $\pm$ 11 µM phenol (Fig. 2.2A). In suspended cells of *N. europaea*, 50% inhibition occurred at only 8 µM phenol and exposure to 40 µM phenol caused over 95% inhibition. The results indicate that *N. europaea* biofilms are more tolerant to phenol exposure than suspended cells (Fig. 2.2A). Resuspending biofilm-grown cells in liquid medium eliminated the increased tolerance to phenol (Fig. 2.2A).

Similar to phenol results, biofilms of *N. europaea* were more resistant to toluene inhibition than both the suspended cells and biofilm-grown cells resuspended in liquid medium (Fig. 2.2B). In both the suspended and biofilm-grown resuspended batch tests, NH_3 oxidation was 50% inhibited by 21-25 µM toluene, while the biofilms were 50% inhibited by 97-120 µM toluene.

The concentration of phenol or toluene necessary for 50% inhibition was 5 to 7 fold higher in the biofilms than in either batch-grown cells or biofilm-grown cells in suspension. Similarly, a previous study of biofilm populations of *N. europaea* reported that biofilms were also more resistant than cell suspensions to NH_3 oxidation inhibition by the nitrification inhibitor, nitrapyrin (77). Possible explanations for the increased tolerance to inhibition in biofilms include slow or incomplete diffusion of the inhibiting species (106). Incomplete diffusion of some antimicrobial compounds has been a factor in biofilm resistance (3). In the case of co-metabolic substrates, the

reaction of the inhibitor combined with diffusion limited transport creates concentration gradients resulting in a lower concentration inside the biofilm compared to the bulk fluid. In this study, the maximum co-metabolism rates during exposure of 60 μM phenol and 100 μM toluene were 0.0011 and 0.01 mmol/(mg protein-d), respectively. The order of magnitude difference in co-metabolism rates between phenol and toluene, despite the similarity in the physiological response of the biofilms to the two compounds, suggests that concentration gradients of phenol and toluene did not play a large role in the biofilm tolerance.

The possibility that stationary cells are protected from inhibition has been examined for antibiotics that affect actively growing cells, but it may also apply during co-metabolic inhibition that is dependent on substrate turnover by an enzyme such as AMO. Comparisons of average growth rates between batch and biofilm cultures have revealed lower growth rates in biofilms, which were a result of averaging over stratified conditions in biofilms with large zones of inactive and nutrient limited cells (81). In this study, average specific (normalized to cell protein) NH_3 oxidation rates in *N. europaea* biofilms and exponential cells were 0.31 and 3.41 mmol/(mg protein-d), respectively, in the same growth medium. Upon resuspension of biofilm cells into batch reactors, specific NH_3 oxidation rates increased to 1.6 mmol/(mg protein-d). Experiments with resuspended biofilm cells were repeated in the presence of the protein synthesis inhibitor chloramphenicol (400 μg/mL) with identical NH_3 oxidation rates and inhibition results. The five-fold increase in activity after a return to nutrient replete medium suggests that the biofilm cells were able to recover quickly from deprived conditions upon exposure to substrates, and presumably without requiring *de novo* protein synthesis. The higher NH_3 oxidation rate of biofilm cells when resuspended into fresh medium indicates that inactive cells are still capable of NH_3 oxidation when oxygen and NH_3 are supplied. A previous study of ammonia oxidation gene expression during oxygen deprivation suggested that *N. europaea* may maintain AMO for quick recovery when nutrients become available (115). The

increase in ammonia oxidation activity in resuspended cells corresponded to an increase in phenol and toluene inhibition, which may be dependent on AMO turnover.

Oxygen Concentration in Biofilms

Oxygen is a substrate for AMO during both NH_3 oxidation and co-metabolic oxidation, and its limitation will affect the dynamics between the competing processes. Since an excess of NH_3 was supplied in the media, dissolved O_2 was expected to be the limiting substrate for AMO. The NH_3 oxidation rate of 0.31 mmol NH_3/(mg protein-d) in control biofilms was 30-300 times higher than the rates of phenol and toluene co-metabolism reported for the biofilms in the previous section. Therefore, the co-metabolized substrates were not expected to be as depleted inside the biofilm as oxygen. This is supported by the observations that only about 10% of the phenol was co-metabolized to hydroquinone in the DFR (Fig. 2.1A).

To determine if oxygen limitation was present in the biofilms, steady-state dissolved oxygen concentrations were measured with biofilm depth using microelectrodes. Measurement of oxygen concentration profiles was done at locations on the coupons where the biofilm depth was measured to be greater than 200 μm. Oxygen concentration was 20% of atmospheric saturation at the biofilm surface and completely depleted at a biofilm depth of 100 μm (Fig. 2.3). The depletion of O_2 in the biofilms also indicates that NH_3 limitation is not likely influencing the rate of NH_3 oxidation. These dissolved oxygen concentration profiles in the biofilms indicate that cells greater than 100 μm from the biofilm surface were oxygen limited.

Although greater than half of the biofilm depth was under O_2 deprivation, the specific rates of ammonia oxidation were 10-fold lower than suspended cells. This indicates that not all of the reduced activity is associated with oxygen limitation. The biofilm cells are likely in a stationary phase of growth, which is a previously observed characteristic of bacterial biofilms (9). In biofilms, both oxygen deprivation and slow growth rate have been factors in tolerance to antimicrobials (57, 106). In *N. europaea*, co-metabolic inhibition by phenol and toluene is related to interaction with the AMO

enzyme (45). Therefore, the biofilm tolerance observed in this study may be due to reduced cell activity during oxygen deprivation and cells in stationary growth.

Transcriptional Responses to Phenol and Toluene

Genome-wide gene expression was analyzed in *N. europaea* biofilms exposed to either 60 μM phenol or 100 μM toluene (Table 2.2). Toluene exposed biofilms did not differentially express any genes greater than 2-fold with 95% confidence, compared to uninhibited biofilms. In phenol exposed biofilms, two genes NE1545, a putative pirin protein, and NE1546, a putative inner membrane protein, were up-regulated over biofilm controls 24- and 28-fold, respectively. The genes NE1547-NE1551 were also differentially expressed in the microarrays of phenol-exposed biofilms, although the statistical analysis concluded that the results were not significant (Table 2.2). This resulted from lower fold-changes of these genes in one of the phenol-exposed biofilms, although the expression was still above that of the biofilm controls.

In a similar microarray study with suspended cells of *N. europaea*, the same 7 genes were expressed during phenol inhibition and no genes were up-regulated with toluene inhibition (79). Since phenol and toluene exposed biofilms exhibited the same gene expression as suspended cells during inhibition, transcriptional response to short-term inhibition cannot account for the apparent biofilm tolerance to phenol and toluene.

qRT-PCR Analysis

The genes NE1545-NE1551 were measured in the biofilms via qRT-PCR analysis for microarray validation (Table 2.2). The genes *amoA* and *hao* were also measured as controls that were not up-regulated in microarrays. No significant changes in *amoA* and *hao* expression were observed in phenol or toluene exposed biofilms. During qRT-PCR of phenol treated biofilms, the genes NE1545-NE1551 were up-regulated, although only NE1545 and NE1546 showed a statistically significant fold-change over control biofilms according to 95% confidence, which is consistent with microarray results (Table 2.2).

The most highly up-regulated gene in phenol-exposed biofilms, NE1545, was measured via qRT-PCR in *N. europaea* exposed to various phenol concentrations. NE1545 was up-regulated in biofilms exposed to 10-80 µM phenol, compared to control biofilms (Fig. 2.4), and the average of 13-fold up-regulation was essentially constant over the range of phenol concentrations. In comparison, suspended cells of *N. europaea* exposed to phenol exhibited higher up-regulation of NE1545 than biofilms and expression increased with increasing phenol concentration (Fig. 2.4). It is interesting to note that up-regulation of NE1545 is observed in the biofilms at phenol concentrations that caused only 10% inhibition of NH_3 oxidation. This is significant for the application of *N. europaea* sentinel gene expression for detection of inhibitors. The sensitive transcriptional response of NE1545 to phenol at low concentrations is favorable for the potential of *N. europaea* as a microbial biosensor.

The difference in biofilm and suspended cell fold-changes may result from averaging expression in biofilm cells that are growing under heterogeneous conditions. Cells for the microarray and qRT-PCR analyses were sampled over the entire biofilm thickness. As mentioned above, chemical gradients are typically observed in biofilms, such as the dissolved oxygen gradient observed in our test, and can result in differential growth rates with biofilm depth (110, 113). Recent research has also shown that expression of selected genes in biofilms can vary in cells at different biofilm depths (53). *N. europaea* cells that were in proximity with the biofilm surface may have expressed higher levels of NE1545 than the cells deeper in the biofilm.

CONCLUSIONS

NH_3 oxidation rates in biofilms of *N. europaea* were less inhibited by phenol and toluene than in suspended cells. However, when biofilm cells were resuspended into liquid medium, the resistance to inhibition was eliminated. Concentration profiles of oxygen in the biofilm showed that it was essentially depleted by a depth of 100 µm and the cells at greater depths were likely starved in comparison with nutrient rich conditions in the batch suspended cell reactors. The influence of oxygen depletion

and stationary-phase activity of biofilm cells is supported by lower specific rates of NH_3 oxidation in biofilms and an increase in both rates and inhibition of NH_3 oxidation after resuspension of biofilm grown cells in liquid medium. The relationship between slow ammonia oxidation rates and resistance in the biofilms points to a turnover dependent inhibition of AMO activity.

The genes up-regulated in phenol-exposed biofilms were the same as those detected in the previous, suspended cell microarray study. Thus there was not sufficient evidence that would indicate a transcriptional resistance mechanism unique to cells in the biofilm in response to phenol exposure.

The combined transcriptional and physiological results show that *N. europaea* biofilm cells up-regulate NE1545 at phenol concentrations that cause less than 20% inhibition of NH_3 oxidation. This early detection of transcriptional response to phenol exposure may be useful in the application of microbial biosensors for phenol contamination in wastewater treatment. Future research will incorporate microelectrode profiles with a biofilm model to explore the hypothesis that concentration gradients influence the physiological response of *N. europaea* biofilms to phenol and toluene. Relationships between cell activity and inhibition by phenol and toluene also need to be investigated.

Table 2.1 Primers sequences used in qRT-PCR analysis

Primer	Sequence
16S For	5'-GGCTTCACACGTAATACAATGG-3'
16S Rev	5'-CCTCACCCCAGTCATGACC-3'
NE 1545 For	5'-GGATGATCTGACGCAAGTGA-3'
NE 1545 Rev	5'-CTGCGACAAAGTCGAAAGTG-3'
NE 1546 For	5'-TTCCAAAATCAGCAGCTACG-3'
NE 1546 Rev	5'-TCGGCAAGATTCTTCTCAAA-3'
NE 1547 For	5'-CTGAAGGGTTGTGGCAAAAT-3'
NE 1547 Rev	5'-AAAGCTTGACAGCCGTTCAT-3'
NE 1548 For	5'-CTCGATGAATGGCACATCAC-3'
NE 1548 Rev	5'-TTGGGCACCATTACAGTCAC-3'
NE 1549 For	5'-GATGTACGCCAGACAGGTGA-3'
NE 1549 Rev	5'-ACCTGTGCACTGCTGTATGC-3'
NE 1550 For	5'-ATGCATCCTGGTTTCTTTGC-3'
NE 1550 Rev	5'-AATTGTTCCATTTCGGCGTA-3'
NE 1551 For	5'-TCCAGTACACCATTCACAGCA-3'
NE 1551 Rev	5'-CGGTTCAAGGTTCAAGCAAT-3'
amoA For	5'-TGGCGACATACCTGTCACAT-3'
amoA Rev	5'-ACAATGCATCTTTGGCTTCC-3'
hao For	5'-CAAACTTGCCGAAATGAACC-3'
hao Rev	5'-GCTGGTGATGTTCTCTGCAA-3'

Figure 2.1 Effluent aromatic hydrocarbons and transformation products (A and C) and NO_2^- production (B and D) in biofilms exposed to 70 µM phenol (A and B) and 97 µM toluene (C and D). **A)** NO_2^- production activity of biofilms exposed to 0 µM (○) and 70 µM (●) phenol. **B)** Effluent concentrations of phenol (□) and hydroquinone (■) during 3 h addition of 70 µM phenol. **C)** NO_2^- production activity of biofilms exposed to 0 µM (○) and 97 µM (●) toluene. **D)** Effluent concentrations of toluene (□), benzyl alcohol (■), and benzaldehyde (▲) during 3 h addition of 97 µM toluene. Error bars represent the range of duplicate treatments.
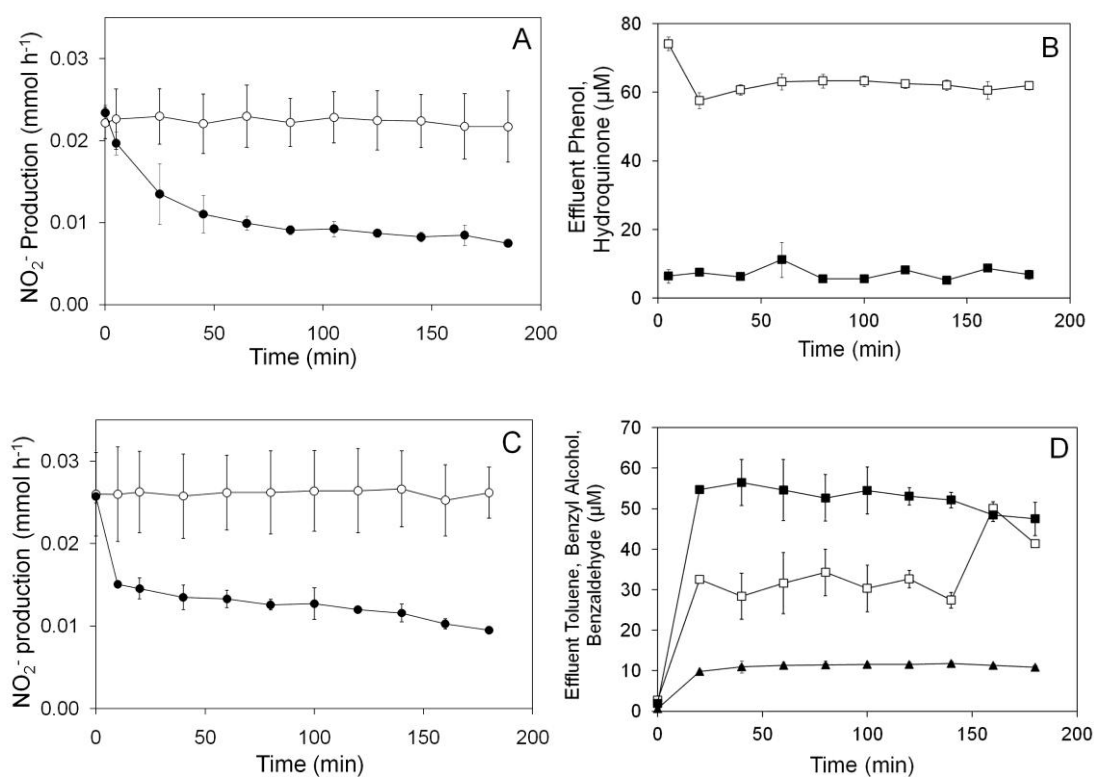
Figure 2.2 **A)** Phenol and **B)** toluene inhibition of NH_3 oxidation in biofilms (▲), suspended cells (□), and biofilm-grown cells dispersed in liquid media (■). Error bars represent range of duplicates in biofilm experiments and standard deviation of triplicates in suspended cell tests. Percent inhibition is given by

$$\% = \left(1 - \frac{r_{inh}}{r_{cont}}\right) \times 100\%$$

, where r_{inh} is the rate of NO_2^- production during inhibition and r_{cont} is the control rate of NO_2^- production.
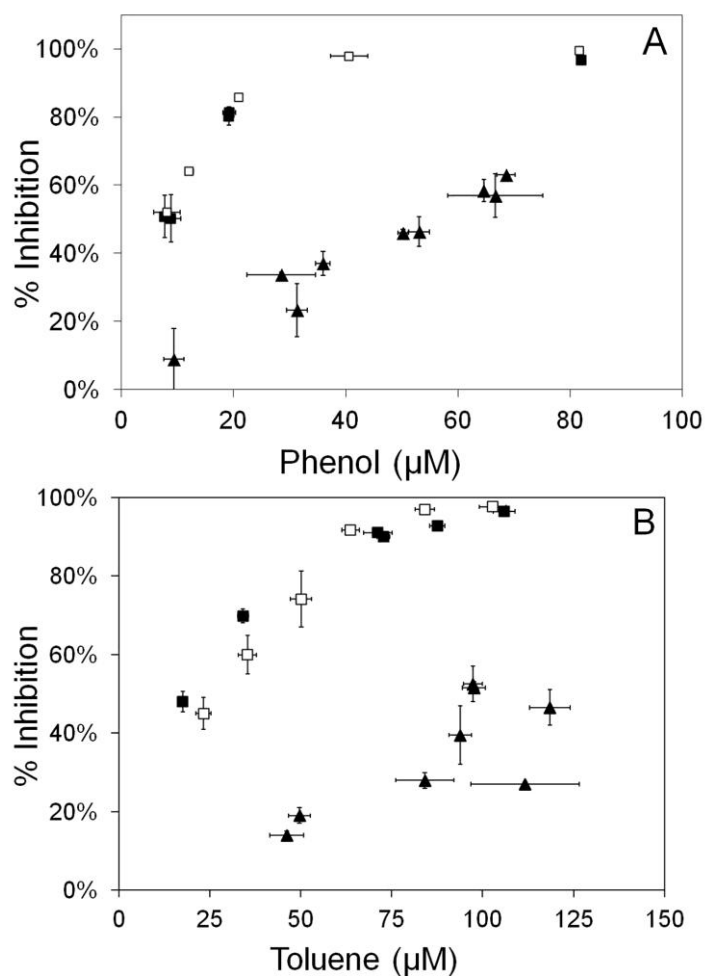
Figure 2.3 Oxygen concentration profiles in *N. europaea* biofilms at 22ºC. Depth of 0 µm corresponds to biofilm surface. Five replicate profiles from different locations on the same biofilm are shown.
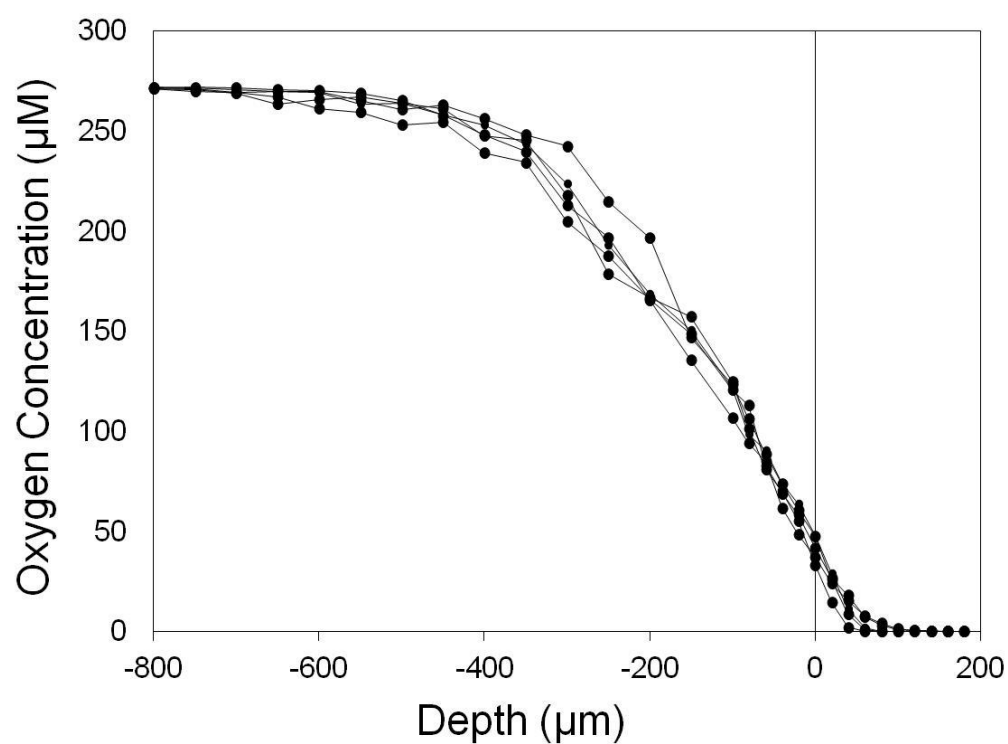
Table 2.2 Microarray and qRT-PCR analysis of *N. europaea* biofilms upon exposure to 100 μM toluene or 60 μM phenol. P-values were calculated in ArrayStar using the modified t-test. *Values were statistically significant according to 95% confidence of triplicates.

	Gene ID	Gene name	Microarray fold-change	p-value	qRT-PCR fold-change
Toluene		None detected			
Phenol	NE1545	DUF 209 (*Putative pirin protein*)	24.82	0.00193	14.92*
	NE1546	*Putative inner membrane protein*	28.43	0.00361	14.79*
	NE1547	Hypothetical protein	10.16	0.922	4.89
	NE1548	Acyl-CoA dehydrogenase	3.63	0.963	2.37
	NE1549	AMP-dependent synthetase and ligase	3.08	0.504	1.93
	NE1550	Hypothetical protein	5.11	0.944	3.66
	NE1551	Hypothetical protein	4.40	0.892	3.43

Figure 2.4 Fold-change of NE1545 in *N. europaea* biofilms (●) and suspended cells (○) vs. phenol concentration. Error bars represent standard deviation of triplicates, biofilm values are from single samples.
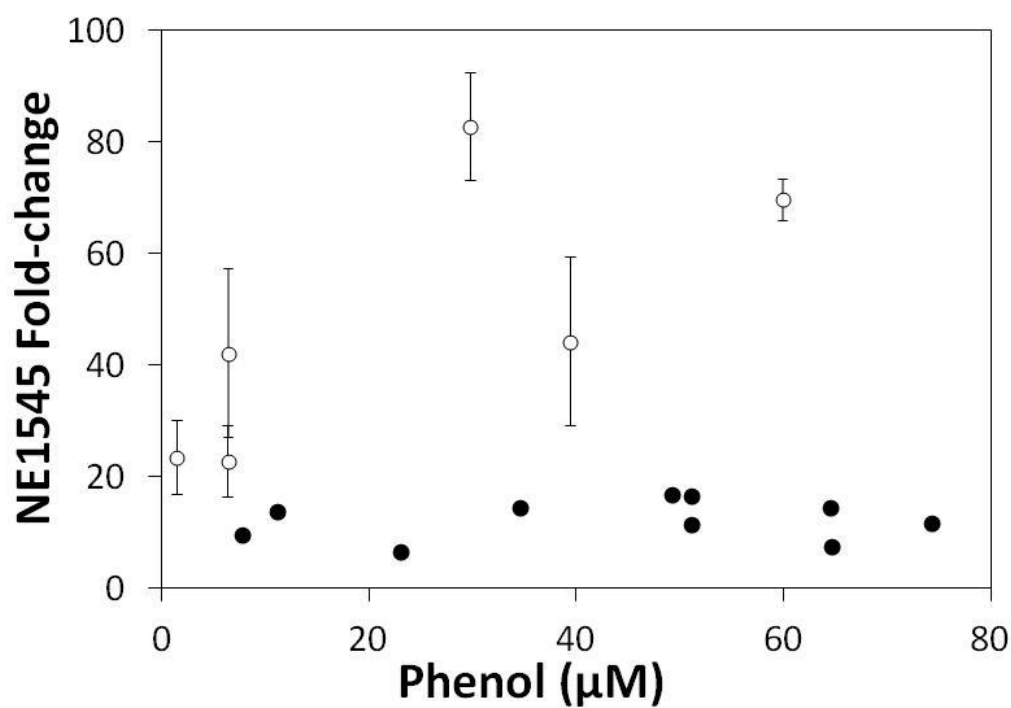
Chapter 3

Gene expression in biofilms of *Nitrosomonas europaea* and correlation with growth rate in suspended cells

Ellen G. Lauchnor, Tyler S. Radniecki and Lewis Semprini

ABSTRACT

Nitrosomonas europaea is a well characterized species of ammonia oxidizing bacteria (AOB) that exists in biofilms in natural and engineered systems. We cultivated single species biofilms of *N. europaea* in a Drip Flow Biofilm Reactor to analyze gene expression patterns between biofilms and suspended cells. To determine if the gene expression in biofilms can be induced in suspended cells during slow growth, the expression of selected genes was tracked under different growth conditions of suspended cells. First, genes were identified as differentially expressed between batch exponential and biofilm cells using whole-genome microarrays. A selection of genes up-regulated in the biofilm microarrays was tracked in suspended cell continuous cultures at various growth rates. In the microarrays, a total of 240 genes were differentially expressed by at least 2-fold, with 105 genes up-regulated and 135 genes down-regulated in biofilms with at least 95% confidence. Down-regulated genes in the biofilms were involved in metabolism of lipids, amino acids and nucleotides, while up-regulated genes in the biofilms included cell motility and adhesion, DNA replication and repair, and inorganic ion transport. A subset of the genes up-regulated in the biofilms were analyzed further via RT-qPCR and found to be highly expressed under continuous culture grown at slow dilution rates. The up-regulation of the genes was correlated to the growth rate of the suspended cells. In batch culture, the biofilm expressed genes were also up-regulated upon entry into stationary phase. This research demonstrates that genes expressed in *N. europaea* biofilms are also induced in suspended cells under continuous culture, and the level of expression increases with slower dilution rate of the culture.

INTRODUCTION

Biofilms, or surface associated communities of bacteria, are often the dominant form of bacterial growth in both natural and engineered environments. In engineered systems such as wastewater treatment plants (WWTP) biofilm reactors can be used for aerobic processes such as nitrification (88). Ammonia oxidizing bacteria (AOB) perform the first step of nitrification, the oxidation of ammonia (NH_3) to nitrite (NO_2^-), in natural systems and WWTP (78, 112). Multiple *in situ* analyses have identified *Nitrosomonas europaea*, a model AOB, as an important species in nitrifying WWTP reactors, indicating the importance of understanding *N. europaea* under various growth conditions (33, 94).

Bacterial cells undergo changes in gene expression when transitioning from planktonic to biofilm growth (52). Cells in biofilms also tend to have slow growth similar to stationary phase cells because the diffusive transport of nutrients into the biofilm causes substrate limitations (114). Additionally, changes in transcription and gene regulation can occur when exponential cells enter stationary phase or nutrient limited conditions (56) and similarities between the gene expression of biofilms and stationary phase cells has been reported (9).

Genome-wide microarrays have been used widely to compare transcriptional profiles between biofilms and planktonic cells of various bacterial species (84, 105, 111). Microarrays have been used to identify transcriptional changes in *N. europaea* during periods of starvation (109), and genes up-regulated in response to aromatic hydrocarbons (79), chlorinated hydrocarbons (36), and heavy metals (68). To our knowledge, no transcriptional analysis has been performed on biofilms of *N. europaea,* which will allow for identification of genes expressed in biofilms that can be tracked in other growth conditions of *N. europaea*.

Previous research has shown that *N. europaea* produces acyl-homoserine lactones (AHL) (6, 15), quorum sensing molecules that can mediate biofilm formation and gene expression (24). The presence of AHL has been shown to decrease lag phase from starvation in suspended cells of *N. europaea* and produce a starvation recovery

response similar to that observed in *N. europaea* biofilms (6). Nitric oxide gas has also been postulated as an inducing agent for biofilm formation in *N. europaea* (96). The examination of gene-expression in *N. europaea* biofilms may elucidate potential genes involved in biofilm formation.

In this study, microarrays were used to identify transcriptional differences between *N. europaea* biofilms and suspended cells of *N. europaea* in exponential growth. To evaluate the relationship of gene expression to growth rate, ten representative genes differentially expressed in the microarrays were tracked via RT-qPCR in suspended continuous culture at various growth rates. Gene expression was also tracked in batch cultures to evaluate transcriptional changes during the transition into stationary phase.

EXPERIMENTAL PROCEDURES

N. europaea culture

Cultures of *N. europaea* (ATCC 19718) were grown in batch as previously described (79) for biofilm inoculation and suspended cell studies. In brief, 25 mL of inoculum was added to 2 L of liquid growth medium and shaken in the dark at 100 RPM and 30ºC for 3 d. Cells were harvested in late exponential phase ($OD_{600} = 0.07$).

Exponential Batch Cell Experiments

N. europaea exponential phase cells were washed and placed in 1 L fresh AOB medium in batch reactors. AOB medium consisted of 25 mM $(NH_4)_2SO_4$, 3.77 mM Na_2CO_3, 20 mM HEPES buffer (pH 7.8), 730 μM $MgSO_4$, 200 μM $CaCl_2$, 9.9 μM $FeSO_4$, 16.5 μM EDTA free acid, and 0.65 μM $CuSO_4$. Cells were stirred for 2 h at 750 RPM and 30ºC, and NH_3 oxidation was monitored by taking liquid samples every 30 min for detection of NO_2^- accumulation. At the end of 2 h, 120 mL of cells (6 mg protein L^{-1}) were harvested for microarray analysis, pelleted by centrifugation, fixed in 0.5 mL Trizol reagent (Invitrogen, Carlsbad, CA) and stored at -80ºC until RNA extraction described below.

Drip Flow Biofilm Reactor

Biofilms of *N. europaea* were cultivated in a Drip Flow Biofilm Reactor (DFR) (BioSurface Technologies, Inc., Bozeman, MT) according to methods described elsewhere (50). To facilitate attachment, the biofilms were grown on frosted glass microscope slides. *N. europaea* inoculum for the DFR was prepared by centrifuging late exponential phase cells for 20 min at 9000 RPM, and removing supernatant until a cell concentration of 20 mg L^{-1} was achieved. Following inoculation, cells were allowed a 3 d attachment period of no flow in the DFR. Subsequently, growth medium was pumped through the DFR at 15 mL h^{-1} per channel. The flow rate of 15 mL h^{-1} to each channel was sufficient to wash out all unattached cells. Biofilm growth medium (pH 7.8) consisted of AOB medium with 2.5 mM $(NH_4)_2SO_4$. Samples were collected from the DFR effluent over 10 min periods. Aseptic techniques were used during DFR operation and effluent samples were plated periodically to test for contamination.

Slides containing mature biofilms grown for 4-6 weeks were removed from the DFR and biofilms were scraped off of the slides, suspended in 1 mL HEPES buffer (20mM, pH 7.8) and centrifuged for 1 min. The cell pellets were suspended in 500 μL of cold Trizol reagent (Invitrogen, Carlsbad, CA) and stored at -80ºC until Total RNA was extracted. For all analyses in this study, the complete biofilm on each slide was sampled for RNA extraction.

Continuous Flow Bioreactor

A Bioflow 110 bioreactor (New Brunswick Scientific, Edison, NJ) was used to continuously culture *N. europaea* cells at a hydraulic and cell residence time of 7 days. The bioreactor was operated according to methods described previously (80). Concentrations of NH_3, NO_2^- and optical density were measured in liquid samples taken aseptically from the reactor, and pH 7.8 was maintained by automated addition of Na_2CO_3. Periodically, 120 mL liquid samples were removed from the bioreactor and cells were harvested for Total RNA extraction as described above for exponential batch cell experiments.

Fill-and-Draw Reactors

N. europaea cultures were maintained in 500 mL flasks operated as fill-and-draw reactors by daily addition of fresh medium to mimic continuous culture. Triplicate flasks were operated at four different hydraulic and cell residence times of 100, 50, 20, and 5 d in order to compare the gene expression of cells at different growth rates. The fill-and-draw reactors each contained 200 mL sterile AOB medium with an additional 20 mM HEPES buffer (total 40 mM HEPES) to aid in maintenance of pH 7.8. The reactors were inoculated with 2 mL of late exponential phase *N. europaea* culture and shaken for 3 d at 200 RPM and 30ºC until the cultures arrived at stationary phase. Medium with suspended cells was aseptically removed from the reactors and replaced with an equal volume of fresh, sterile medium daily, to simulate continuous fed bioreactors. OD_{600}, NO_2^- and pH were measured in the spent reactor samples. The reactor pH was adjusted with NaOH to maintain a pH of 7.8. The triplicate reactors were maintained for 45 days at transfer volumes of 2 mL, 4 mL, 10 mL and 40 mL. Liquid samples were spread plated on LB agar to verify absence of heterotrophic contamination. Total RNA extraction was performed at the end of the 45 days as described previously for batch cells.

Batch growth curve

Expression levels of selected genes were tracked during the batch growth of *N. europaea* in liquid culture using qRT-PCR. During the growth phase experiment, batch cells were harvested aseptically on days 3, 4, 5 and 7, to track gene expression during progression through exponential and stationary phases. Liquid samples were also taken for determination of OD_{600} and NO_2^-.

Total RNA extraction

Total RNA extraction was performed on *N. europaea* cells according to methods described previously (79). RNA was purified using the Qiagen RNeasy Mini-kit (Qiagen Inc., Valencia, CA) as per manufacturer's instructions. Concentration and purity of total RNA was measured by UV absorption with a Nanodrop Spectrophotometer (Thermo Scientific, Wilmington, DE). An Agilent

Bioanalyzer (Agilent Technologies, Santa Clara, CA) was used to verify the quality of total RNA samples for microarray analysis.

Microarray Analysis

Whole-genome gene expression was analyzed in biological triplicates of *N. europaea* biofilms and exponentially growing suspended cells. Analyses were performed using microarray chips containing all genes in the *N. europaea* genome in 4-plex format (Roche NimbleGen, Inc., Madison, WI). Synthesis of cDNA from total RNA using random hexameric primers, labeling of cDNA and hybridization to microarray chips were performed according to the manufacturer's instructions (Roche NimbleGen, Inc.). Labeled cDNA was hybridized to microarrays at 42ºC for 16 h in a 4-bay NimbleGen Hybridization Station. After washing, microarrays were scanned at 532 nm with an Axon GenePix 4200A scanner (Molecular Devices, Sunnyvale, CA).

Scanned array images were aligned and raw expression data was extracted using Roche Nimblegen software (Roche NimbleGen, Inc., Madison, WI). Expression data was normalized with using quantile normalization (12) and gene calls were generated using a Robust Multichip Average algorithm (43). Microarray data was analyzed with ArrayStar software (DNAStar, Madison, WI). Statistical significance of 2-fold or greater changes in gene expression was determined by a confidence level of 95%, which was calculated in ArrayStar using the Student's t-test. Complete microarray data is available on the NCBI Gene Expression Omnibus (GEO) database with the accession number GSE22646. BLASTX searches (NCBI database, http://blast.ncbi.nlm.nih.gov) were performed on unknown genes that were differentially expressed. When the BLASTX search resulted in putative identities and functions, e-values of the top match for each gene are supplied in the appendix Table A1.

Real Time quantitiative PCR

Real-Time quantitative PCR (RT-qPCR) was performed to track expression of selected genes under various suspended cell culture conditions. The primer sequences for 10 genes chosen from the microarray results were designed using Primer3 software

(Table A2). Synthesis of cDNA and RT-qPCR reactions were carried out as described previously (79). Efficiencies of all genes were between 0.7 and 1. Raw fluorescence data from the RT-qPCR reactions were extracted and expression values were calculated using the Data Analysis of Real-Time PCR (DART-PCR) program, which takes efficiencies of the reactions into account (70). Fold-changes were determined by normalizing gene expression to 16S rRNA expression and comparing normalized values of the experimental groups.

Analytical Methods

NO_2^- concentrations were measured by colorimetric assay (37). Cell protein concentrations were measured by a microbiuret assay after cell digestion for 30 min at 65ºC in 3M NaOH (39). The OD_{600} measurement was correlated to protein concentration by a standard curve with the microbiuret protein analysis, and used with liquid cell cultures as a surrogate protein measurement. Biofilm thickness and structure was observed with a Leica Z16 APO stereomicroscope (Leica Microsystems, Inc., Bannockburn, IL) on biofilm samples grown for the same length of time and with similar activity as those used for microarray analysis.

RESULTS

Growth of *N. europaea* biofilm and batch cultures

N. europaea biofilms were cultivated in a Drip Flow Reactor (DFR) under continuous flow for several weeks to develop mature biofilms for microarray analysis. The NO_2^- production increased over 4 weeks of operation arriving at a steady level between 0.02-0.03 mmol NO_2^- h^{-1} per DFR channel with the pH of the DFR effluent remaining above 7.5. The steady-state rates of protein normalized NO_2^- production are shown in Table 3.1. Biofilm coverage of slides was heterogeneous, with estimated biofilm depth of 100 – 300 μm. Total biomass protein was 1-2 mg protein per biofilm sample and the differences in protein content contributed to the range in specific NO_2^- production rates as presented in Table 3.1.

Suspended *N. europaea* cells were maintained and harvested during exponential batch tests to compare gene expression with biofilms. Nitrite concentration increased as a linear function of time for the duration of incubation, verifying that NH_3 and O_2 were not limiting. The measured nitrification rates were an order of magnitude higher than those in the biofilms when normalized to protein concentration (Table 3.1). The rates were similar to NO_2^- production rates measured in previous *N. europaea* batch tests (36, 79).

Microarray results

Gene expression microarrays of *N. europaea* biofilms and exponentially growing cells revealed 240 genes that were differentially expressed at least 2-fold with 95% confidence, of which 105 genes were up-regulated and 135 genes were down-regulated in the biofilms. A table of all genes identified as differentially expressed between biofilms and batch suspended cells in the microarrays is included as Table A1 in Appendix A. The differentially expressed genes make up 9.8% of the 2,460 predicted protein-encoding genes in the *N. europaea* genome. Fifty-seven genes were poorly characterized genes including hypothetical proteins or domains of unknown function. Hypothetical proteins and unknown genes make up 19% of the *N. europaea* genome (17), so the high number of these genes expressed in the biofilms may also be a result of the large number of uncharacterized genes in the *N. europaea* genome. Of the total 240 genes that were differentially expressed, 20 were up-regulated greater than 4-fold in the biofilms, and 22 were down-regulated greater than 4-fold. The most highly expressed gene in the biofilms was a hypothetical protein (NE1576) that was up-regulated 7.1-fold. The most down-regulated gene in the biofilms was the gene NE0923, a putative cyanophycin synthetase which was repressed 10.8-fold.

Differentially expressed genes in the microarrays were classified based on clusters of orthologous groups (COGs) that were divided into four general categories in the GenBank database (GenBank, NCBI), shown in Figure 3.1. Three categories represent the broad functional groups of metabolism, cellular processes, and

information storage and processing, and a fourth category includes poorly characterized genes, such as domains of unknown function and hypothetical proteins.

Seventy-seven genes related to metabolism (Fig. 3.1, category II) were differentially expressed in *N. europaea* biofilms in comparison to exponentially growing cells. In this group, 48 genes were down-regulated, including amino acid, nucleotide and coenzyme biosynthesis genes. Several lipid metabolism genes in the fatty acid biosynthesis pathway (NE0653, NE0695, NE1649/50 and NE1708) were down-regulated in biofilms. Genes in energy production encoding cytochromes and cytochrome biogenesis proteins were both up- and down-regulated, with a cytochrome c encoding gene (NE1493) and the cytochrome c biogenesis gene *ccmH* (NE0770) down-regulated in biofilms 2-fold and another cytochrome c (NE1274) up-regulated 4-fold.

Of the 29 metabolism genes up-regulated in biofilms, 18 were classified as inorganic ion transport and metabolism (Fig. 3.1, category II). This COG had the highest percent of differentially expressed genes, where 23 genes were either up- or down-regulated in biofilms. Six TonB-dependent receptor proteins were up-regulated in the biofilms (NE0321, NE0556, NE0758, NE1088, NE1721 and NE2140). TonB-dependent receptor proteins are thought to be involved in iron uptake (108). However, none of the TonB-dependent receptor genes up-regulated in the biofilms correlated with proteins expressed in a previous study of iron limitation (108).

In the cellular processes functional group (Fig. 3.1, category III), seven genes classified as cell motility related were up-regulated in biofilms, and four were identified by homology as putative Type IV pili assembly proteins (NE0596/7 and NE1749/50), were all up-regulated between 2- and 4-fold. In the cell wall/membrane biogenesis group, two genes putatively involved in capsular polysaccharide synthesis and transport (NE1332, NE1386) were up-regulated in the biofilms approximately 2-fold more than exponential cells.

In the information storage functional group (Fig. 3.1, category IV), 19 genes encoding proteins for DNA replication, recombination and repair were up-regulated in biofilms. Of these, 13 genes encoded IS4 transposases or putative transposases.

RT- qPCR validation

A subset of 10 genes was chosen from the microarrays for examination of gene expression via RT-qPCR under varying growth conditions (Table 3.2). The genes NE0597 and NE1749 were chosen due to the potential involvement of Type IV pili in biofilm formation (63). NE0923 was selected as the most highly down-regulated in biofilms according to the microarray analysis. The other genes presented in Table 3.2 were chosen to explore a diverse range of genes from the microarray results, including iron siderophore acquisition (NE0556), polyssacharide production (NE1332), cytochrome biogenesis (NE0770), osmotic stress response (NE1944), c-di-GMP based signal transduction (NE1909), and DNA repair and uptake (NE1479, NE2408). Expression of each gene was determined via RT-qPCR to validate the microarray results for biofilm and exponential batch cells. The ammonia monooxygenase gene *amoA* was also detected by RT-qPCR, which helped to verify the sample quality by measuring a constitutively expressed gene. The RT-qPCR results of *N. europaea* biofilms agreed with the microarray results, although the levels of expression calculated from RT-qPCR and normalized to 16S rRNA concentration were higher than in the microarrays (Fig. 3.2).

RT-qPCR was also performed with RNA harvested from *N. europaea* cells cultivated in a chemostat at a constant dilution rate of 0.14 d^{-1}, which equated to a hydraulic residence time of 6.9 d. During continuous operation over several weeks, the chemostat arrived at a steady state NO_2^- production rate of 0.63 mmol NO_2^- (mg protein-d)$^{-1}$, which was greater than five-fold lower than the NO_2^- production by batch cells in exponential phase (Table 3.1). The normalized expression of the selected genes in chemostat cells was similar to the expression in biofilms relative to exponential cells (Fig. 3.2). Levels of *amoA* did not change between the biofilms, chemostat cells and exponential cells used in the microarray analysis (data not shown).

Gene expression in continuous suspended cultures

Fill-and-draw reactors operated to mimic continuously operated chemostats at four different hydraulic residence times (HRTs) of 5, 20, 50 and 100 d. Rates of NO_2^- production for each reactor varied less than 7% over the final 18 days of operation and were assumed to be at steady-state when cells were harvested from reactors for analysis of gene expression using RT-qPCR. The average NO_2^- production rates of triplicate reactors were normalized to protein concentration and are reported in Table 3.1. The highest rates of NO_2^- production were associated with the 5 d HRT and the lowest rates with the 100 d HRT. The rate of NO_2^- production in the chemostat was closest to the fill-and-draw reactors with 20 d HRT, and the protein normalized rates for the biofilms were between those of the 50 d and 100 d HRT reactors.

Transcriptional levels of the chosen subset of 10 genes differentially expressed in the microarrays were also up-regulated in the fill-and-draw reactors as compared to suspended cells in exponential growth. Transcript levels increased with slower dilution rate of the reactors (Fig. 3.3), which also corresponded to lower rates of NO_2^- production (Table 3.1). Consistent trends of greater up-regulation with lower NO_2^- production rates and longer HRT were observed with all of the genes analyzed. Linear regression analysis of NO_2^- production rates vs. fold-change in the fill-and-draw reactors was performed and revealed correlations between the two variables ($R^2 > 0.81$) for all the genes (Appendix A, Table A3). Positive linear correlations were also observed between the fold-changes of the selected genes and the reactor HRT (Table A3).

The genes NE0770 and NE0923, which were down-regulated in biofilms, were slightly up-regulated in cells grown in the 100, 50, and 20 d HRT fill-and-draw reactors and were down-regulated only in the 5 d HRT reactors compared to exponential cells (Fig. 3.3). An inverse relationship with NO_2^- production was also observed with expression of these genes. However, normalized levels of the constitutively expressed reference gene *amoA* in all fill-and-draw reactors were less than 1.6-fold different than exponential cells (data not shown).

The 5 d HRT fill-and-draw reactors were operated at a similar dilution rate as the chemostat at an HRT of 6.9 d. The genes NE0923 and NE0770 were down-regulated in both and the other eight genes examined via RT-qPCR were up-regulated. Linear regression analysis comparing the fold-change values for the chemostat and 5 d HRT reactors showed positive correlation between gene expression in the reactors (R^2=0.7) although the magnitude of expression was slightly higher in the chemostat (Appendix A, Fig. A1). The similarity in gene expression between the two reactors provides confidence that the fill-and-draw reactors behaved like continuously flowing chemostats.

Biofilm gene expression in stationary phase

Suspended cells were monitored over the course of batch growth for seven days and five genes from those chosen from the microarrays for further analysis were tracked by RT-qPCR to determine if transition into stationary phase induced gene expression (Table 3.3). The genes were chosen from Table 3.2 for their potential roles in biofilm formation, including pili formation (NE0597, NE1749), capsular polysaccharide production (NE1332) and c-di-GMP control (NE1909). Gene expression was calculated using the same DART-PCR threshold value for all samples of a given gene. After arrival at stationary phase on day 5, as determined by NO_2^- production and optical density, the expression of the genes NE0597, NE1749 and NE1909 between 5- and 20-fold over the exponential phase levels (Table 3.3). The batch cells used in the microarray analysis were harvested on day 3 of batch growth, where they were in mid- to late-exponential phase. The expression of *amoA* increased almost 4-fold by the end of exponential growth on day 4, and then decreased through day 7. The reduction in *amoA* expression during stationary phase has been observed previously and is potentially a result of reduced cell energy (115).

DISCUSSION

Microarray comparisons

The biofilm microarrays did not share any up-regulated genes with the microarray results of *N. europaea* cells during NH_3 and carbonate starvation (109). In the starved planktonic cells, 1,631 genes were down-regulated, of which only 78 were also down-regulated in the biofilm microarray. The genes selected for RT-qPCR did not show changes in transcription in batch cultures of *N. europaea* after NH_3 starvation for 7 days (data not shown). This suggests that NH_3 or O_2 starvation in suspended cells is not likely to be responsible for the observed gene expression.

A proteomic study was performed on *N. europaea* biofilms (96) and none of the up-regulated genes in the biofilm microarrays correlated to up-regulated proteins in the previous work. Transcriptional results do not always correlate with proteomic results, due to either post-transcriptional modifications or differences in the sensitivity of the methods. Another possible explanation for this may be that the same chemostat was used to cultivate the suspended cells (chemostat liquid) and biofilm cells (chemostat walls) used in the proteomic study, which would eliminate differences in media conditions that were present in this study. Other differences between the experimental conditions that could have caused the different results include variations in shear stress, dissolved oxygen conditions and potentially different stages of growth of the cells.

Chain et al. hypothesized that the gene NE1184 encodes a putative AHL synthase, which may produce cell-signaling molecules in *N. europaea* (17). Interestingly, this gene was not up-regulated in the biofilm microarrays and no genes for AHL synthesis or AHL receptor proteins were identified in this study. However, three of the genes up-regulated in *N. europaea* biofilms (NE0579, NE1909, NE2075) encode homologs of diguanylate cyclase/phosphodiesterase which putatively catalyzes the synthesis and degradation of the cellular signaling molecule, c-di-GMP (38). Cellular levels of c-di-GMP influence the control of multiple cellular functions and may trigger post-transcriptional changes that lead to biofilm formation (95).

Gene expression in stationary phase

Upon entry into stationary phase, batch cells of *N. europaea* up-regulated selected genes that were also up-regulated in the biofilms (Table 3.3). These results agree somewhat with previous studies, where similarities were found between transcriptional profiles of stationary phase cells and biofilms of *E. coli* (10) and *P. aeruginosa* (105). The observed up-regulation of biofilm-expressed genes in batch cultures of *N. europaea* during stationary phase may signal the beginning of biofilm formation in the culture, upon arrival at stationary phase.

Gene expression dependence on growth rate

A comparison of the relative rates of NH_3 oxidation between biofilms and batch cells indicates that the biofilm cells have slow growth rates compared to exponential growth of *N. europaea*. Suspended cells of *N. europaea* cultivated at long HRT of 50- and 100-d had similar rates of NH_3 oxidation as the biofilms and exhibited up-regulation of a subset of genes identified by the microarrays as up-regulated in biofilms. These results suggest that the observed gene expression in the biofilms may be due to slow growth rates in both suspended and biofilm cells.

The fill-and-draw reactors were operated to behave similar to the chemostat. It is interesting to note that similar transcriptional up-regulation was observed in both reactor types. The fill-and-draw reactors at 5-d HRT were most similar to the gene expression in the chemostat at 7-d HRT. Interestingly, the NH_3 oxidation rates in the chemostat were closer to those in the 20-d HRT fill-and-draw reactors, due to the higher biomass concentration in the chemostat (Table 3.1). The gene expression levels correlated better on the basis of dilution rate rather than NH_3 oxidation rate. This may be a result of normalizing NH_3 oxidation rates to total protein, where the fraction of protein that was active biomass was not determined although it may have been less than the total or could have varied between the different reactors.

The specific ammonia oxidation rates in the biofilms were lower on a protein averaged basis than the fill-and-draw reactors at 50- and 100-d HRT, however the observed up-regulation of the selected genes was much higher in the fill-and-draw

reactors than in the biofilms (Fig. 3.2 and 3.3). This discrepancy may be caused by heterogeneity in biofilm cells, where localized gene expression in some areas of the biofilm can occur due to gradients in activity (53), which may result in lower expression when averaged over the entire biofilm. Additionally, factors such as build-up of soluble microbial products in the fill-and-draw reactors with long HRTs, compared to the DFR (~10 min). Cell signaling molecules AHLs have been identified from suspended cell cultures of *N. europaea* (15). Others have also shown that suspended cells of *N. europaea* respond to the addition of AHL by decreasing the lag phase of starvation recovery, similar to biofilm response (6). If microbial products, such as AHL, in the fill-and-draw reactors act as signaling molecules for biofilm formation, they may cause an increasing transcriptional response with slower dilution rate.

In this research, selected genes that were up-regulated in biofilms of *N. europaea* were also expressed in continuously cultured suspended cells, with the levels of expression inversely relating to growth rate of the cells. This study has shown that expression of biofilm-related genes may be used to determine the metabolic state of suspended cells of *N. europaea*. The results of this research indicate that it is important to note the suspended cell growth phase in transcriptional studies of *N. europaea* due to differences in transcription between suspended cultures.

Acknowledgements

Table 3.1. Nitrite production rates in batch culture, continuous culture and biofilms. Values in parentheses are standard deviation of triplicates.

	NO_2^- production [mmol (mg protein-d)$^{-1}$]	Biomass [mg protein (L)$^{-1}$]
Batch cells (exponential)	5.01 (0.29)	5.48
Chemostat (HRT 6.9 d)	0.63 (0.05)	10.4
Fill-and-Draw reactors		
5 day HRT	1.63 (0.11)	4.26
20 day HRT	0.72 (0.084)	3.05
50 day HRT	0.33 (0.049)	2.75
100 day HRT	0.16 (0.01)	2.61
Biofilms	0.38 (0.14)	

Figure 3.1. Gene numbers in functional categories that were differentially expressed in microarrays. up-regulated (black bars) and down-regulated (grey bars) 2-fold or higher in microarrays of biofilms compared to suspended cells of *N. europaea* harvested in late exponential growth. Negative values denote down-regulation in biofilms. (**I**) Poorly Characterized Genes (**II**) Metabolism (**III**) Cellular Processes (**IV**) Information Storage and Processing.
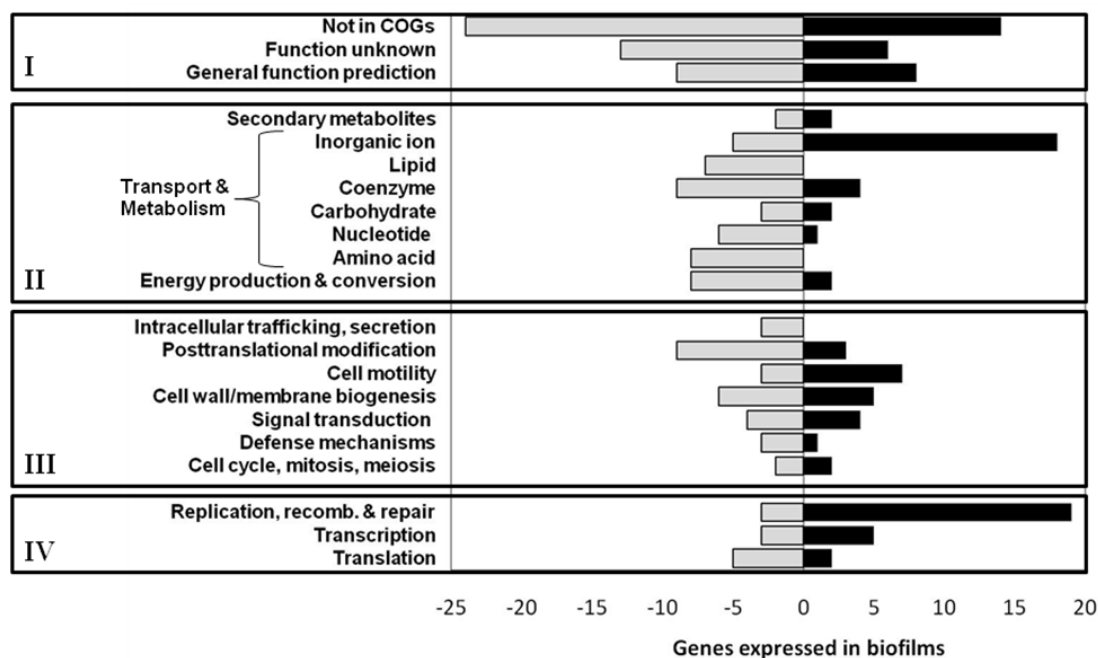
Table 3.2. Genes expressed in microarrays selected for RT-qPCR analysis. Categories refer to Figure 1: (**I**) Poorly Characterized Genes (**II**) Metabolism (**III**) Cellular Processes (**IV**) Information Storage and Processing.

Category	Gene name	Function	Fold change	P-value
II	NE0556	TonB-dependent iron siderophore receptor	3.66	0.0471
II	NE0770/*ccmH*	Putative cytochrome C-type biogenesis protein	-2.86	0.0408
III	NE0597/*pilD*	Type IV pili assembly protein	3.38	0.0413
III	NE1749/*pilW*	Type IV pili assembly protein	4.05	0.0488
III	NE1332/*rkpI*	Capsular polysaccharide biosynthesis/export	2.16	0.0485
III	NE1944	OsmC osmotically inducible protein	4.87	0.0400
III	NE1909	Diguanylate cyclase/phosphodiesterase	3.65	0.0429
III	NE0923	Cyanophycin synthetase	-10.8	0.0356
IV	NE2408	DNA competence protein	2.88	0.0385
IV	NE1479/*recN*	DNA repair protein	3.03	0.0383

Figure 3.2. Fold-changes of genes analyzed by microarray and RT-qPCR in biofilm and chemostat cells compared to exponential cells. Microarray (filled bars) and RT-qPCR (open bars) of biofilms and RT-qPCR of chemostat cells (shaded bars). Dashed lines represent changes of ± 2-fold.
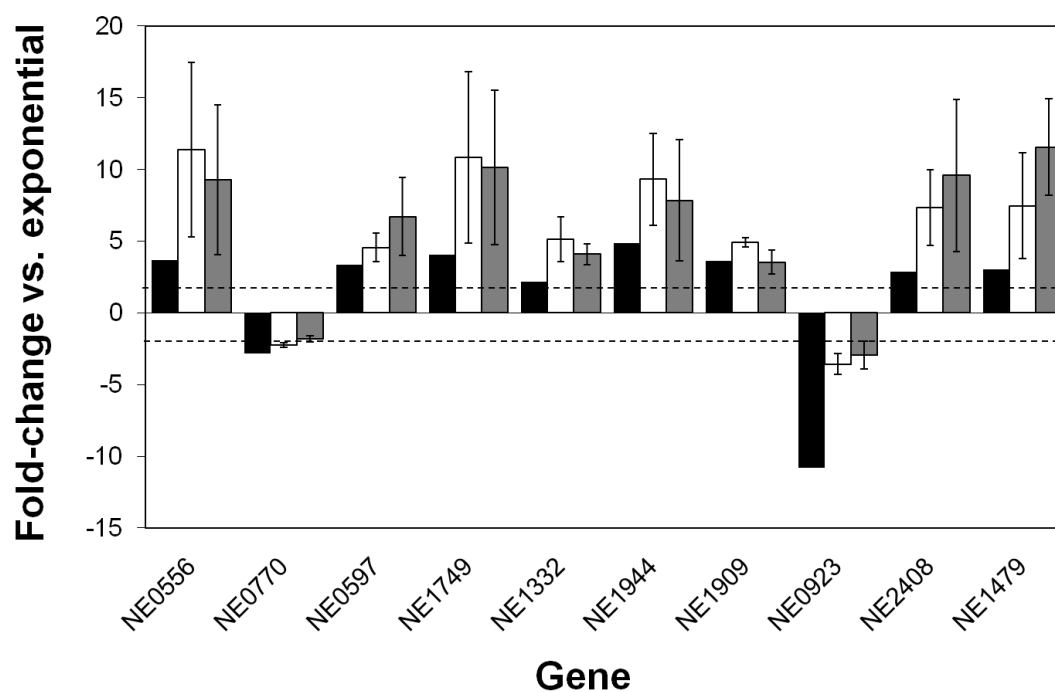
Figure 3.3. Expression of genes in fill-and-draw reactors determined by RT-qPCR. Expression of cells at HRT of 100 days (open bars), 50 days (light shaded bars), 20 days (dark shaded bars), and 5 days (filled bars), compared to cells in batch culture. Error bars represent 95% confidence of triplicates.
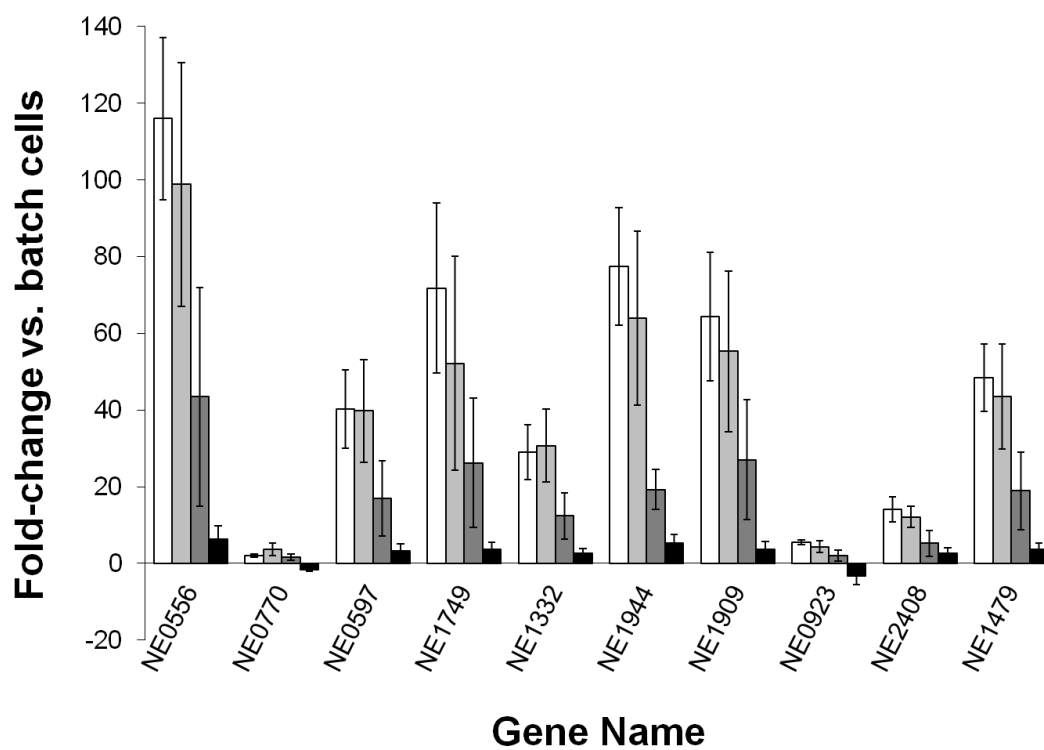
Table 3.3. Growth of suspended batch culture and fold-change of selected genes. Fold-changes are determined by normalizing gene expression to the expression in log phase (day 3).

		Log Phase	Late Log	Stationary phase	
	Time (d)	3	4	5	7
	OD$_{600}$	0.057	0.1	0.097	0.074
	mM NO$_2^-$	13.7	25.3	27.7	25.2
	NE0556	-	3.1	5.0	4.9
	NE0597	-[a]	2.3	11.2	10.8
Fold-change	**NE1749**	-	2.9	17.5	17.6
	NE1332	-	1.9	9.0	7.6
	NE1909	-	3.1	13.6	14.7
	amoA	-	4.2	3.7	2.1

[a]Fold-change value is expression via RT-qPCR, normalized to 16S rRNA gene and divided by expression on day 3.

Chapter 4

Correlation of phenol inhibition to rates of ammonia oxidation in *Nitrosomonas europaea* grown under batch, continuous fed, and biofilm conditions

Ellen G. Lauchnor and Lewis Semprini

ABSTRACT

Ammonia oxidation by *Nitrosomonas europaea*, a prevalent ammonia oxidizing bacterium, is inhibited in the presence of the aromatic hydrocarbon phenol, due to interaction of the phenol with the ammonia monooxygenase enzyme. Suspended cells of *N. europaea* were cultured in batch reactors and continuous flow reactors at dilution rates of $0.01 - 0.2$ d^{-1}. The rate of ammonia oxidation in the continuous cultures correlated to the dilution rate in the reactor. The batch and continuous cultures were exposed to 20 μM phenol and ammonia oxidation activity was measured by specific oxygen uptake rates (SOURs). Inhibition of NH_3 oxidation by 20 μM phenol ranged from a 77% reduction of SOUR observed with exponential cells, to 26% in biofilms. The extent of inhibition was correlated with ammonia oxidation rates in both suspended and biofilm cells, with greater inhibition observed with higher activity. In biofilm grown cells, an increase in activity and phenol inhibition were both observed upon dispersing the biofilm cells into fresh, liquid medium. Under higher oxygen tension, an increase in the NO_2^- production of the biofilms was observed and biofilms were more susceptible to phenol inhibition. Oxygen limited conditions in the biofilm were used for dissolved oxygen microsensor measurements, where the predicted rate of NO_2^- production was much lower and the biofilms were less inhibited during phenol exposure. The results clearly indicate that in both suspended and attached cells of *N. europaea*, NH_3 oxidizing activity is a key factor in the extent of phenol inhibition.

INTRODUCTION

Nitrosomonas europaea is a well-characterized ammonia oxidizing bacterium (AOB) that oxidizes ammonia to nitrite and is prevalent in wastewater treatment processes that treat nitrogen using biological nitrogen removal (78). The presence of aromatic hydrocarbons in wastewater, such as phenol, inhibits NH_3 oxidation by *N. europaea* and can result in failure of nitrogen removal (2). The use of biofilms, microbial communities attached to surfaces, for wastewater treatment provides protection for sensitive bacteria such as *N. europaea*.

N. europaea, like all AOB, uses an enzyme called ammonia monooxygenase (AMO) to oxidize ammonia (NH_3) to nitrite (NO_2^-) as their source of energy for growth and metabolism (112). The oxidation of NH_3 to NO_2^- is a two-step process, the first step of NH_3 oxdiation to hydroxylamine (NH_2OH) is catalyzed by AMO, while the second oxidation step to NO_2^- is catalyzed by a second enzyme, hydroxylamine oxidoreductase (HAO) (4). AMO is a non-specific enzyme with a wide substrate range capable of co-metabolic oxidation of aliphatic (82) and aromatic hydrocarbons (44, 45) such as phenol, which is oxidized to hydroquinone (41, 45). The oxidation by AMO of co-metabolic substrates, such as phenol, inhibit NH_3 oxidation by competing for the enzyme active site or inhibiting electron flow and causing cellular energy drain (27).

In suspended cells of *N. europaea,* 10 μM phenol caused reduction in NH_3 oxidation rates by 66% (79). Pure culture biofilms of *N. europaea* were less inhibited than suspended cells during phenol exposure, with about 60 μM causing a 50% reduction of NH_3 oxidation in biofilms compared to 99% inhibition in suspended cells (50). The *N. europaea* biofilms also had normalized rates of NH_3 oxidation that were an order of magnitude lower than batch cells (50). However, when biofilm cells were detached from the biofilm support and suspended in liquid medium, the rate of NO_2^- production increased and the degree of inhibition increased compared to the biofilm test. These observations prompted our interest in exploring whether the inhibition was related to the state of cell growth and NH_3 oxidation rates.

N. europaea has also been examined under different growth states to study inhibition of NH_3 oxidation (18, 80). A study of *N. europaea* biofilms reported that established biofilms were less inhibited by the nitrification inhibitor nitrapyrin and exhibited reduced growth rates compared to suspended cells (77). Additionally, exponential cells of *N. europaea* exhibited greater inhibition of NH_3 oxidation when exposed to nitrapyrin compared to stationary-phase cultures (76). A previous study of cadmium inhibition of *N. europaea* determined that the inhibition kinetics depended upon the growth state of the cells, and cells in stationary phase were less inhibited over time than during exponential growth, based on O_2 uptake rates (18). More investigation of the factors involved in phenol inhibition of *N. europaea* is needed, with an emphasis on the growth state and NH_3 oxidation rates of the cells.

Stationary phase or slow growth of bacteria has been linked to resistance to antimicrobial agents in other bacterial species and is thought to be a factor in biofilm resistance (57, 99). Antimicrobial agents have been shown to be less effective on eradication of slow growing or stationary cells (13). In biofilms, cells are often slow-growing due to nutrient or oxygen limitations (114), which has also been observed in *N. europaea* biofilms (50). Exposure of *N. europaea* to phenol under different culture conditions is examined here to determine the role of cell growth rate in phenol resistance of *N. europaea* biofilms.

The goal of this study was to compare phenol inhibition of *N. europaea* grown under different growth conditions including batch culture, chemostats, fill-and-draw reactors and biofilms, to determine if inhibition was a function of cell activity or growth rate. The activities of the cells from the different reactors were evaluated by measuring oxygen uptake rates with and without exposure to phenol. In biofilms, different tests were performed to examine the influence of O_2 availability in the biofilm on the rates of NH_3 oxidation in control biofilms and during phenol exposure.

EXPERIMENTAL PROCEDURES

Inhibition tests with suspended cells

N. europaea cells were cultivated in batch reactors, chemostats and fill-and-draw reactors for comparison of NH_3 oxidation rates and phenol inhibition between cells from the different reactors. Batch reactors were used to cultivate exponentially growing cells and the chemostats and fill-and-draw reactors were maintained at various dilution rates to cultivate cells with a range of growth rates. For inhibition tests of the suspended cells, samples were taken from the reactors and placed into sample bottles containing 0 or 20 µM phenol for 60 min. The O_2 uptake rates of the cells were then measured via SOURs at the end of the exposure to evaluate the extent of NH_3 oxidation inhibition by the phenol.

N. europaea cell growth in batch reactors

Batch cultures of *N. europaea* were grown in 4L flasks for inoculation of attached growth and suspended growth reactors and for batch inhibition tests. Batch AOB medium consisted of: 25 mM $(NH_4)_2SO_4$, 3.77 mM Na_2CO_3, 40 mM KH_2PO_4, 730 µM $MgSO_4$, 200 µM $CaCl_2$, 9.9 µM $FeSO_4$, 16.5 µM EDTA free acid, and 0.65 µM $CuSO_4$.

Cell growth in fill-and-draw reactors

Suspended cells of *N. europaea* were cultured in fill-and-draw reactors where volumes of the liquid cultures were replaced by fresh medium daily to mimic continuous flow conditions and create long cell residence times. In the fill-and-draw reactors, HEPES medium was used, consisting of AOB medium with 20 mM HEPES buffer (pH 7.8) and 10 µM KH_2PO_4 in lieu of 40 mM KH_2PO_4 buffer. Reactors consisted of 500 mL flasks with 200 mL of HEPES medium inoculated with *N. europaea*. Cells and medium from each flask were removed daily and aseptically replaced with fresh HEPES medium at volumes to achieve desired dilution rates. The pH was adjusted daily to 7.8. Triplicate reactors were maintained at each of four different dilution rates of 0.01, 0.02, 0.05, and 0.2 d^{-1}, which corresponded to

hydraulic and cell residence times of 100, 50, 20 and 5 d, respectively. Biomass protein concentration, NO_2^- accumulation and pH were monitored in the flasks.

Cell growth in chemostat reactors

N. europaea was cultivated at dilution rates of 0.14 and 0.03 d^{-1} in continuous fed Bioflow 110 bioreactors (New Brunswick Scientific, Edison, NJ) with HEPES medium as described previously (80). For phenol inhibition experiments and specific oxygen uptake rate measurements, completely mixed liquid samples were taken aseptically from a port in the vessel into sample vials.

SOUR inhibition tests

Specific oxygen uptake rate (SOUR) tests were performed to evaluate the rate of oxygen consumption in *N. europaea* under various culture conditions and during phenol exposure. The SOUR assay provides immediate rate measurements of O_2 consumption that can be converted to NH_3 oxidation or NO_2^- production rates based on the following stoichiometry: $NH_3 + 1.5O_2 \rightarrow NO_2^-$ (79). SOUR measurements were made with 10-50 mL of liquid samples with cells from the batch, chemostat, and fill-and-draw reactors. The pH was adjusted to 7.8 and supplemented with 2.5 mM $(NH_4)_2SO_4$. Samples were incubated with either 0 µM or 20 µM phenol while shaking at 100 RPM and 30 °C for 60 min prior to SOUR tests.

SOUR measurements were taken with a Clark-type oxygen electrode (Yellow Springs Instrument, Inc.) in a water-jacketed cell at 30°C (Gilson Medical Instruments, Inc.). Oxygen uptake in the cell was measured over time using a strip chart recorder and the rates of consumption were compared for the control and phenol-treated samples. The cell contained 1.8 mL liquid and a stir bar for complete mixing of the sample. For measurement of AMO-SOUR, 2.5mM $(NH_4)_2SO_4$ was added to provide an excess of substrate. To halt AMO activity 100 µM allylthiourea was added and the AMO-independent oxygen uptake, or HAO-SOUR, was measured by addition of 750 µM NH_2OH as alternative substrate for HAO. The percent inhibition was determined by dividing the AMO-SOUR of phenol exposed cells by that of the control

cells for each reactor using the following equation: % Inhibition = (100% - AMO-SOUR $_{treated}$/AMO-SOUR$_{control}$)×100%.

Biofilm growth and inhibition tests

Biofilms of *N. europaea* were cultivated in a Drip Flow Biofilm Reactor (DFR) fed with with HEPES medium for 4-6 weeks and inhibition experiments were performed on mature biofilms according to methods developed previously (50). In brief, phenol was added via a syringe pump to the influent media of two DFR channels for a period of 3 h, with the other two DFR channels as controls. During phenol addition, effluent samples of the DFR were taken to monitor NO_2^- production and concentrations of phenol and its oxidation products. The rates of NO_2^- production were calculated by multiplying the effluent NO_2^- concentrations by the liquid flow rates in the DFR channels.

The oxygen concentration in the DFR headspace was elevated to eliminate O_2 limitation and achieve higher rates of NH_3 oxidation in the *N. europaea* biofilms. Biofilms were grown to maturity under atmospheric oxygen conditions. One hour prior to the phenol addition, O_2 gas was added at 1 L min^{-1} to the headspace of the DFR channels through 0.45μm syringe filters. Phenol inhibition tests were then performed under the elevated O_2 conditions to evaluate the effect of higher O_2 and increased rates. Headspace addition was performed for 2 min every 30 min until the end of the inhibition experiment to maintain high O_2 conditions.

Microsensor profiles

Clark-type oxygen microsensors were used for measuring profiles of dissolved oxygen concentration in the biofilms. The biofilm samples were cultivated in the DFR identically to those used in the inhibition tests described above. The biofilms were removed from the DFR and placed into a flow cell connected to a recirculating water batch with media containing 2.5 mM $(NH_4)_2SO_4$ and 10 mM HEPES buffer (pH 7.8) kept at a 25°C. Microsensor measurements were made using a micromanipulator as described previously (50). After control profiles of dissolved oxygen in the presence of NH_4 with no phenol added to the medium, additions of 40 μM and 80 μM phenol

were made to the medium. After each addition of phenol, the recirculating system was allowed to equilibrate for 2 hours prior to microsensor measurements. Triplicate oxygen profiles were taken and steady-state in oxygen uptake was determined by taking repeated profiles and verifying that profiles were not changing.

The areal O_2 fluxes in the biofilms were calculated from the microsensor profile data, according to the diffusion-reaction equation at steady-state, approximated by the following difference equation (34):

$$J = D_{eff} \frac{c_a - c_b}{\Delta x} \tag{4.1}$$

Where J is flux in $\mu mol\ cm^{-2}\ s^{-1}$, D_{eff} is the diffusion coefficient, c_a and c_b are measured DO concentrations, and Δx is the depth interval between c_a and c_b. The reduction in O_2 flux upon phenol exposure in biofilms was calculated by dividing the flux of O_2 into the phenol exposed biofilms by the flux in the control biofilms with no phenol. The diffusion coefficient, D_{eff}, drops out of the equation and the calculation of inhibition is reduced to the ratio of concentration gradients of phenol exposed and control biofilms at the biofilm surface.

Analytical methods

NO_2^- accumulation in liquid media was used to determine rates of NH_3 oxidation in DFR biofilm inhibition tests and during long term growth of suspended cell reactors. NO_2^- was measured using a colorimetric assay (37), which was quantified by spectrophotometric analysis at a wavelength of 540nm. Phenol concentrations were measured by high performance liquid chromatography (HPLC), according to methods reported elsewhere (79). Biomass protein concentrations were determined using a microbiuret assay after a 30 minute cell digestion in 3M NaOH at 65°C. Optical density at 600 nm was used with suspended cultures as a surrogate measurement for the biuret assay, and a standard curve was used for conversion to biomass protein concentration.

RESULTS

Suspended cell cultivation

Fill-and-draw reactors

Continuous cultures of *N. europaea* were maintained in fill-and-draw flasks at four different dilution rates and phenol inhibition was evaluated at different rates of growth and NH_3 oxidation. The fill-and-draw reactors were maintained for 45 days while monitoring NO_2^- production and cell growth. Triplicate reactors at each dilution rate were maintained and the concentrations of NO_2^- and protein achieved pseudo-steady-state for all dilution rates (Fig. 4.1). During the first 15 days of operation, the 5 d HRT reactors began to washout due to insufficient agitation, which was increased and the reactors subsequently arrived at pseudo-steady state. The activity of the cells was calculated by dividing NO_2^- concentration by the biomass protein concentration and dilution rate of the reactor. At pseudo-steady-state of the reactors, the NO_2^- production rates showed an increasing trend with increasing dilution rates of the reactors (Table 4.1). The steady-state NO_2^- concentrations were 40-45 mM for all reactors, and protein concentrations ranged from 2.5-4.5 mg L^{-1}. Control SOUR measurements in the fill-and-draw reactors were compared to NO_2^- production rates taken during growth of the cells in the reactors and a positive correlation was observed between the rates (Fig. 4.2).

Batch reactor

Batch reactors were maintained and cells were harvested during exponential growth for phenol inhibition experiments. In the batch cell experiments, activity was measured in a short-term 30 minute rate experiment where NO_2^- concentration was measured every five minutes and the rate of accumulation was calculated. The results of NO_2^- production rates and SOURs were almost equivalent in the batch reactors, although based on stoichiometry, the SOURs should be about 1.5 times the NO_2^- production rates (Table 4.1).

Chemostats

Chemostats at dilution rates of 0.14 and 0.03 d^{-1} were maintained to evaluate phenol inhibition and to compare with the results of fill-and-draw reactors. NO_2^- production was measured and normalized to biomass concentration in each reactor by dividing the NO_2^- concentration in the chemostat by the dilution rate and normalizing to protein concentration determined by OD_{600} measurements. Control SOURs in the chemostats fell along the same linear trend with the NO_2^- production rates as the fill-and-draw reactors (Fig. 4.2).

The two different measurements of NH_3 oxidation activity, SOURs and NO_2^- production rates, were compared for the continuous reactors (Fig. 4.2). There was a positive correlation between NO_2^- production and SOURs, although the SOURs were higher than NO_2^- production rates and deviated more at lower dilution rates. The cells at the slowest dilution rates were the most nutrient limited and increased activity in response to the addition of NH_3 during the SOUR tests. The SOUR measurements were performed with added substrate at the onset of the test, which allowed for measurement of the maximum rate of NH_3 turnover for the cells. It was determined that the SOUR assay was representative of the differences between AMO activity in the cells, and the SOURs were therefore used for inhibition comparisons. SOURs were also found to be the most sensitive measurement to growth phase and inhibition response by others studying *N. europaea* exposure to cadmium (18).

During continuous culture of *N. europaea*, it is possible that the active fraction of cells in the chemostats and pseudo-chemostats was lower than the total biomass concentration measured in the reactors. Here, the total protein was measured by correlating OD_{600} measurements to a standard curve with the microbiuret protein assay and the fraction of protein comprising active cells was not determined.

Suspended cell exposure to phenol

After 45 days of fill-and-draw reactor operation, phenol inhibition studies were performed by taking cells from the reactors and exposing them to 0 (control) or 20 μM phenol while shaking at 100 RPM for 60 min and performing SOUR measurements

for both control and treated cells at the end of the test. The SOUR measurements determined that oxygen consumption rates of control cells (no phenol) were positively correlated with the dilution rates in the reactors (Fig. 4.3A). The rates for the chemostat-grown cells and fill-and-draw cells fell along the same linear trend between dilution rate and SOUR measurement, providing confidence that cells grown in the fill-and-draw reactors were representative of chemostat-grown cells.

The phenol inhibited AMO-SOURs were essentially the same over the range of growth rates in the chemostats and fill-and-draw reactors, within the standard deviations of the measurements (Fig. 4.3A). Upon exposure to the same phenol concentration, cells grown at faster dilution rates showed greater reduction in SOUR activity. HAO-SOURs were equal in the control and phenol treated samples (data not shown); only the AMO dependent oxygen uptake was inhibited, which supports previous evidence that the inhibition is specific to the AMO enzyme (79). This result also indicates that phenol inhibited NH_3 oxidation was not imparting toxicity to the cells.

The inhibition of phenol treated cells was determined from SOURs by the equation shown in the above Methods section. The inhibition of the phenol treated cells measured by SOURs increased with increasing dilution rate at the same phenol exposure of 20 μM (Fig. 4.3B). This indicates that the phenol inhibition was correlated to the activity of the continuously cultured cells, which was dependent upon dilution rates of the chemostat and fill-and-draw reactors.

Suspended cells of *N. europaea* cultured in batch reactors were exposed to 20 μM phenol and inhibition was determined via SOUR measurements with the same methods as the cells grown in the chemostats and fill-and-draw reactors. The inhibition results for batch, chemostat and fill-and-draw grown cells were compared on a basis of control SOURs (Fig. 4.4). Regardless of the type of suspended cell growth reactor (batch, fill-and-draw or chemostat), the degree of inhibition of suspended cells increased with increasing SOURs (Fig. 4.4).

Biofilm exposure to phenol and comparison to suspended cells

For a comparison between attached and suspended growth states, biofilms were exposed to 20 μM phenol and NO_2^- production was monitored to determine extent of inhibition. Biofilms exposed to 18 ± 1 μM phenol in the DFR resulted in 26% inhibition of NO_2^- production after 2 hours of exposure (Fig. 4.5). It was not feasible to measure the inhibition via oxygen uptake rate in the biofilms, so the change in NO_2^- production was used to determine percent inhibition. A basis of NO_2^- production was used for activity comparisons between the reactors since SOURs were not taken for biofilms. The biofilm results are similar to results of our previous study on *N. europaea* biofilm exposure to phenol and toluene (50). The previous study showed that biofilm cells were more tolerant to phenol than batch cells, as is shown in Figure 4.5 where batch cells exhibited 77% inhibition compared to 26% inhibition in biofilms. However, cells from the fill-and-draw reactors at the slowest dilution rate were only 28% inhibited, which was not statistically different than the biofilms. The results of these inhibition comparisons at 20 μM phenol demonstrate that with decreasing NH_3 oxidation activity in continuous cultures, suspended cells of *N. europaea* may potentially become as tolerant to phenol as attached biofilms.

The phenol inhibition in the suspended cells was compared with previous results of phenol inhibition in biofilm cells that were suspended in fresh, liquid medium and exposed to phenol (Fig. 4.5). The biofilm grown cells had been directly scraped from the biofilm support, dispersed into liquid medium and immediately used for phenol inhibition experiments, while monitoring NO_2^- production (50). Prior to removing the cells from the biofilm, their activity was equivalent to the biofilm activity shown in Fig. 4.4, and the activity of the biofilm cells increased to 50% of the batch rates upon dispersing them into fresh medium. It is possible that the 50% difference in rates between batch and resuspended biofilm cells indicates that the biofilms had a lower active cell fraction and up to 50% of the biofilm cells were dead or inactive. Regardless, the inhibition was equal to that of the batch cells, which increased from the percent inhibition observed in the intact biofilms. This comparison

indicates that growth in biofilms did not affect the extent of inhibition since the cells were as inhibited as batch grown cells.

Microsensor profiles of biofilms

To determine the dissolved oxygen (DO) concentration in the biofilms and the changes in DO upon phenol inhibition, oxygen profiles were measured in control biofilms and those exposed to 40 and 80 μM phenol. The biofilms were removed from the DFR and placed into a measuring chamber with liquid medium flowing through it and recirculating in a water bath with 5 L of liquid. The bulk fluid phase in the measuring chamber had a constant atmospheric concentration of DO (257 μM at 25ºC), which differed from the DFR where the thin film flow allowed for more O_2 transfer from the headspace. This was evidenced by the increase in NO_2^- production when O_2 was added to the DFR headspace (Fig. 4.5). In comparison, the bulk fluid phase used in the measuring chamber provided only 257 μM O_2. Dissolved oxygen (DO) microsensor measurements were performed to determine the rate of DO uptake in the biofilms.

DO profiles were measured in biofilms prior to phenol exposure in the presence of 5 mmol L^{-1} NH_4-N and 10 mmol L^{-1} HEPES buffer (pH 7.8) (Fig. 4.6). The uninhibited profiles showed that DO is consumed in the biofilms and reaches negligible concentrations before reaching a depth of 200 μm. The concentration of DO in the medium at 25ºC was 257 μM, which is much lower than the total NH_4 in the medium, indicating that excess NH_3 was present. The fact that the DO profiles were depleted to essentially zero inside the biofilms also indicates that O_2 was the limiting substrate for the cells.

Upon addition of both 40 and 80 μM phenol, the O_2 concentration increased in the biofilm as NH_3 oxidation was reduced due to inhibition (Fig. 4.6). The O_2 profiles taken during phenol exposure demonstrate that O_2 is limiting and phenol exposure results in an increase in O_2 concentration inside the biofilm due to inhibition of NH_3 oxidation. The flux of O_2 into the biofilm was calculated for each case using Equation 4.1. Percent inhibitions were determined by dividing the fluxes during phenol

exposure by the control flux. The percent reduction of O_2 flux into the biofilm was only 17% and 19% for 40 µM and 80 µM phenol exposure, respectively. In the DFR, exposure to similar phenol concentrations of 36 µM and 69 µM resulted in 37% and 63% inhibition, respectively, based on decrease in NO_2^- production (Table 4.2).

Phenol inhibition of biofilms vs. oxygen

Based on the microsensor measurements, which demonstrated that O_2 was limiting in *N. europaea* biofilms, additional O_2 was supplied in the DFR headspace to increase NH_3 oxidation rates. This permitted evaluation of phenol inhibition at two different rates of NH_3 oxidation in the biofilms. For these tests, the biofilms of *N. europaea* in the DFR were exposed to 50 µM phenol first under atmospheric conditions and subsequently under pure oxygen headspace for a higher rate comparison. The atmospheric inhibition test was performed on the biofilms and then a recovery period of two days was allowed before the second 50 µM phenol inhibition test was performed. The control NO_2^- production rates during the initial atmospheric test were on average 0.0229 mmol NO_2^- h^{-1} per channel (Fig. 4.7). After the initial test (1-4 hours), NO_2^- production rates of phenol exposed biofilms recovered to 97% of the control rates between 5 and 50 hours, demonstrating essentially complete recovery of the treated biofilms between exposures. After the addition of pure O_2 gas in the DFR headspace at 52.5 hours, the rates of NO_2^- production showed a 56% increase from atmospheric headspace conditions to an average of 0.0384 mmol NO_2^- h^{-1} per channel.

Under the atmospheric headspace conditions, NO_2^- production decreased in the biofilms by 61% upon phenol exposure (Fig. 4.7). In the high O_2 test, NO_2^- production was inhibited 85% compared to rates prior to the inhibition test. The phenol inhibition of 85% in the biofilms under elevated O_2 availability was greater than the 61% inhibition observed under atmospheric conditions. This result is consistent with the relationship in suspended cells where increased NO_2^- production rates correlated with increased inhibition. The experimental conditions of using the same biofilms for subsequent testing under elevated O_2 conditions allowed for direct comparison of results without variation in biofilm age, thickness or activity. The fast

response of the cells to higher oxygen concentration in the headspace suggests that under these conditions, O_2 limitations control the NH_3 oxidation kinetics of the biofilms. The results showing increased inhibition with increased activity are consistent with the observations of biofilm grown cells that were dispersed and inhibited by phenol while in suspension (Fig. 4.5).

DISCUSSION

Growth rate dependence of phenol inhibition in suspended cells

In this study, the SOUR measurements showed that phenol inhibition increased with increasing dilution rate in continuous suspended cultures of *N. europaea* (Fig. 4.3B). The same increase in phenol inhibition with greater NO_2^- production rate was shown for all suspended cell reactors on a protein normalized basis (Fig. 4.5). A common trend between the extent of inhibition and NH_3 oxidation activity was observed, regardless of the reactor type used to cultivate the cells. The lowest inhibition was observed in fill-and-draw cells grown at the lowest dilution rate. Our results indicate that harvesting cells at different stages of growth would affect the degree of inhibition observed.

Phenol is oxidized by AMO, as evidenced in previous studies of *N. europaea* (41), although the rate of phenol oxidation to hydroquinone was at least two orders of magnitude lower than NH_3 oxidation. The oxidation of phenol therefore would not be expected to significantly deplete the reductant supply in the cell. However, the inhibition of a co-metabolic substrate such as phenol may disrupt the flow of reductant in the cell by inhibiting the energy-generating process of NH_3 oxidation and therefore cause energy drain (27). These inhibitory actions may have more effect on cells that are more rapidly oxidizing NH_3 and have greater flow of reductant, such as during exponential phase growth.

Influence of activity on phenol inhibition in biofilms

Microsensor profiles have been used to study rates of substrate consumption in nitrifying biofilms (34) as well as changes in NH_3 and O_2 uptake during exposure to

inhibitory compounds (54, 93). In this study, fluxes of measured substrate and consumption rates were calculated from microsensor profiles and compared between phenol inhibited and control biofilms.

A notable difference between the microsensor profiles (Fig. 4.6) and biofilm inhibition tests performed in the DFR (Fig. 4.7) is the fluid environment around the biofilms in the DFR and the microsensor measuring chamber. There was a significant bulk liquid phase in the microsensor measuring chamber compared to a thin film layer in the DFR, which resulted in greater O_2 transfer through the thin film in the DFR. The difference in O_2 uptake is evidenced by the NO_2^- production in the DFR, where 2.75 mM NO_2^- was present in the reactor effluent. Assuming that the stoichiometry of NH_3 oxidation predicts 1.5 O_2 consumed per NO_2^-, the O_2 consumed in the DFR would be 4.1 mmol O_2 L^{-1}, which is much higher than the atmospheric DO concentration measured in the bulk liquid of the microsensor chamber.

The NO_2^- production rates in biofilms can be calculated in the DFR and the microsensor setup to determine if activity is a factor in the different extents of phenol inhibition in the two systems. A biofilm model described in Chapter 5 of this dissertation was used to simulate the DO microsensor profiles in the biofilm and predict NO_2^- production rates (Table 4.2). Under the same conditions in the model, the control (no phenol) DO profile was simulated and the total NO_2^- production rate for the biofilm depth was $6.5*10^{-8}$ mol m^{-1} s^{-1}. Using the slide dimensions of 7.5 cm by 2.5 cm and assuming 50% biofilm coverage of the slide, a protein normalized rate of 0.0015 mmol NO_2^- mg protein^{-1} h^{-1} was estimated from the DO profile which was an order of magnitude lower than in the DFR and two orders of magnitude lower than batch cells (Table 4.2). The results of inhibition tests at higher concentrations of phenol in both suspended and biofilm cells shown in Table 4.2, agree with the same trend as the results at 20 μM phenol exposure. This lower NH_3 oxidizing activity in the biofilm is consistent with the lower degree of inhibition observed compared to the DFR.

Biofilm resistance and slow growth rate

The results of biofilm inhibition with elevated O_2 confirmed that with attached cells as well as suspended cells, increasing the NH_3 oxidation rates resulted in increased inhibition. In the biofilms, O_2 availability controlled the rates of NO_2^- production. Conversely, in suspended cell reactors O_2 limitation was not present and NH_3 was the limiting substrate controlling rates of growth in the fill-and-draw and chemostat cultures, which was confirmed by stoichiometric mass balances of NO_2^- production. Regardless of whether the limiting substrate was O_2 or NH_3, the same general trend was observed in both suspended and biofilm cultures, where the increased rates of NO_2^- production caused greater inhibition during phenol exposure. The results suggest that increased AMO turnover rate dictates the sensitivity to phenol by increasing the potential interaction of phenol with the enzyme.

CONCLUSIONS

This research suggests that the biofilm did not provide protection from phenol inhibition, though the biofilm cells were less inhibited than exponentially growing cells due to slower rates of NH_3 oxidation. The phenomenon of biofilm resistance to antimicrobials has been well documented and attributed to various factors including nutrient limitation in biofilms causing slow or stationary growth (113). However, suspended cells in stationary phase have also exhibited similar resistance to antibiotics as biofilms, suggesting that slow growth is an important factor in the observed resistance (57, 99).

The results indicate that one of the key factors that make biofilms more resistant to inhibition by phenol is the lower metabolic activity of the cells. This was observed in this study with an inhibitor that interacts directly with the AMO enzyme, which catalyzes the first reaction in the energy-generating pathway for these organisms. A similar correlation was also observed in Chapter 3, where the genes identified in biofilms were increasingly up-regulated with slower growing suspended cells.

The observations presented here are significant for wastewater treatment operations, where both biofilm and suspended cell reactors can be used during nitrification (89). Phenol was demonstrated to cause greater inhibition of nitrification in batch assays than in an activated sludge reactor operating continuously (2). Additionally, the nitrification process in wastewater treatment has been shown to be inhibited by other aromatic hydrocarbons, such as benzene and toluene (117). It would be of interest to determine if correlations between activity and inhibition exist with other inhibitors of NH_3 oxidation in *N. europaea*.

Table 4.1. Activity and culture conditions of continuous and batch reactors prior to phenol exposure.

	Dilution rate	OD$_{600}$	NO$_2^-$ production	Control SOURs
	d^{-1}		mmol NO$_2^-$ mg protein^{-1} h^{-1}	mmol O$_2$ mg protein^{-1} h^{-1}
Batch		0.070	0.16	0.176
Fill-and-Draw reactors	0.01	0.030	0.007	0.041
	0.02	0.031	0.014	0.061
	0.05	0.038	0.030	0.070
	0.2	0.053	0.068	0.131
Chemostats	0.03	0.073	0.009	0.052
	0.14	0.072	0.045	0.097

Figure 4.1. Protein normalized rates of NO_2^- production in fill-and-draw reactors. Reactor dilution rates of 0.01 ($\bullet$), 0.02 ($\square$), 0.05 ($\blacksquare$) and 0.2 d^{-1} ($\circ$). Error bars represent standard deviations of triplicate reactors.
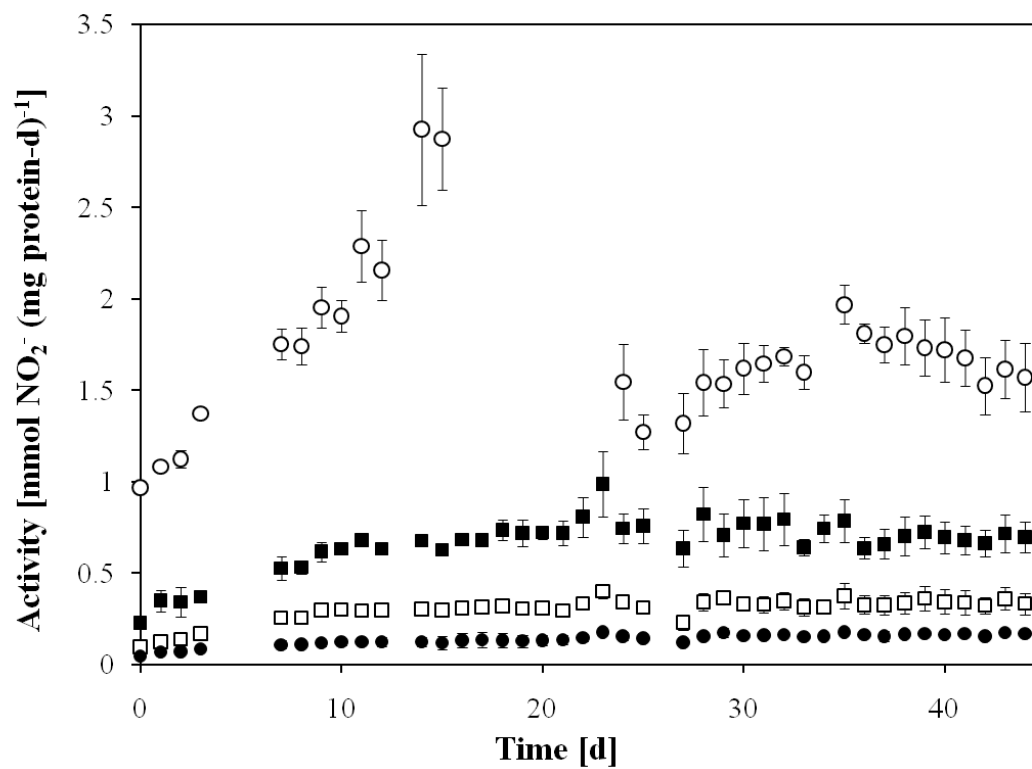
Figure 4.2. Comparison of nitrite production rates and SOURs of suspended cell reactors. Rates of batch reactors (○), chemostats (◊) and fill-and-draw reactors (●). Error bars represent standard deviation of triplicate reactors for batch and fill-and-draw, and triplicate samples taken from chemostats.
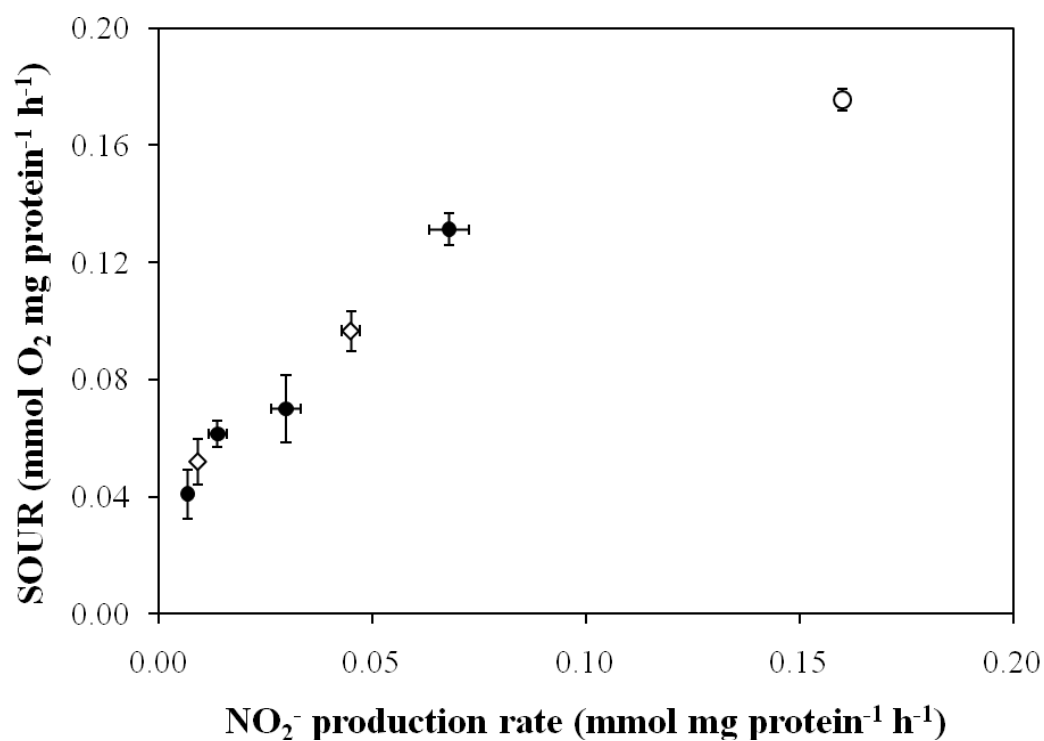
Figure 4.3. Oxygen uptake rates and percent inhibition of chemostat and fill-and-draw cells. **A)** Cells from fill-and-draw reactors (triangles) and chemostats (circles) exposed to 0 µM phenol (open symbols) and 20 µM phenol (closed symbols). **B)** Inhibition of fill-and-draw cells () and chemostat cells () determined by ratio of phenol and control SOURs. Error bars represent standard deviations of biological triplicates.
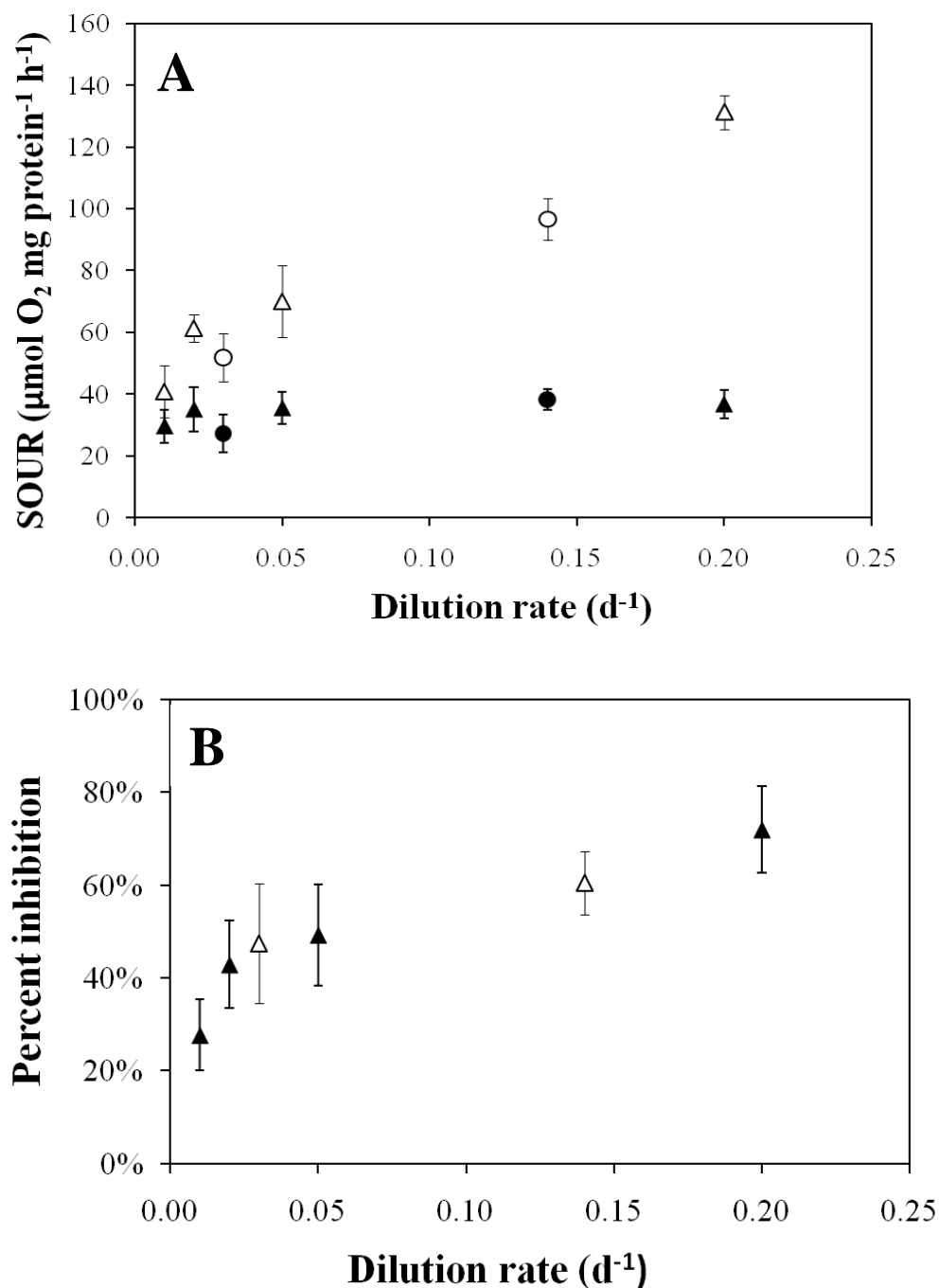
Figure 4.4. Percent inhibition compared to SOURs during exposure to 20 µM phenol with cells from batch and continuous suspended cultures of *N. europaea.* Inhibition of batch cells (○), fill-and-draw cells (▲), and chemostat cells (Δ). Error bars represent standard deviation of triplicate reactors.
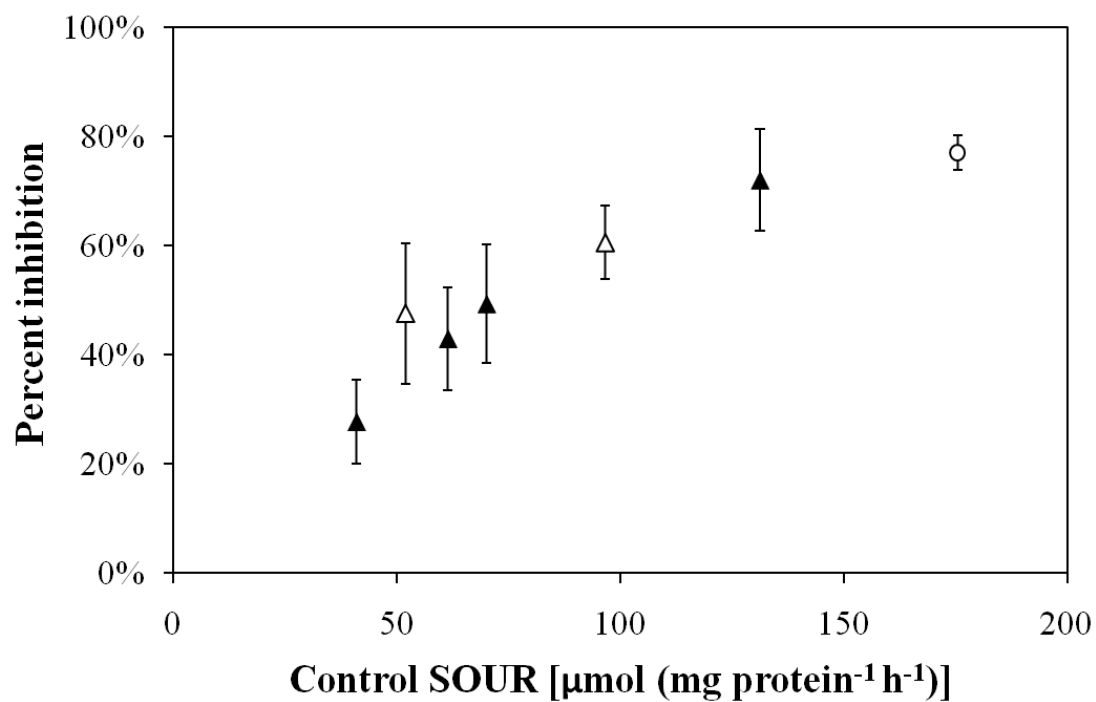
Figure 4.5. Percent inhibition of NH_3 oxidation during exposure to 20 μM phenol under different culture conditions of *N. europaea.* Inhibition of batch cells (○), fill-and-draw cells (▲), chemostat cells (Δ), biofilm-grown cells suspended into liquid (●) and biofilms (□). Biofilm inhibition was determined by nitrite production measurements and suspended cell rates were measured using SOURs. Error bars represent standard deviation of triplicates for suspended cell data and range of duplicate for biofilms. Data for biofilm cells suspended in liquid were taken from Lauchnor et al. (50).
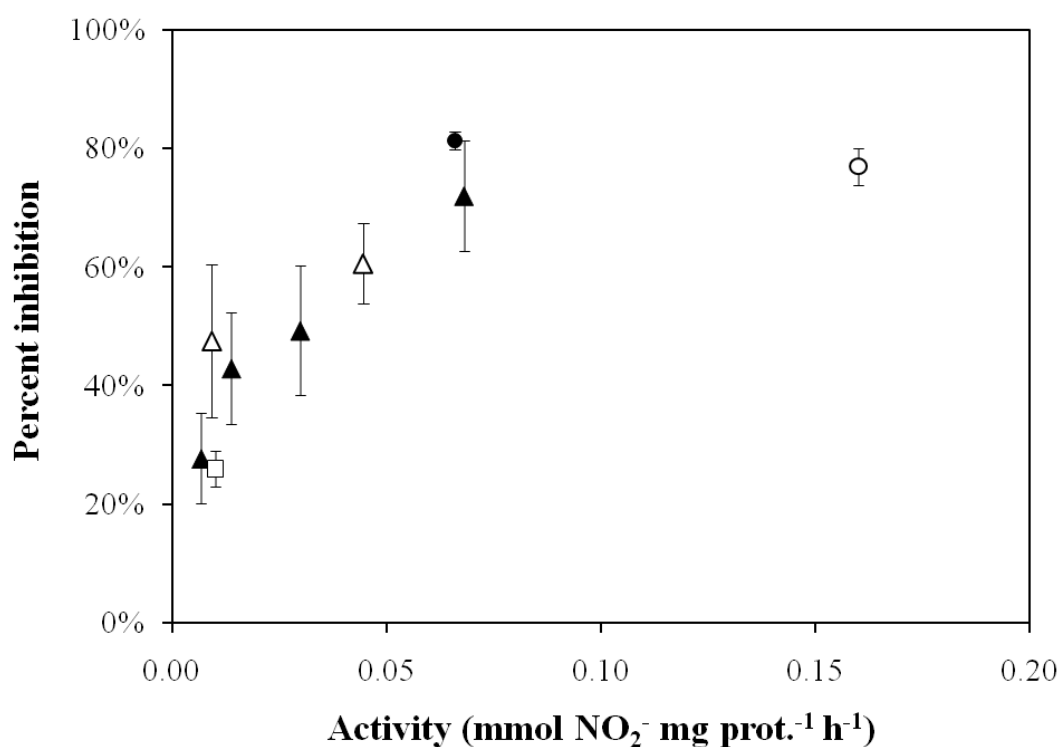
Figure 4.6. DO microsensor profiles of biofilms exposed to 0 µM (■), 40 µM (○), and 80 µM phenol (●). The biofilm surface was located at a depth of 0 µm. Error bars represent standard deviations of triplicate profiles.
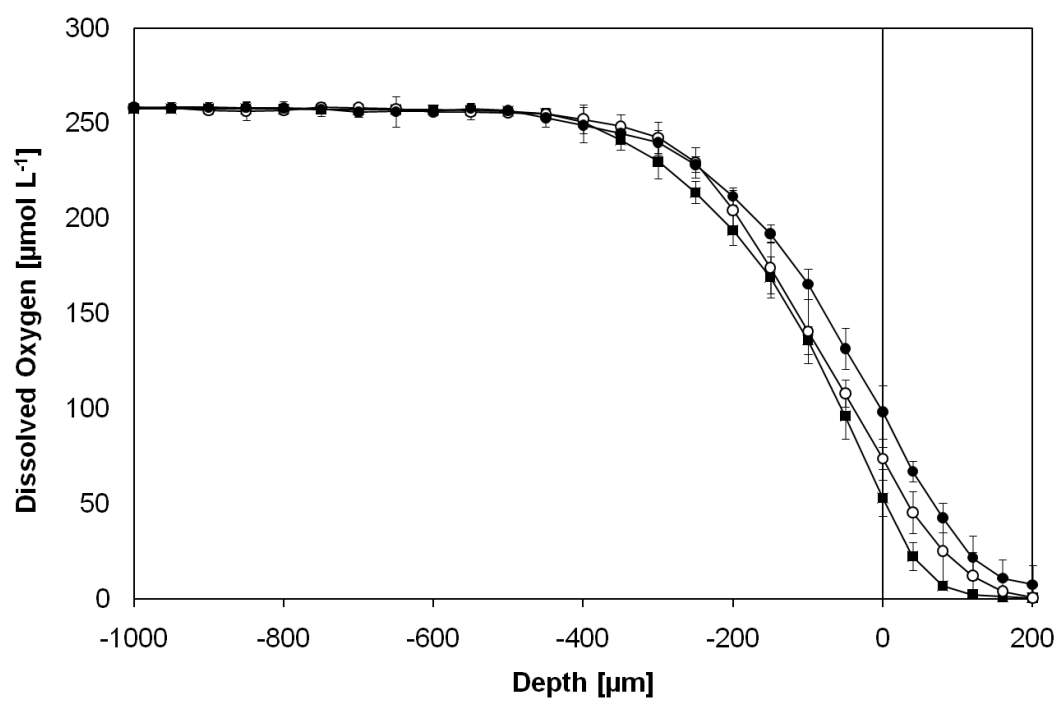
Figure 4.7. Nitrite production by *N. europaea* biofilms in DFR during phenol exposure under different O_2 conditions. Phenol exposure under atmospheric O_2 (1 h – 4 h) and pure O_2 headspace (53 h – 57 h)), during addition of 0 μM phenol (○) and 50 μM phenol (●). Arrow denotes beginning of O_2 gas addition to headspace. Error bars represent range of duplicate biofilms.
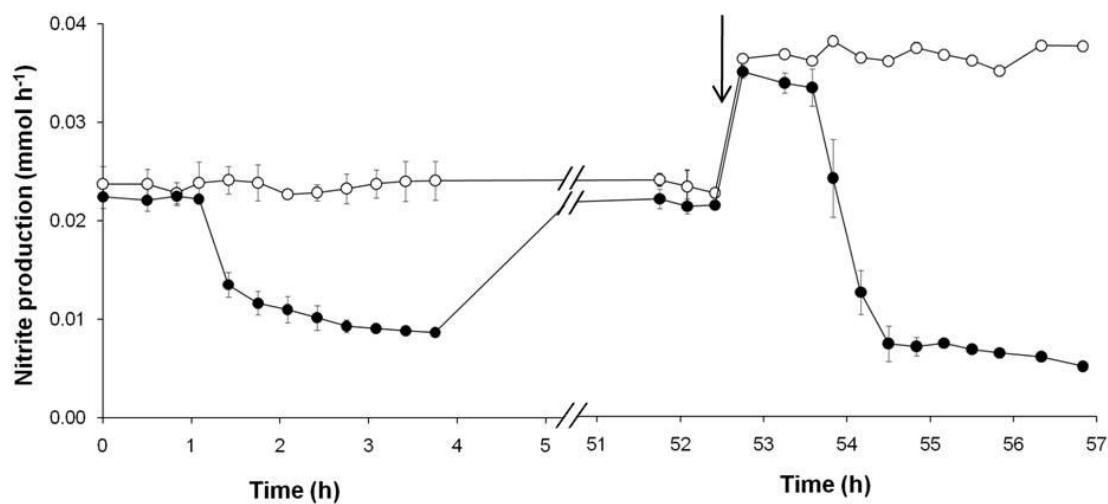
Table 4.2. Inhibition comparisons between biofilms and batch cells exposed to high phenol concentrations.

	NO_2^- production mmol mg protein^{-1} h^{-1}	Phenol (μM)	% inhibition
Batch reactor	0.116	40	98%
Biofilm – suspended into liquid (50)	0.066	82	97%
Biofilm – DFR	0.018	36	37%
	0.011	69	63%
Biofilm – Microsensor chamber	0.0015*	40	17%
		80	19%

*Estimated from model simulation in Chapter 5

Chapter 5

Evaluation of kinetic parameters in *N. europaea* biofilms using microelectrodes and a reactive transport model

Ellen G. Lauchnor, Brian D. Wood, and Lewis Semprini

ABSTRACT

Kinetic parameters in biofilms are essential to evaluate for the accuracy of biofilm models, although it is not often clear whether the kinetics of batch systems can be used for biofilm models. Biofilms of the ammonia oxidizing bacterium *Nitrosomonas europaea* have been cultivated in Drip Flow Reactors and are useful for studying pure culture kinetics of ammonia oxidation. By developing pure culture biofilms of *N. europaea* we explored the hypothesis that the kinetics of ammonia oxidation in *N. europaea* biofilms are equal to batch suspended cells and the observed differences in rates are due to mass transfer limitations. This was done by in situ measurement of dissolved oxygen and pH inside biofilms using microsensors and applying a 2-D advection-diffusion reactive transport model. The model simulated the experimental data and was used to evaluate the Monod equation half-saturation coefficient K_m for NH_3 oxidation. A 2-D model was required to effectively simulate both fluid transport parallel to the biofilm surface, and diffusive transport into the biofilms. The model was fitted to the experimental data from of dissolved oxygen and pH profiles with the biomass concentration as the main adjusted parameter. Three experimental studies of microsensor measurements were performed with biofilms as follows: 1) NH_3 concentrations close to and above the batch K_m value 2) Low NH_3 concentrations well below the half-saturation coefficient 3) Limited buffering capacity which resulted in a pH gradient within the biofilms. The calibration of the biomass parameter resulted in lower values than estimated from experimental results, indicating that either inactive biomass protein is present or the cells in the biofilm have a lower maximum rate of NH_3 oxidation. The measurements of DO and pH profiles under insufficient buffering capacity allowed for simulation of pH shift and DO consumption simultaneously. The same kinetic parameters simulated the result of pH gradient and DO consumption under reduced NH_3 concentration at a lower pH. The 2-D model simulated the experimental results using a uniform biomass and Monod kinetics.

INTRODUCTION

Kinetic parameters in biofilms are difficult to determine experimentally due to mass transfer limitations that result in gradients of substrates and heterogeneous activity within a biofilm (87). The kinetic parameters determined for batch systems of an organism are often used to represent the kinetics in biofilms (11, 67). The assumption that kinetic parameters are the same in biofilms and suspended cells of an organism may not be valid and needs to be investigated for the organism of interest. It is possible to evaluate biofilm kinetics using models that incorporate reaction and diffusive mass transport correlated with overall rates of microbial activity (66, 73).

The use of microsensors allows for direct measurement of local substrate concentrations inside biofilms (34, 86). The concentration profiles of dissolved oxygen have been used to calibrate biofilm models and determine biokinetic parameters while accounting for mass transport (116, 118). The modeling of microsensor profiles has mainly focused on 1-D diffusive transport along the dimension of the measured profile.

The concentrations of O_2, NH_4^+, NO_2^- and NO_3^- have been measured inside nitrifying biofilms using microsensors and resulting rates of nitrifying activity have been determined from the concentration profiles (33, 64, 65). The kinetics of nitrifying bacteria have been examined with microsensor profiles, using the diffusion-reaction equation to determine local rates (98). A simplifying assumption involved with calculating the microbial activities from concentration profiles is that a diffusion boundary layer exists in the liquid above the biofilm where advective transport of the fluid is neglected (34). While this may be a valid assumption, models that incorporate advection of solutes in the fluid phase more accurately depict the transport of solutes into the biofilm.

Biofilm models in 1-D can describe transport and reaction of chemical species and growth of biomass when assuming that gradients are only in the dimension of the biofilm depth (60, 90, 107). However, the 2-D approach to biofilm modeling is necessary when heterogeneity or mass transport is occurring in a direction

perpendicular to the biofilm depth. Specifically, multidimensional modeling is important for simulation of species transport where advection is a significant contribution to mass transport (26, 104). 2-D biofilm models have been developed to study surface heterogeneity in biofilms and the influence of fluid-flow on detachment and biofilm geometry (74, 75). Here, fluid-flow is incorporated into a 2-D model to accurately simulate the advective transport of species in the direction parallel to the biofilm surface.

Ammonia oxidizing bacteria (AOB) are a group of the nitrifying bacteria that carry out the first step of nitrification in wastewater treatment plants (WWTP). *Nitrosomonas europaea* is an AOB that exists in wastewater nitrifying biofilms and has been well-characterized in pure cultures of suspended cells (4). *N. europaea* has been identified as a prevalent AOB in nitrifying biofilms and is a model AOB for kinetic parameter studies. In pure culture, biofilms of *N. europaea* exhibited greater resistance to inhibition by phenol and toluene than suspended cells (51). Construction of an *N. europaea* biofilm model and evaluation of the NH_3 oxidation kinetics in biofilms is the first step to determining if the observed difference in inhibition is due to mass transport effects.

The kinetic model typically used for NH_3 oxidation is the Monod equation with dual substrate dependence on NH_3 and O_2 (25, 67, 72). To effectively model ammonia oxidation in biofilms using this equation, the kinetic parameters including the half-saturation coefficients and maximum rate coefficient associated with ammonia oxidation must be determined. The K_m of 23-58 μM NH_3 was experimentally determined in suspended cells of *N. europaea* by Suzuki et al, who also determined that the substrate for AMO is NH_3, not NH_4^+ (102). Kinetic studies of mixed nitrifying cultures with *N. europaea* determined K_m values 0.4-1.7 mM N, corresponding to 7-30 μM NH_3 at pH 7.5 used in the experiments (48, 49). More recently, kinetics comparisons made between AOB and NH_3 oxidizing archaea determined a K_m of 553 μM NH_4+NH_3 in *N. europaea* strain 19718, which equates to 10 μM NH_3 at the experimental pH 7.5 (58).

The research presented here uses microelectrode measurements and a 2-D advection-diffusion reactive transport model to evaluate the kinetics of ammonia oxidation in pure culture *N. europaea* biofilms. The aim of modeling in 2-D was to accurately model the boundary layer of fluid above the biofilm surface, where advective flux in the fluid increases with distance from the surface. Another goal of the study was to determine if the half-saturation coefficient, K_m for NH_3 oxidation in the exponential batch system works in biofilm system of the same species. Microelectrode experiments under highly buffered conditions were performed at varying concentrations of NH_3 to evaluate kinetics at constant pH. Under the constant pH conditions, the NH_3 concentration remains fairly constant as it is replenished by acid-base equilibrium with a larger pool of NH_4^+. With decreasing pH, the equilibrium shifts to NH_4^+, so that in acidic conditions the NH_3 becomes depleted. Therefore, to explore the kinetics of *N. europaea* as NH_3 is depleted in the biofilm, buffering capacity was reduced to allow for pH gradients and resulting NH_3 gradients.

EXPERIMENTAL PROCEDURES

Bacterial cultures and batch experiments

Batch cultures of *N. europaea* cells (ATCC strain 19718) were grown for biofilm reactor inoculation and suspended batch tests. Batch reactors used for cell cultivation consisted of 4L flasks containing 2L of medium as described previously (79). The flasks were inoculated with 25 mL of *N. europaea* culture and shaken (100 RPM) at 30°C in the dark and cells were harvested upon reaching late exponential phase on day 3 (OD_{600}=0.07).

Batch experiments were performed to evaluate ammonia oxidation kinetics using batch grown cells harvested after 3 days of growth. Cells were pelleted and rinsed in HEPES buffer (20 mM, pH 7.8) and resuspended into 150 mL bottles containing either 1 mM or 20 mM HEPES buffer solution at pH 7.8, with an $(NH_4)_2SO_4$ concentration of 0.125, 0.25, 0.5 or 2.5 mM. Rates of ammonia oxidation were evaluated at NH_4-N concentrations of 0.25 – 5 mM by monitoring NO_2^-

production at five minute intervals for 30 minutes. Rate experiments in low buffered medium (1 mM HEPES) and 2.5 mM $(NH_4)_2SO_4$ were also conducted to provide data that could be used to demonstrate the model was able to simulate the change in pH and the NH_3 oxidation rates that occurred under simple batch reactor kinetic conditions.

Biofilm reactor

A drip flow biofilm reactor (DFR) was used to cultivate biofilms of *N. europaea* according to methods developed previously (51). Biofilms were grown on glass slide coupons within four isolated DFR channels for 4-8 weeks prior to experiments. AOB biofilm growth medium consisted of the following: 25 mM $(NH_4)_2SO_4$, 3.77 mM Na_2CO_3, 20 mM HEPES buffer, 730 µM $MgSO_4$, 200 µM $CaCl_2$, 9.9 µM $FeSO_4$, 16.5 µM EDTA free acid, and 0.65 µM $CuSO_4$. Ammonia oxidation activity in the biofilms was monitored by sampling the effluent media from the DFR and measuring NO_2^- concentration in the effluent.

The biomass volumetric concentration in the biofilms was estimated based on dimensions of the coupon, biofilm depth, and total protein measurements. Total protein measurements of *N. europaea* biofilms yielded 1-2 mg per coupon, and average estimates of biofilm depth from microscopy were 100-200 µm. The coupon dimensions were 7.5 cm by 2.5 cm and coverage of biofilm on the slides was estimated around 50%. From these measurements, the calculated volumetric biomass concentration was 5-10 mg protein cm^{-3}.

Oxygen and pH microsensor measurements

Mature biofilm samples on coupons were removed from the DFR for microsensor measurements after being cultivated to steady-state, determined by NO_2^- production. For microsensor profiling, the coupon containing the biofilm was placed inside a flow cell that was connected to a 5 L media reservoir maintained at 25°C with a heater. The system was open to the atmosphere. The media from the reservoir was recirculated through the flow cell via an aquarium pump at a flow rate of 50 mL min^{-1}. The media reservoir was continuously sparged with air to ensure constant DO

saturated under atmospheric conditions. A schematic of the microsensor experimental apparatus is shown in Figure 5.1.

Dissolved oxygen (DO) and pH microelectrodes with tip diameters of 8-12 μm (Unisense AS, Denmark) were used to take vertical concentration profiles within the biofilm samples. The O_2 sensors were Clark-type microelectrodes described in detail elsewhere (85). A two-point calibration was performed for DO sensors using medium at atmospheric saturation of DO and medium sparged with pure $N_{2(g)}$ for 5-10 minutes for a zero measurement. The pH microelectrodes were calibrated with buffered solutions at pH 4.0, 7.0 and 10.0. Calibrations were performed at least once per day to ensure accuracy of measurements.

The pH microelectrode consisted of a redox sensitive tip 150 μm in length, which measured the pH over the depth of the tip (Unisense AS). Therefore, for each measurement, the pH reading was an integrated measurement from the tip up to 150 μm above the tip. For analysis of the pH profiles, an interpolated function of the pH measurements was generated and integrated to derive pH values at each location from the depth averaged measured values. The calculations for determining the adjusted pH profile values are shown in Appendix B.

A micromanipulator with a motor controller (Marzhauser, Germany) was used to position the microelectrodes on the biofilm surface and make vertical spatial steps while profiling. A Leica S8 APO Stereozoom microscope (Leica Microsystems, Inc., Bannockburn, IL) was used to visualize the biofilm surface while positioning the microelectrodes. Data acquisition was performed on a computer with the SensorTrace Pro program (Unisense AS).

Biofilm depth and coverage on the slides was heterogeneous, with the depth varying between 0-300 μm. The biofilm was examined using the Stereomicroscope and locations on the slide where the biofilm was at least 200 μm in depth were used for microsensor measurements. Three to five replicate profiles were taken for each experimental condition tested.

Experimental conditions

The liquid media for microsensor experiments contained HEPES buffer (1 or 10 mM) at pH 7.8. Ammonia additions were made by aliquoting volumes of a 0.5 M $(NH_4)_2SO_4$ stock solution to the media bath and allowing the fluid to recirculate into the flow cell for at least one hour to ensure well-mixed conditions. Increasing concentrations of $(NH_4)_2SO_4$ were added to the bath in order to compare O_2 profiles under different conditions on the same biofilm samples. The residence time in the chamber of ~12 minutes was determined by the flow rate of 50 mL min^{-1} and volume of the measuring chamber.

The experimental conditions for microsensor measurements are outlined in Table 5.1. Three studies were conducted, beginning with the initial microsensor measurements under well buffered conditions and high NH_4-N concentrations in Study 1. Study 2 was conducted for evaluation under NH_3 limiting conditions and Study 3 examined DO profiles in the presence of pH gradients due to limited buffer capacity. Steady state was determined by taking multiple measurements over time and verifying no change in the profiles.

MODEL DEVELOPMENT

Batch model

The COMSOL program was used to create a kinetic model of NH_3 oxidation in a batch system in the absence of mass transport. The model was used to verify the Monod equation kinetic parameters K_m and k_{max} for batch cells. The model was also used to evaluate the performance of COMSOL with a pure kinetic model for NH_3 oxidation and to simulate pH change during NH_3 oxidation in batch tests with insufficient buffering capacity.

Biofilm model description

A 2-D biofilm model was developed with two adjacent subdomains consisting of fluid and biofilm. The conceptual representation is shown in Figure 5.2, with the key model equations. The fluid subdomain was 7.5 cm by 0.1 cm, and contained

advection in the x-direction (Fig. 5.2). The biofilm subdomain geometry was assumed to have a depth of 0.03 cm, which was the approximate maximum depth measurement, determined by microscopic examination of *N. europaea* biofilm samples.

In the model, steady-state was assumed with respect to biofilm growth and detachment and growth of biofilm biomass was ignored due to the short-term duration of experiments. Conservation of mass equations were solved for chemical species involved in the reactions for AOB respiration and aqueous chemistry. The 2-D model incorporated both advective and diffusive transport of aqueous species in the fluid domain and only diffusive transport in the biofilm domain.

Model equations

Parameters used in the model are shown in Table 5.2. Mass balance equations were developed for each of ten aqueous species in the biofilm: NH_4^+, NH_3, DO, NO_2^-, H^+, HEPES acid, HEPES base, H_2CO_3, HCO_3^- and CO_3^{2-}. Two buffering systems were present: HEPES buffer (pH 7.8) was added to the medium and carbonate buffering was present due to the dissolution of CO_2 from the air. The fluid subdomain contains both convective and diffusive transport of solutes and equilibrium reactions may also take place in the fluid, thus the mass balance equation for all species in the fluid subdomain, incorporating advection, diffusion and reaction, is the following:

$$\frac{\partial C_i}{\partial t} = -u_x \frac{\partial C_i}{\partial x} + D_{eff} \left(\frac{\partial^2 C_i}{\partial x^2} + \frac{\partial^2 C_i}{\partial y^2} \right) + \sum R_j \qquad (5.1)$$

In equation 5.1, u_x is the fluid velocity, individual reaction rates are designated as R_j for species C_i and D_{eff} is the effective diffusion coefficient. Here, it is assumed that fluid flow only occurs in the x-direction according to the equation for fluid velocity described below.

The fluid flow equation was generated from the Navier-Stokes equation, as a solution for fluid flow close to a flat surface with no flow at the surface and an upper boundary of maximum velocity, u_{max}. It was determined by tracer tests that the fluid flow was not completely uniform or well defined by an analytical equation above the

biofilm surface. However, very close to the biofilm surface, the flow could be assumed laminar and solved analytically, with the fluid velocity increasing to a maximum rate of u_{max} above the biofilm surface. The model maximum velocity was calculated using the pump flow rate of 50 mL min^{-1} and the area of the inlet to the flow cell. The equation for velocity field was input as the fluid velocity used in the advective term of the transport equation.

$$u_x = \frac{u_{max}}{D^2} * (2Dy - y^2)$$

$$u_{max} = \frac{Q_T}{A_{inlet}}$$

(5.2)

Equation 5.2 was developed from Navier-Stokes using a boundary condition of $u_x = 0$ at the biofilm surface (y=0), and a second boundary condition of $u_x = u_{max}$ at y = D. The depth parameter (D) represented the distance above the biofilm surface to u_{max} and was calibrated to the DO microsensor profiles. The parameter influenced the depth location on the profiles where DO concentration began to decrease below the bulk fluid concentration, which was 450 μm above the biofilm surface for all the measured profiles. Due to the influence of the parameter D on the fluid portion of the profile and not the biofilm, it was possible to calibrate the flow regime independent of the kinetic parameters. A sensitivity analysis of the flow parameter D is presented in Appendix B, which illustrates that the DO profile in the fluid phase is affected by changing D.

In the biofilm it was assumed that transport of solutes was solely by diffusion, therefore the non-steady-state mass balance equation in 2-D for a reacting solute in the biofilm is as follows:

$$\frac{\partial C_i}{\partial t} = D_{eff}\left(\frac{\partial^2 C_i}{\partial x^2} + \frac{\partial^2 C_i}{\partial y^2}\right) + \sum R$$

(5.3)

For the reaction term, NH_3 oxidation and reactions for acid-base equilibria were incorporated. The stoichiometric matrix of species and their reactions is

included in the Appendix B. Ammonia is oxidized to nitrite by *N. europaea* according to the following equation: $NH_3 + 1.5O_2 \rightarrow NO_2^- + H^+ + H_2O$ (103). Monod kinetics with dual substrate dependence (21) were used to model the kinetics of ammonia oxidation in the biofilm.

$$R_{AOB} = K_{max} X \frac{NH_3}{K_{sn} + NH_3} \frac{O_2}{K_{so} + O_2} \tag{5.4}$$

Endogenous respiration was included in the model to account for decay inside the biofilm. An endogenous respiration term was used to represent the rate of oxygen consumption independent of NH_3 oxidation. The endogenous respiration term was fitted to the DO consumption with no NH_3 present, as shown in Appendix B (Fig. B1) and the term was held constant while simulating the DO profiles with NH_3 oxidation.

Acid-base equilibrium

The aqueous chemistry of the system and acid-base equilibria need to be taken into account to determine the fraction of total ammonium that is available as NH_3 for microbial reaction and to model the pH in the system as a function of HEPES buffering capacity. Due to the limitations of the COMSOL program, the equilibrium reactions had to be represented as rates. To achieve this, the equilibrium reactions were represented as reversible reactions with high rate constants.

$$K_a = \frac{k_1}{k_2} = \frac{NH_3 * H^+}{NH_4^+} \tag{5.5}$$

$$R_{eq} = k_2 \left[K_a NH_4^+ - NH_3 * H^+ \right] \tag{5.6}$$

Three equations in the form of 5.6 were used to account for equilibria of NH_3/NH_4^+, HEPES acid/base, and H_2CO_3/HCO_3^-, which are shown in Appendix B (Table B1). The equilibria between species were verified in the model solution by comparing the right side of equation 5.6 with the equilibrium constants.

Boundary conditions

The following boundary conditions were used for the biofilm boundaries in the model, and are designated with the same notation in Figure 5.2:

BC 1.
$$\frac{dC_i}{dx} = 0 \tag{5.7}$$

BC 2. $\quad J_{fluid} = J_{biofilm}$ Equal flux at phase boundary (5.8)

BC 3. $\quad C_i(x, y_{max}) = C_{i,Bulk}$ Bulk fluid boundary (5.9)

BC 4. $\quad C(0, y) = C_B$ Inlet concentration (5.10)

Model Solution

The reactive transport model was solved using the COMSOL 4.1 Multiphysics package with the Chemical Reaction Engineering module. COMSOL uses a finite element method to solve the PDEs describing the species concentrations at each node in the model geometry. The computational grid was 200 nodes in the x-direction (fluid flow), and in the y-direction there were 40 nodes in the fluid and 30 nodes in the biofilm domain. A transient solver was used to iteratively solve for all chemical species until arriving at the steady-state solution. The solution was compared over the solver times to verify that steady-state had been reached.

Least Squares Method

A least-squares error method was used for comparison of experimental data and model results to determine the best fit kinetic parameters. The sum of squared error was determined between the data points and model solution at the same points for the entire profile. The parameter calibration and comparison to the data was done manually for a range of parameter values, until the minimum value for the sum of squared error was found.

RESULTS AND DISCUSSION

Model verification

A simplified 1-D model in COMSOL was used to solve for a first-order reaction rate with diffusive transport. The model was compared with the analytical solution for 1-D diffusion and reaction (Appendix B). The model result matched the analytical solution exactly, providing confidence that the COMSOL model could accurately solve the reactive transport model for the biofilm system.

Batch kinetics for *N. europaea*

A non-steady-state batch model was used to simulate the kinetics of suspended cells of *N. europaea* and to verify the reaction kinetics of the COMSOL model prior to adding solute transport. Short term batch tests with *N. europaea* were used to determine the kinetic parameters k_{max} and K_m for NH_3 oxidation without O_2 limitation and compare with literature values. In medium containing 2.5 mmol L^{-1} $(NH_4)_2SO_4$, NH_3 was in excess and the rate of NO_2^- production over 3 h by linear regression was 0.05 mol mg protein^{-1} s^{-1} (Fig. 5.3A). This value was used as k_{max} in the batch model, which fit the data well (Fig. 5.3A). This parameter is in the range of maximum NH_3 oxidation rate from previous studies, which are in the range of 0.023 mol mg protein^{-1} s^{-1} (79) to 0.096 mol mg protein^{-1} s^{-1} (44).

Batch tests were performed with *N. europaea* and concentrations of 0.25 and 1mM NH_4-N at pH 7.8, which resulted in equilibrium concentrations of 9 μM and 34 μM NH_3, respectively. The batch model simulated NO_2^- production in the batch tests with a K_m value of 40 μM. These results agree with a previous study that experimentally determined the K_m value to be 23-58 μM NH_3 for *N. europaea* (102).

A batch model was also used to simulate decreasing pH in the batch system during NH_3 oxidation with insufficient buffering capacity where the microbial reaction acidified the medium (Fig. 5.3B & C). To effectively model the NO_2^- production and pH data from batch experiments, carbonate equilibrium was introduced into the batch model, as well as the HEPES equilibrium. The parameters determined in the well-

buffered, constant pH batch tests were used to simulate the NO_2^- production and co-occurring pH decrease over time.

Experimental results – Study 1

N. europaea biofilm grown for 8 weeks in the DFR was placed into the microsensor measuring chamber and DO profiles were taken with 0, 1 and 5 mmol L^{-1} NH_4-N (Fig. 5.4A). In addition, a run was performed where allylthiourea was added to the medium as an inhibitor of NH_3 oxidation. The rates of DO consumption increased from 1 mmol L^{-1} to 5 mmol L^{-1} NH_4-N, indicating that NH_3 was limiting in the 1 mmol L^{-1} case.

Allylthiourea (ATU), a specific inhibitor of AMO, was added to the bath for a final concentration of 100 μM with 5 mmol L^{-1} NH_4-N present. Upon ATU addition, NH_3 oxidation ceased and DO increased in the biofilms. The response to ATU was rapid and the DO at the biofilm surface returned to 90% of atmospheric DO concentration within 10 minutes of ATU addition. After addition of ATU, a slight decline in dissolved oxygen inside the biofilms was still observed. This indicates that endogenous respiration was occurring as oxygen was being consumed even while NH_3 oxidation was inactivated.

pH microsensor measurements showed that the pH was between 7.6 and 7.8 in the biofilm (Fig. 5.4B). The buffering capacity of the medium prevented a significant decrease in the medium pH by the biofilm cells. The DO profiles measured under the high buffer case were used to evaluate the kinetic parameters of NH_3 oxidation in the biofilms without changes in pH, so that NH_3 availability would not be impacted.

Model simulations – Study 1

A one-dimensional model was initially used to simulate the concentrations of reactive species in the biofilms. The model assumed diffusive transport was dominant above the biofilm in a fluid boundary layer. The 1-D model was not able to fit the profiles in the fluid due to the contribution of advective transport, using K_m of 40 μM, k_{max} of 0.045 mol mg protein^{-1} s^{-1} and biomass concentration of 0.5 g cm^{-3} (Fig. 5.5A). When the fluid flow was added to a 2-D model using equation 5.2, the velocity

increased linearly in the 1 mm length of the vertical fluid dimension and the simulation more accurately depicted the experimental profiles (Fig. 5.5B).

The hypothesis that batch kinetic parameters were valid in biofilms of *N. europaea* was evaluated by using the values of k_{max} and K_m derived from batch experiments in the kinetic biofilm model to simulate the measured DO profiles in Figure 5.4. The biomass concentration parameter (X) has the same effect on the overall Monod rate as the maximum rate coefficient, k_{max} and was adjusted to obtain best fit matches to experimental measurements.

The combined $k_{max}X$ parameter profile was calibrated to the DO profile with 5 mM NH_4-N (Fig. 5.5B). In this case, NH_3 was significantly greater than K_m and changing K_m did not affect the model results. The best fit value for $k_{max}X$, determined by least-squares error method, of 0.025 mol $L^{-1}s^{-1}$ yielded a biomass concentration of 0.5 mg protein cm^{-3} assuming the k_{max} was 0.05 mol mg protein^{-1} s^{-1} as determined for the batch system. This fitted biomass concentration is ten-fold lower than the concentration of 5-10 mg protein cm^{-3} estimated using total protein measurements (see Methods section). Reducing $k_{max}X$ to fit the data suggests the active biomass was much lower than the total measured value. The biuret protein assay that was used to determine biomass measured the total protein in the sample, which may have been greater than the active biomass protein. Alternatively, the maximum rate parameter may in fact be lower in the biofilms than in exponential cells due to lower AMO activity. Interestingly, the 1-D biofilm model used similar parameters as the 2-D model to simulate the profiles inside the biofilm, although the 1-D model did not match the data taken in the fluid phase (Table 5.3).

In our previous biofilm work in Chapter 2, cells from the biofilm that were resuspended into liquid medium recovered to specific NH_3 oxidation rates that were 2-fold lower than batch cell rates. Based on this recovery of activity, the fraction of inactive biomass in the biofilm was less than 50% of the total protein. However, the model results indicate that 90% of the total biomass protein may have been inactive in the biofilm.

With a K_m of 40 µM derived in the batch tests (Table 5.3), the model simulated activity at 1 mmol L^{-1} NH_4-N that matched the DO profile data under the same conditions (Fig. 5.5B). This K_m value was roughly equivalent to the NH_3 concentration at the beginning of the 1 mmol L^{-1} NH_4-N batch test. This simulation fit the experimental value of K_m measured in batch cells, though a more detailed analysis was required to determine K_m under NH_3 limiting conditions.

The simulation results of NH_3 and NO_2^- concentrations for study 1 are shown in Figure 5.5C. As mentioned above, the concentration of NH_3 remains essentially constant as it is replenished by NH_4^+, which is about 96% of the total ammonium in the system at pH 7.8. NH_3 fully penetrates the biofilm according to model results, although the NH_3 concentration in the 1 mM NH_4-N profile is close to the K_m of 40 µM, which influences the Monod rate and results in less DO consumption than with 5 mM NH_4-N. The NO_2^- accumulates inside the biofilm to concentrations above the maximum NH_3 because of this equilibrium. However, the maximum NO_2^- concentration in the biofilm (~180 µM) is much lower than NO_2^- concentrations (~10 mM) that were found to affect NH_3 oxidation by Stein et al. (100).

Experimental results – Study 2

To investigate the K_m for NH_3 in the biofilms with more accuracy, DO profiles were analyzed with low NH_3 concentrations, where NH_3 was the limiting substrate. DO was measured in biofilms under NH_3 limiting conditions at concentrations of 0, 0.05, 0.1, 0.25 and 5 mmol L^{-1} NH_4-N, added as $(NH_4)_2SO_4$ (Fig. 5.6). Under initial conditions with no NH_3 present, DO consumption was still observed, confirming that endogenous respiration was taking place. DO penetrated the entire measured biofilm depth in profiles taken with 0.1 and 0.05 mmol L^{-1} NH_4-N, thus NH_3 was the limiting substrate in these profiles. At NH_4-N concentrations of 0.25 and 5 mmol L^{-1}, the DO profiles did not change very much, which was not in agreement with our initial observations presented in Figure 5.4 with 1 and 5 mmol L^{-1}. It is not know why these results disagree, although the biofilms in Study 2 were grown for about 4 weeks longer than in Study 1, which may affect the active biomass in the biofilm.

The Study 2 profiles were unique in that the DO consumption was limited to the top 100 μm of the biofilm, below which the profiles were constant, indicating no DO uptake deeper than 100 μm. This indicated that the cells below that depth were potentially NH_3 limited or the cells deeper in the biofilm were inactive. In Study 1, the profiles continued to decrease beyond that depth, indicating DO consumption further into the biofilm.

Model simulations – Study 2

The model was used to simulate the DO profiles presented in Figure 5.6 and the least-squares methods was used to fit the K_m parameter (Fig. 5.7A) The DO profiles taken at 0.05 and 0.1 mmol L^{-1} NH_4-N were used in the K_m analysis, which resulted in a K_m of 1.5 μM NH_3 (Table 5.3). A sensitivity analysis of K_m (Appendix B) shows that the model was not very sensitive to K_m when simulating the DO profiles with 0.05 and 0.1 mM NH_4-N. This may be the case because the K_m value was very low and thus did not have a large influence on the Monod rate term for NH_3 oxidation.

The model with the lower K_m value of 1.5 μM NH_3 best fit the simulations of DO profiles in Figure 5.6 for concentrations of 0.25 and 5 mM (Fig. 5.7A). To determine if this solution was unique or if the data could be fit by increasing the rate parameter, another simulation was performed with a higher value of $k_{max}X$ (Fig. 5.7B). Using a biomass concentration of 5 mg cm^{-3}, ten-fold higher than in Study 1, similar DO profiles were predicted as in the solution with K_m of 1.5 μM NH_3. A table of the simulation parameters is shown in Table 5.3. The biomass concentration used in Figure 6B was in the range of calculated biomass concentration, although it contradicts Study 1, which indicated that either the active biomass was much lower or the maximum rate constant was lower than batch cells.

Experimental results – Study 3

Microsensor experiments were conducted in medium with limited buffering capacity (1mM HEPES buffer) to evaluate spatial gradients in pH and observe the effect of the pH change on DO profiles. The results of study 3 confirm that pH gradients develop inside the biofilms when buffering capacity is low (Fig. 5.8). The

DO concentration was greater inside the biofilm than previous studies with 1 and 5 mmol L^{-1} NH_4-N, which was due to less available NH_3 at the lower pH values inside of the biofilm. The DO concentrations decreased over the entire measured depth, which was different than the observed profiles in Study 2.

Model simulations – Study 3

Results of the model simulations for Study 3 are presented in Figure 5.9. In the biofilm model the carbonate system equilibrium was added with 1 mM HEPES buffer concentration. A bulk fluid concentration of 10^{-5} mol L^{-1} H_2CO_3 was used to simulate equilibrium with atmospheric CO_2. The model results with the K_m derived from the batch kinetic tests and the biomass concentration (X) calibrated to the data (Table 5.3) are in general agreement with the microsensor profiles for both pH and DO (Fig. 5.9A & B). A slightly lower $k_{max}X$ was used for the simulation compared to Study 1, which indicates the possibility of variations in biofilm densities with different biofilm samples. The activity in the biofilm occurred over the entire depth of the measured profiles, the DO was not depleted and the lower pH caused NH_3 gradients (Fig. 5.9C). The simulated NH_3 profiles showed more depletion of NH_3 in the biofilm than the simulation of study 1 (Fig. 5.5C), which was a result of the pH reduction in the biofilm. NO_2^- in Fig. 5.9D accumulated in the biofilm to concentrations slightly higher than the NH_3 in the bulk medium, indicating that the NH_3 was still replenished to a small degree by the pool of NH_4^+ in the medium.

CONCLUSIONS

In this research, microsensor measurements were made in *N. europaea* biofilms under a range of NH_3 concentrations and with low and high buffer concentrations. The 1-D model was not able to accurately simulate the profiles due to advection in the fluid phase, although the parameters used in the simulations were similar to those determined for the 2-D model. The 2-D biofilm model was developed including fluid-flow and simulated the DO concentration and pH profiles over the

measured depth. The 2-D model in COMSOL can be used in other systems with microsensor profiles, where the fluid phase hydrodynamics can be characterized.

The kinetic parameters used to simulate the batch experiments and three biofilm studies are shown in Table 5.3. A uniform biomass concentration and activity was used to simulate the DO profiles in the biofilm. In Study 1, the experimental profiles were simulated well with the K_m parameter determined from the batch kinetic tests (Fig. 5.3). However, the $k_{max}X$ term that represented maximum rate and biomass concentration had to be reduced compared to measured values. The resulting parameter predicted that the maximum rate in biofilms was ten-fold lower than the estimated biomass concentration for the biofilm. The range of biomass concentration in biofilms typically used is 10-40 mg cm^{-3} wet weight (59), which is approximately equal to 2-7 mg protein cm^{-3}. The estimated value of biomass concentration of 5-10 mg protein cm^{-3} in the *N. europaea* biofilms is close to this range.

In Study 2, DO profiles were measured in biofilms with limiting NH_3 concentrations (Fig. 5.6). In order to simulate the experimental results, the kinetic parameters had to be adjusted (Table 5.3). The biofilm samples used in Study 2 were cultivated for almost 90 days, compared to 50-60 days for those used in Studies 1 and 3, which may have impacted the concentrations or distribution of active biomass inside the biofilm, even though the NO_2^- production rates remained constant in the DFR during that time.

The model simulated the pH and DO profiles in the low buffered medium in Study 3 where NH_3 was the limiting substrate due to the reduction in pH that shifted the equilibrium towards NH_4^+. A method was developed to calculate the pH profile from the measured pH values, which were averaged measurements over a depth of 150 μm (Appendix B). This method can be used to adjust measured pH profiles from microsensors similar to the ones used in this study.

Microsensors have been used to evaluate kinetic parameters in biofilms before using mass balance equations and ignoring or attempting to eliminate fluid flow effects (116, 118). Fluid flow has also been incorporated into some biofilm models,

where a 2-D approach was used to accurately evaluate the advective transport of species into the biofilms (26). Here, the two methods are combined so that microsensors were used for direct measurement of oxygen uptake in biofilms and a model was used to simulate those direct measurements and calibrate kinetic parameters. The model developed here may be used for further kinetic studies of *N. europaea* as well as in other systems. Future work can include addition of an inhibition model to the kinetics of the 2-D model, and comparison with DO profiles of *N. europaea* biofilms during exposure to inhibitory species such as phenol.

Nomenclature

b	endogenous decay coefficient, mol kg^{-1} s^{-1}
D	Distance between biofilm surface and location of u_{max}, cm
D_{eff}	Diffusion coefficient, cm^2 s^{-1}
K_{aN}	Equilibrium constant for NH_3/NH_4^+, mol L^{-1}
K_{aB}	Equilibrium constant for HEPES buffer, mol L^{-1}
K_{aH}	Equilibrium constant for carbonate buffer, mol L^{-1}
K_o	Half-saturation constant for DO, μmol L^{-1}
K_m	Half-saturation constant for NH_3, μmol L^{-1}
k_{max}	Maximum rate coefficient for NH_3 oxidation, mmol mg protein^{-1} s^{-1}
k_2	Assumed rate constant for reversible equilibrium reactions
Q_T	Volumetric flow rate of fluid, mL min^{-1}
u_{max}	Maximum fluid velocity in measuring chamber, cm s^{-1}
A_{inlet}	Area of fluid flow inlet, cm^2
X	Biomass concentration, mg protein cm^{-3}

Table 5.1. Experimental conditions for microsensor measurements.

	Study 1	Study 2 – NH_3 limitation	Study 3 – pH gradient
NH_4-N (mmol L^{-1})	0, 1, 5, 5 + ATU	0, 0.05, 0.1, 0.25, 5	0.5, 1.5, 5
HEPES buffer (mmol L^{-1})	10	10	1

Figure 5.1. Experimental set up for microsensor measurements.
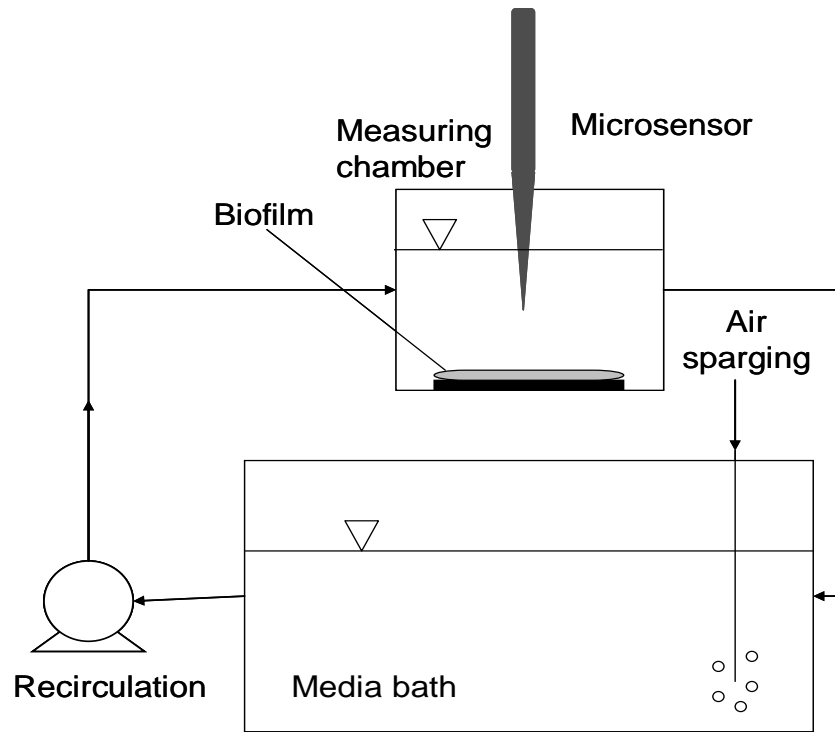
Figure 5.2. Conceptual model of 2-D reaction and transport in biofilm.

BC 3

FLUID

u_x

$$R = u_x \frac{\partial C}{\partial x} - D_{eff} \left(\frac{\partial^2 C}{\partial x^2} + \frac{\partial^2 C}{\partial y^2} \right)$$

BC 3

BC 1

BC 2

BIOFILM

BC 1

$$R = -D_{eff} \left(\frac{\partial^2 C}{\partial x^2} + \frac{\partial^2 C}{\partial y^2} \right)$$

BC 1

BC 1
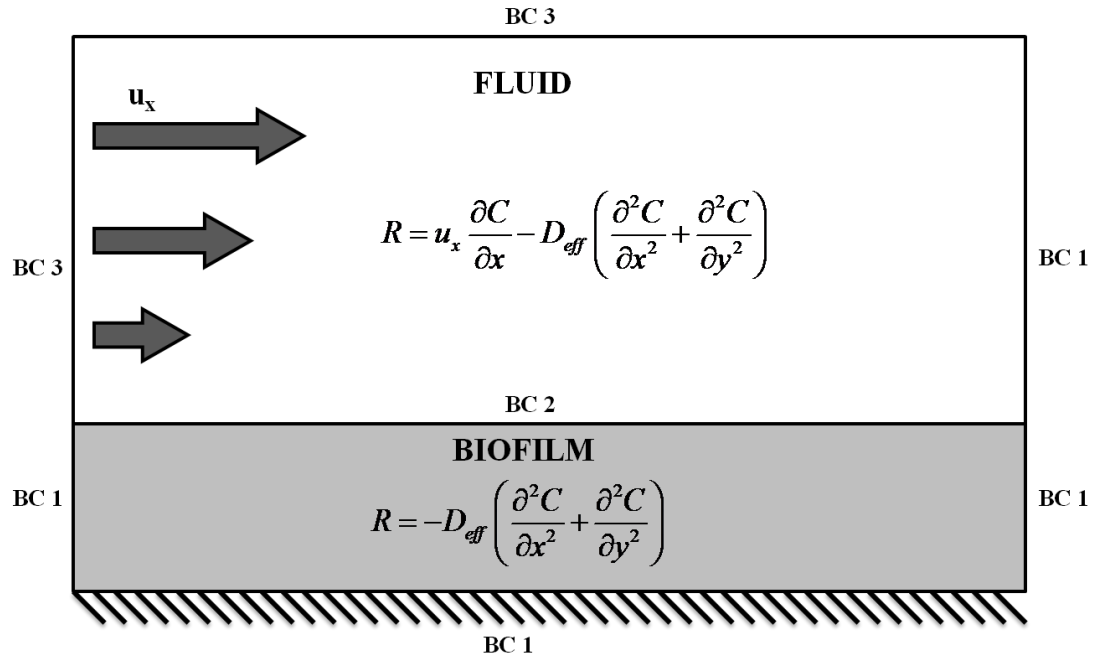
Table 5.2. Physical constants and kinetic parameters for biofilm model.

	Value	Units	Source
Q_T	50	mL min^{-1}	Measured
w	0.5	cm	Measured
D	1.0	cm	Fitted
D_{NH4+}	1.96e-5	cm^2 s^{-1}	(47)
D_{NH3}	1.64e-5	cm^2 s^{-1}	(23)
D_{O2}	2.0e-5	cm^2 s^{-1}	(23)
D_{NO2-}	1.7e-5	cm^2 s^{-1}	(47)
D_{H+}	9.3e-5	cm^2 s^{-1}	(92)
D_{HEPES}	6.2e-6	cm^2 s^{-1}	
K_{aN}	$10^{-9.25}$	mol L^{-1}	(55)
K_{aB}	$10^{-7.8}$	mol L^{-1}	(55)
K_{aH}	$10^{-6.3}$	mol L^{-1}	(55)
K_{so}	0.01	mol m^{-3}	(89)
k_2	10^6		
b	8.2e-4	mol kg^{-1} s^{-1}	Fitted

Figure 5.3. Nitrite production and pH change over time in batch tests and model calibration with 5 mmol L^{-1} NH_4-N. **A)** NO_2^- production data and k_{max} calibration with batch data Lines represent model solutions with k_{max} values of 0.05 (solid line), 0.04 (dashed line) and 0.06 (dash-dot) mol (mg protein-s)$^{-1}$ **B)** Nitrite production with 1 mM HEPES buffer **C)** pH decrease during batch test with 1 mM HEPES buffer. **B and C)** Experimental data (■) and model results (line).
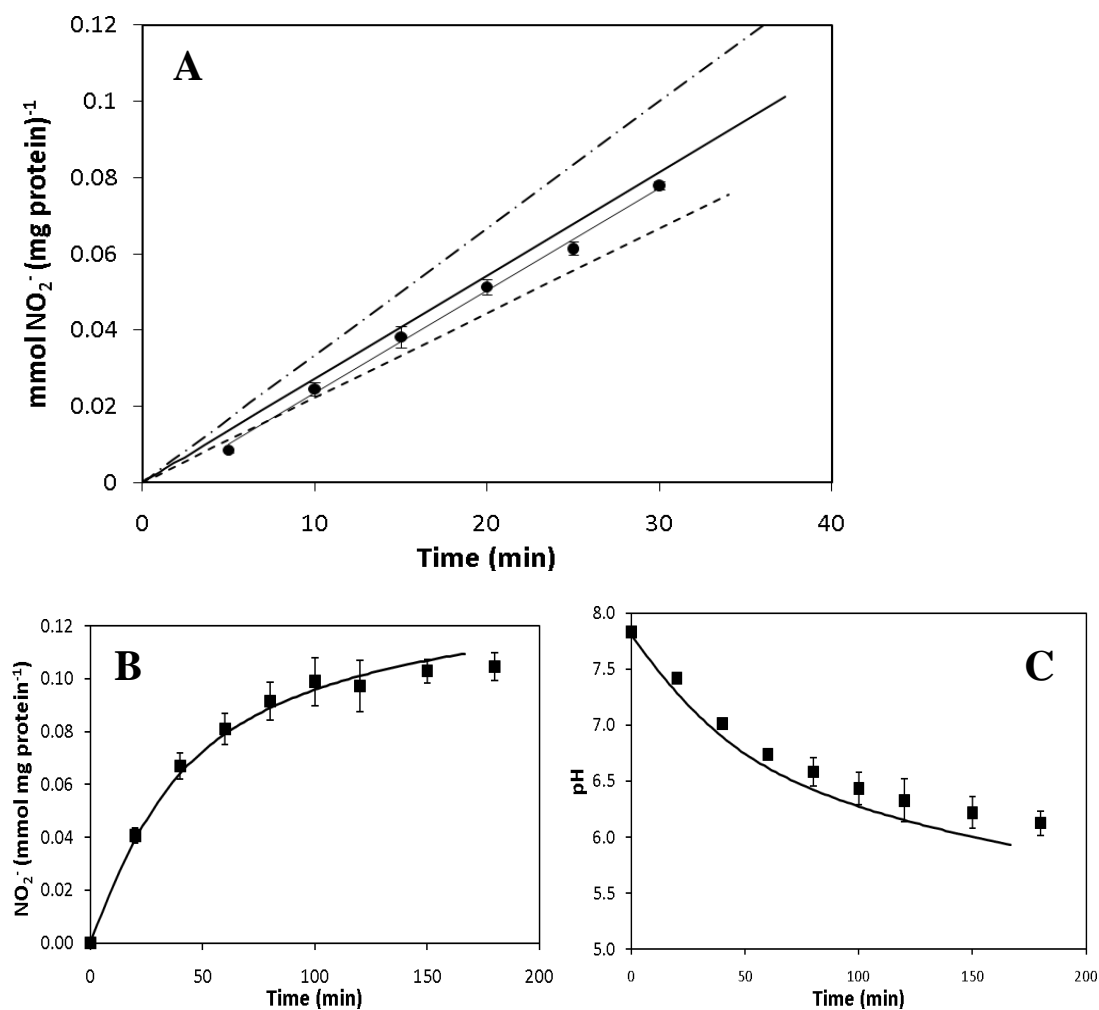
Figure 5.4. DO and pH microsensor profiles of biofilms from microsensor Study 1. **A)** Total concentrations of NH$_4$-N: 0 (■), 1 (□), and 5 mmol L^{-1} (●) and after addition of ATU (○). **B)** pH profile with 5 mM NH$_4$-N. Error bars represent standard deviation of triplicate profiles.
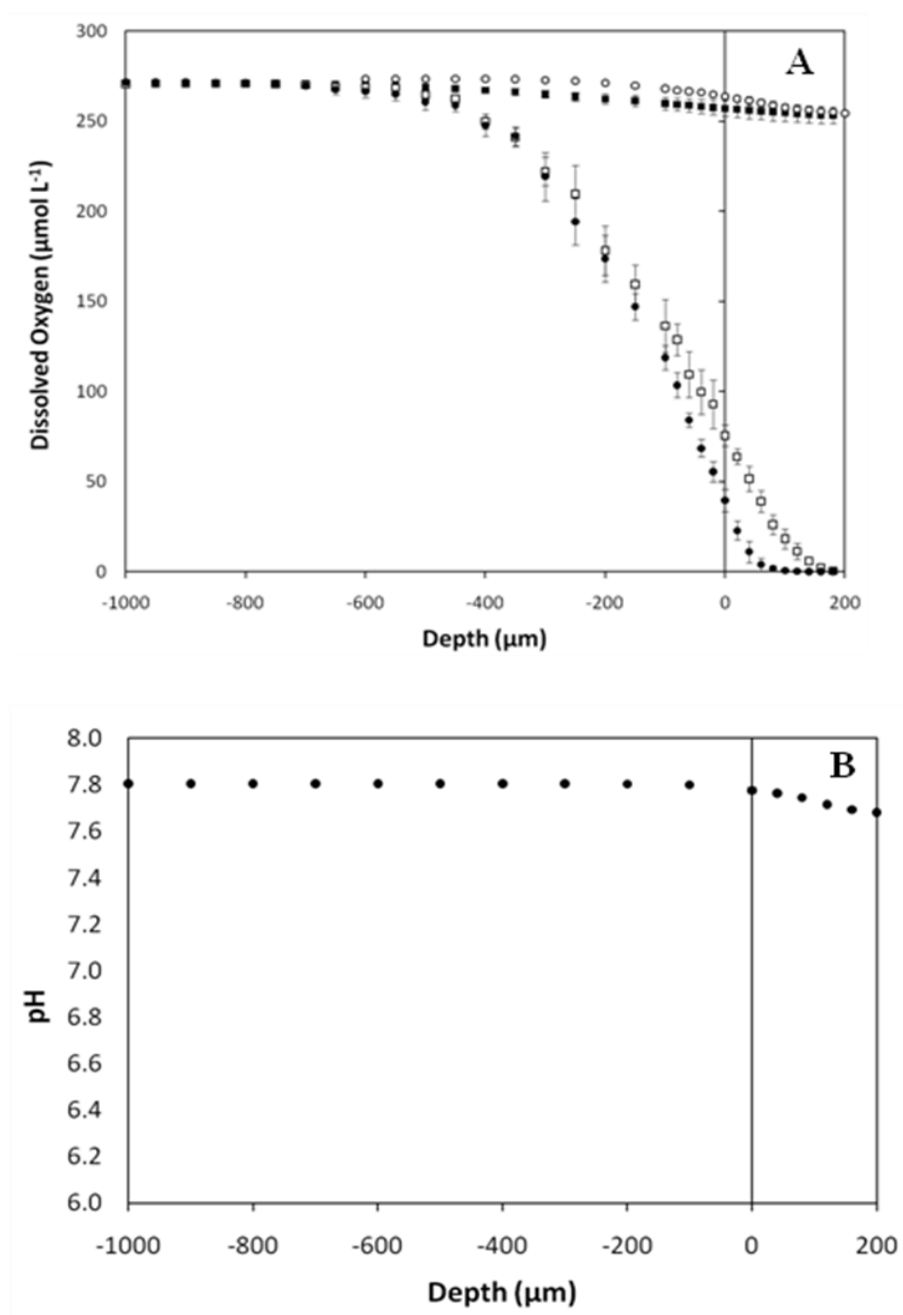
Figure 5.5. Model simulations of Study 1. **A)** 1-D diffusion-based model, **B)** 2-D advection-diffusion model. Profiles are with NH_4-N concentrations of 1 ($\square$) and 5 mmol L^{-1} ($\bullet$). Lines represent model solutions at NH_4-N concentrations of 1 mM (dashed line) and 5 mM (solid line), using a Km of 40 μM NH_3 and biomass concentration of 500 mg L^{-1}. **C)** NH_3 profiles from simulation of 1 mM ($- -$) and 5 mM NH_4-N ($-$), and NO_2^- profiles for 1 mM ($=$) and 5 mM NH_4-N ($- \cdot$) simulations.
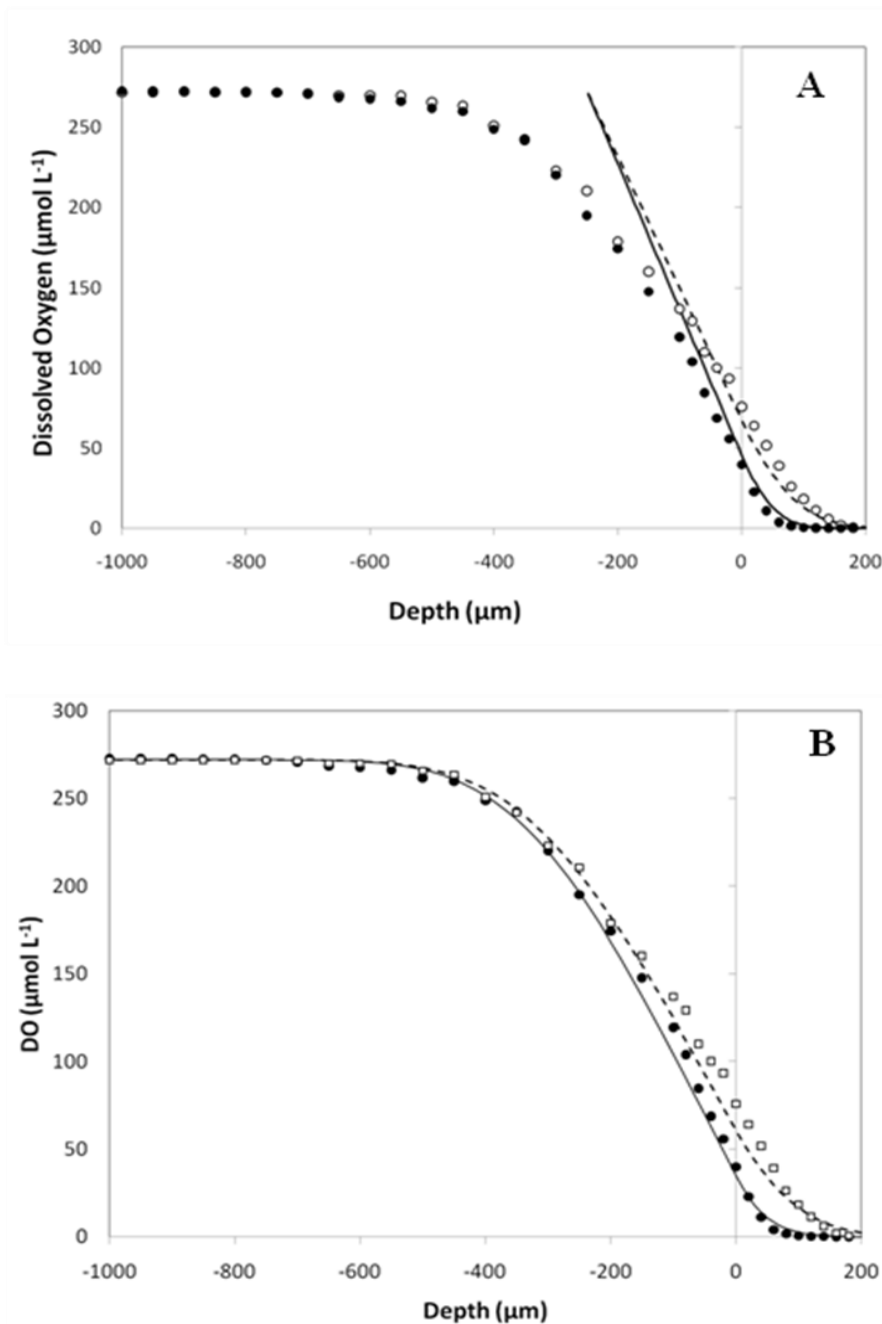
Figure 5.5 (Continued)
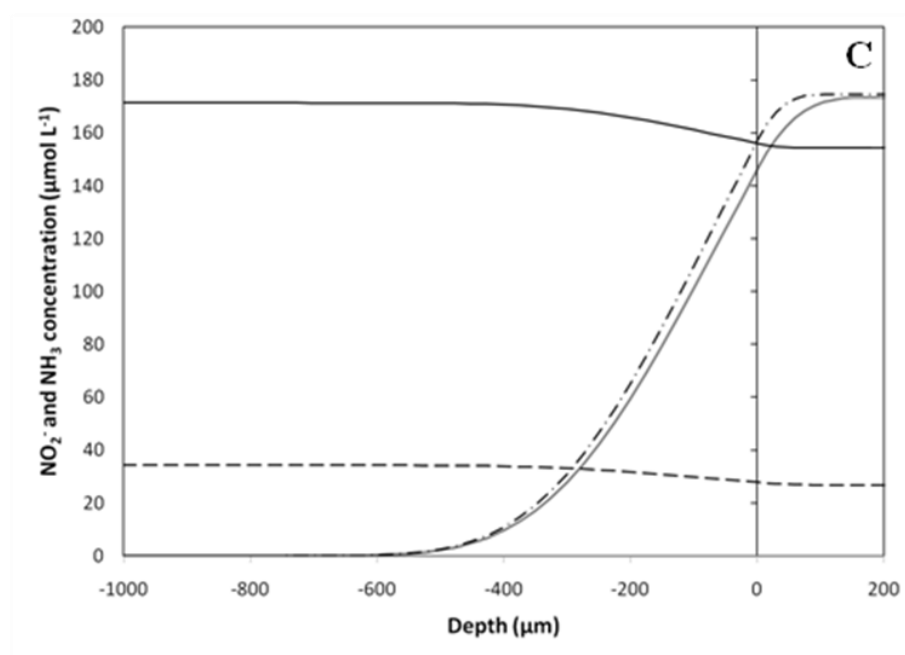
Figure 5.6. DO microsensor profiles of biofilms under limited NH_3 conditions in Sutdy 2. DO profiles with total concentrations of NH_4-N: 0 (■), 0.05 (□), 0.1 (●), 0.25 (○), and 5 (▲) mmol L^{-1}. Error bars represent standard deviation of triplicate profiles.
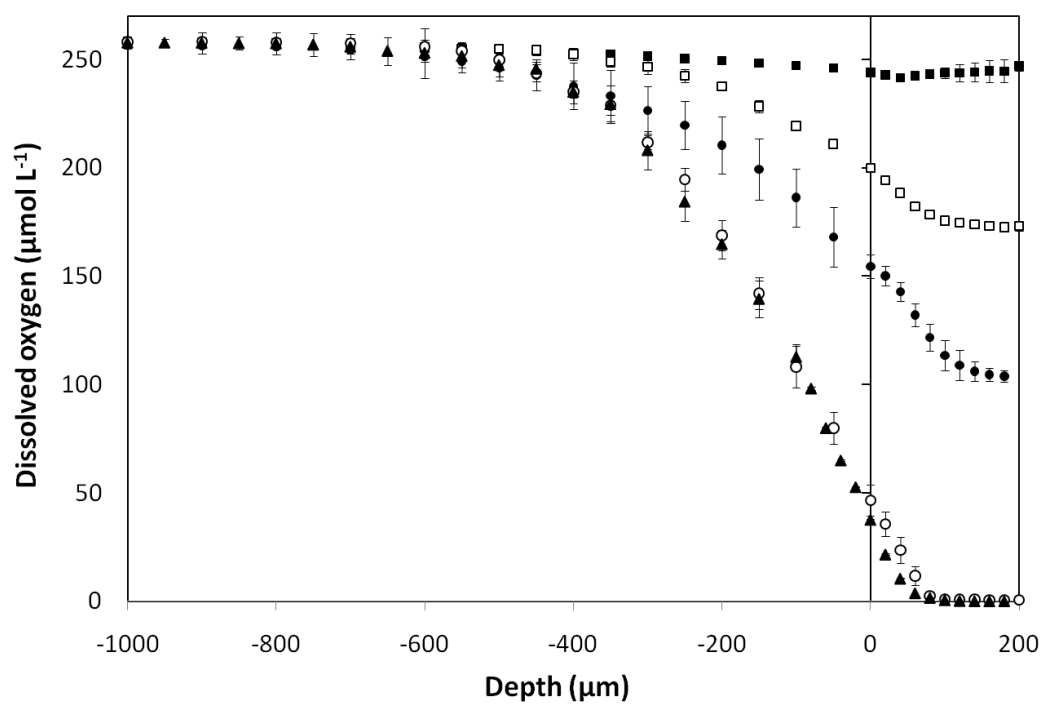
Figure 5.7. Model simulations of DO profiles with low NH_3 concentrations from Study 2. **A)** Model results with $K_m = 1.5$ µM NH_3 and $k_{max}X = 0.025$ mol $L^{-1}s^{-1}$ **B)** Model results with $K_m = 40$ µM NH_3 and $k_{max}X = 0.25$ mol $L^{-1}s^{-1}$. Microsensor data consists of: 0.05 (●), 0.1 (Δ), 0.25 (○), and 5 (▲) mmol L^{-1} NH_4-N. Lines represent model results of 0.05 (solid), 0.1 (long dash), 0.25 (dash dot), and 5 (short dash) mmol L^{-1} NH_4-N.
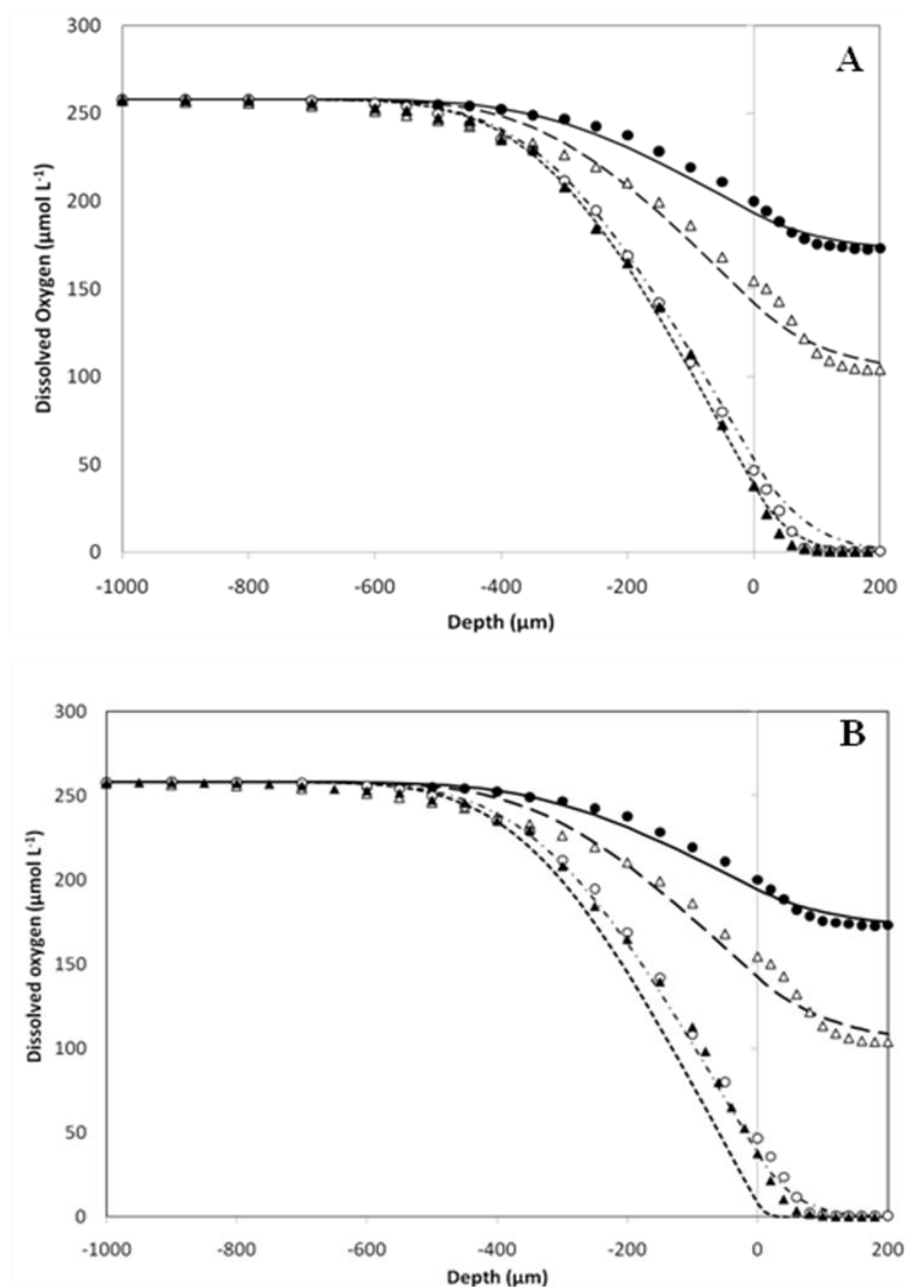
Figure 5.8. DO and pH measured profile data from study 3 with 1 mM HEPES buffer. **A)** DO and **B)** pH profiles. Data for 0.5 mM (▲), 1.5 mM (○), and 5 mM NH₄-N (●).
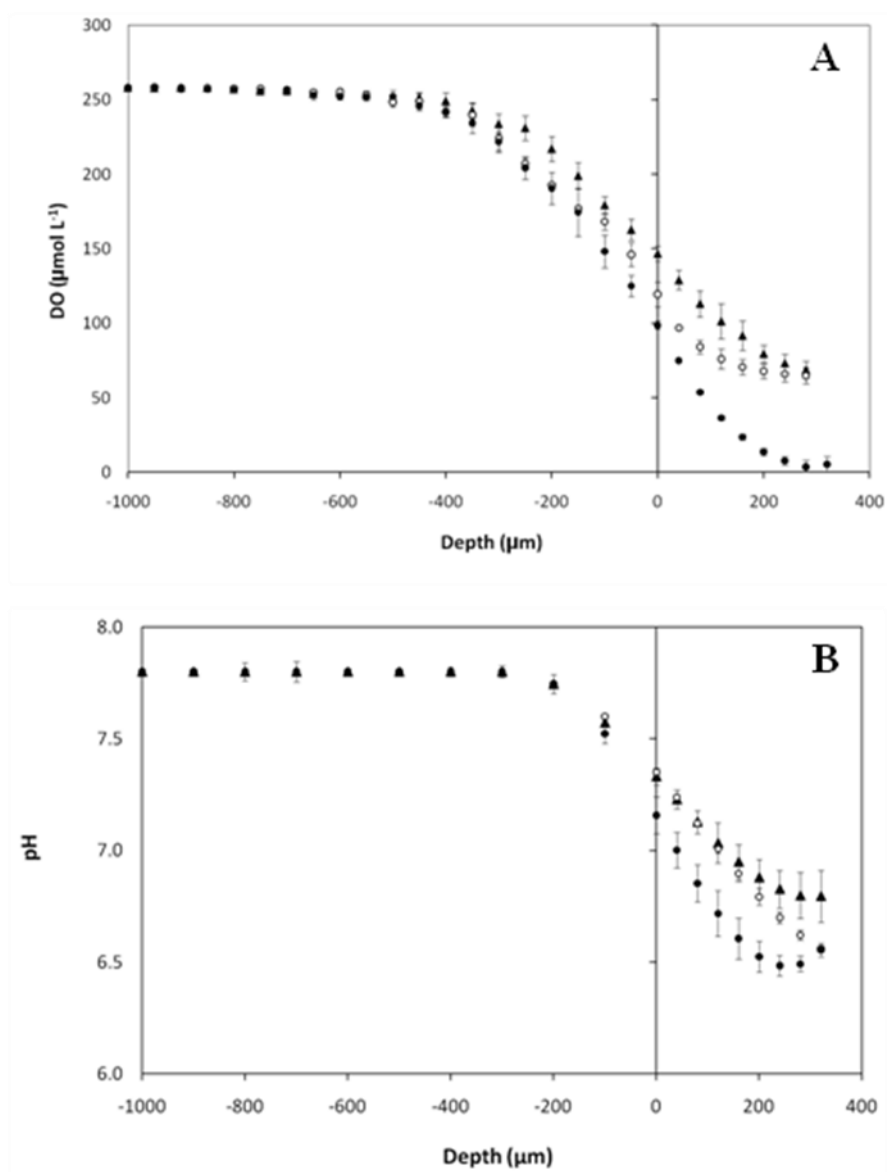
Figure 5.9. Model simulations of profiles from study 3 with 1 mM HEPES buffer, using K_m = 40 μM NH_3 and $k_{max}X$ = 0.025 mol $L^{-1}s^{-1}$. **A)** Dissolved oxygen and **B)** pH profiles. Data for 0.5 mM (▲), 1.5 mM (○), and 5 mM NH_4-N (●). **C and D)** Predicted profiles of **C)** NH_3 and **D)** NO_2^- from model simulations. Lines are model results for 0.5 mM (solid), 1.5 mM (long dash), and 5 mM NH_4-N (short dash).
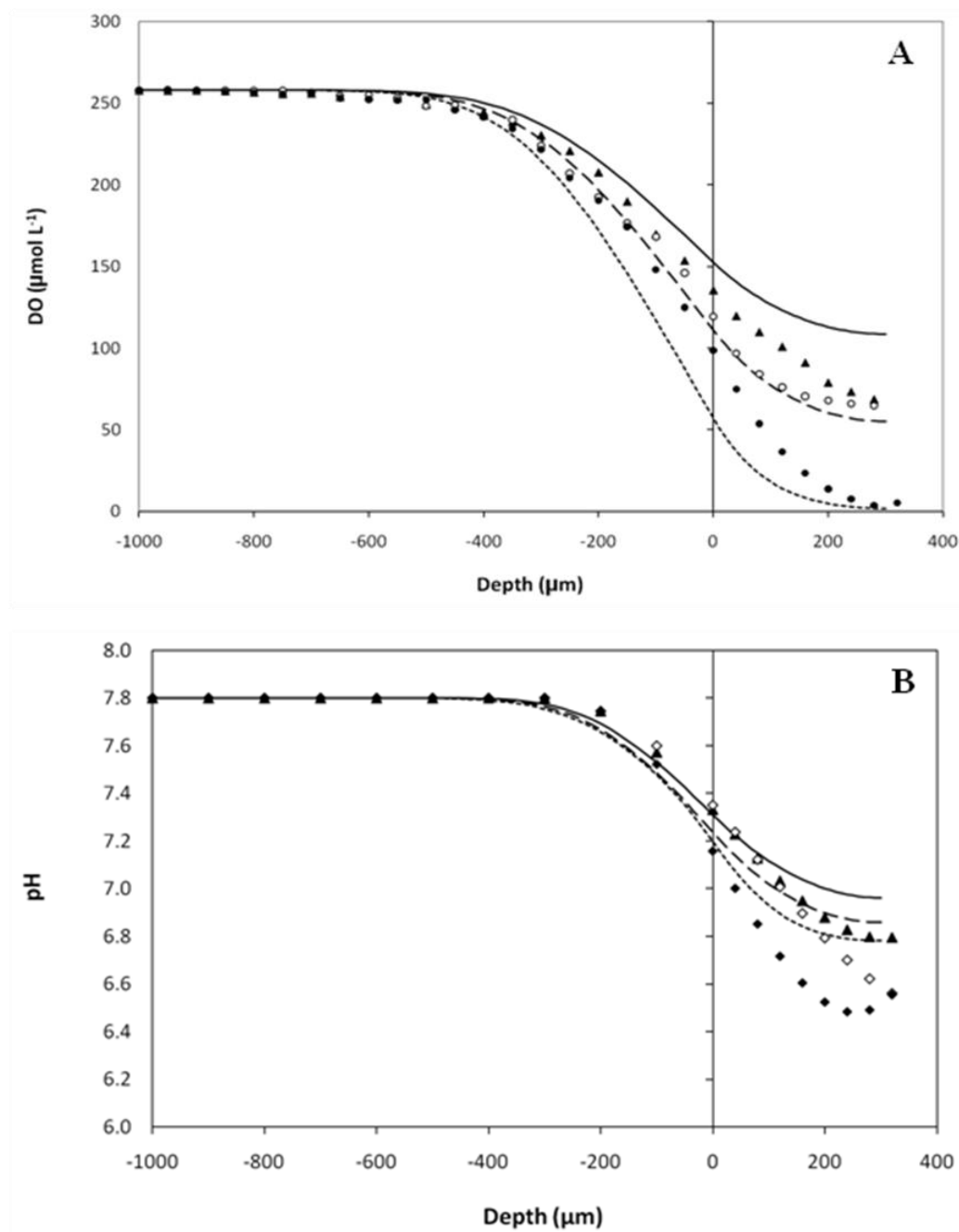
Figure 5.9. (Continued)
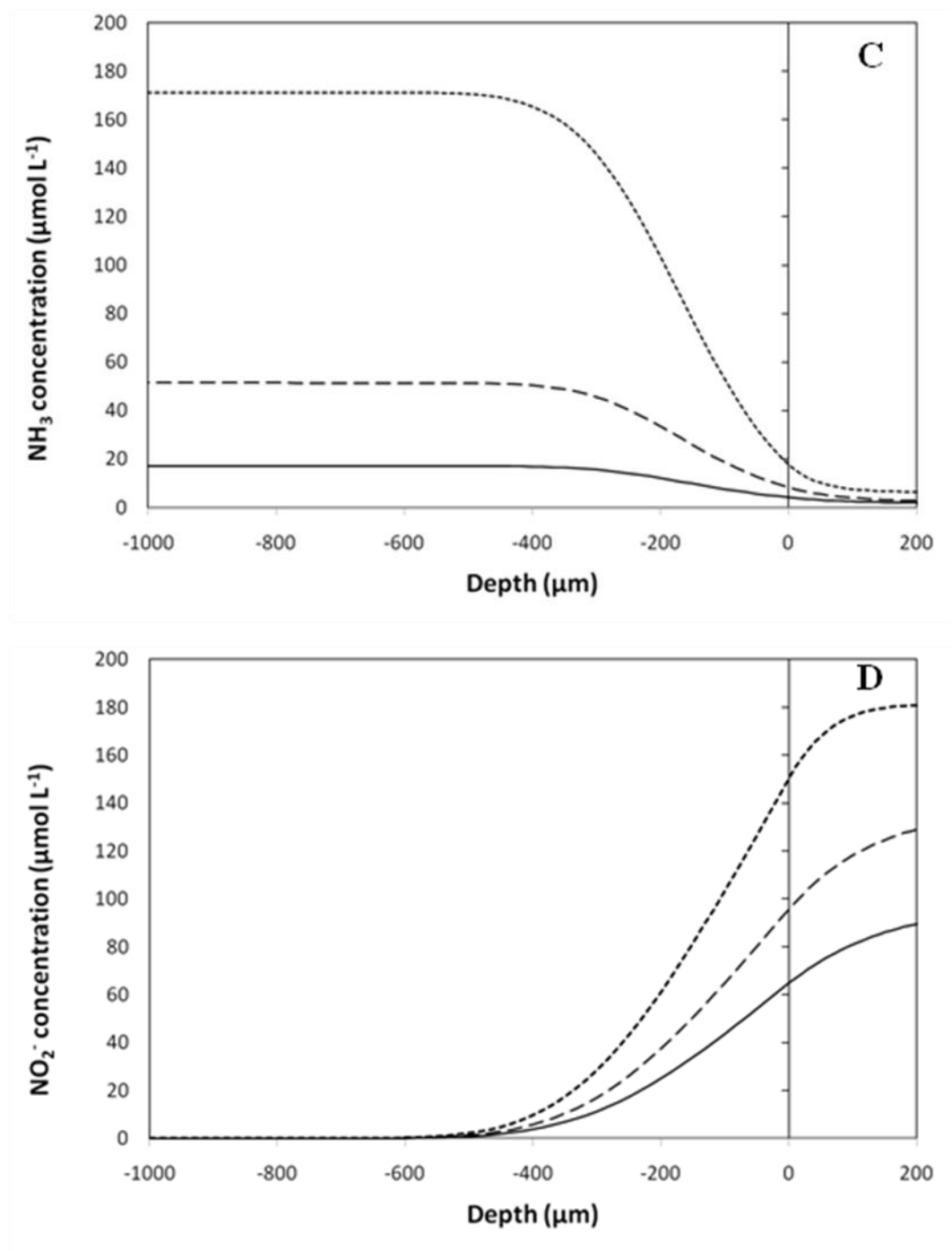
Table 5.3. Kinetic parameters determined with model simulations

	K_m	K_o	k_{max}	X
	μmol L^{-1}	μmol L^{-1}	mol mg protein^{-1} s^{-1}	mg prot. L^{-1}
Batch model	40	NA	0.05	0.0057
1-D Biofilm model	40	0.015	0.045	0.5
2-D Biofilm Study 1	40	0.01	0.05	0.5
2-D Biofilm Study 2	1.5	0.01	0.05	0.5
	40	0.01	0.05	5
2-D Biofilm Study 3	40	0.01	0.05	0.45

Chapter Six

Summary

Increasing attention is being paid to nitrogen removal processes in wastewater and the bacterial species that carry out the transformations involved in nitrification, especially the oxidation of NH_3 to NO_2^-. While *Nitrosomonas europaea* is a well characterized ammonia oxidizing bacterium, only recently have tools been available to study the organism's gene expression under various conditions. Little is known about the physiological and transcriptional behavior of *N. europaea* in biofilms, which is important for potential applications of real-time monitoring systems based on the transcriptional response of *N. europaea* to inhibitors. The relationship between kinetics and mass transport in biofilms of *N. europaea* also has implications for understanding the inhibition of NH_3 oxidation in engineered attached growth systems during exposure to contaminants, such as aromatic hydrocarbons.

The research in this dissertation first explored the transcriptional and physiological responses of *N. europaea* biofilms to the aromatic hydrocarbons phenol and toluene. Biofilms of *N. europaea* experienced less inhibition of NH_3 oxidation than suspended cells grown in batch reactors when exposed to the same concentrations of phenol and toluene. The rates of NH_3 oxidation were an order of magnitude lower in the biofilms than in suspended cells. However, cells from the biofilm quickly increased NH_3 oxidation rates upon being removed from the biofilm and dispersed into batch reactors. When exposed to phenol and toluene, the previously biofilm-grown cells exhibited similar inhibition as batch cells. The transcriptional profiles of the biofilms identified potential sentinel genes NE1545 and NE1546 up-regulated during phenol exposure and no genes up-regulated in response to toluene, which was the same in batch cells. However, the level of up-regulation of the gene NE1545 increased in batch cells with higher phenol concentrations, while it remained at a constant level in the biofilms.

Although the transcriptional responses to phenol and toluene were the same in batch and biofilm cells, the basal transcriptional profiles were found to be different

between the two growth phases, revealing 240 genes that were differentially expressed between biofilms and exponential growth batch cells. It was of interest to determine if conditions of slow growth or stationary phase in suspended cells also induced the gene expression observed in the biofilms. A subset of 10 genes identified from the biofilm microarrays were tracked in suspended cells cultivated at various dilution rates. The genes identified in the biofilm microarrays were increasingly up-regulated with decreasing dilution rate. The same biofilm genes were tracked in batch suspended cells and also showed up-regulation in batch cultures upon entry into stationary phase. The level of up-regulation in the suspended cells was inversely related to the rate of NH_3 oxidation, indicating that the expression was more related to factors associated with slow growth instead of biofilm specific. In the slow growth reactors that exhibited up-regulation, the limitation of nutrients or accumulation of microbial products may have been influential factors in the gene expression. The observed trend also suggests that physiology of the cells in biofilms is potentially similar to stationary phase growth or slower growth rates of suspended cells.

The similarities observed in the gene expression between biofilms and stationary growth phase cells provided an incentive to examine the inhibitory response to phenol with respect to growth rate as well. Phenol inhibition of NH_3 oxidation in batch suspended cells was compared to continuous cultures in a range of dilution rates, revealing that the inhibition did in fact change with the growth rate of the cells. The inhibition, normalized to the rate of NH_3 oxidation rate in control cells, decreased with lower NH_3 oxidation activity, with the slowest dilution rates of suspended cultures exhibiting activity and inhibition similar to that observed in biofilms.

The result that phenol inhibition decreased with decreasing NH_3 oxidation rate proved to be the same in biofilms as well as suspended cells. In biofilms of *N. europaea,* a correlation between growth rate and phenol inhibition was investigated by increasing or decreasing DO supply to the biofilms and thus changing their rates of NH_3 oxidation. The results led to the conclusion that rate of NH_3 oxidation is a key controlling factor in the phenol inhibition and the observed biofilm protection from

phenol resulted from slow activity of the cells, which was caused by substrate depletion in the biofilms due to mass transport limitation.

The biofilm activity was dependent upon the DO availability and NH_3 oxidation increased with elevated O_2 in the headspace. However, the concentrations of substrates in biofilms were lower than measured in the bulk fluid, due to diffusive transport limitation which creates substrate gradients in the biofilm. Therefore, to examine the kinetics of the biofilm cells in more detail, the actual concentrations of DO in the biofilms were measured with microsensors.

The microsensor measurements of DO concentration profiles in the biofilms also enabled the use of a reactive transport model to analyze the kinetic parameters in the biofilms. A 2-D biofilm model was created to simulate the DO profiles and predict the concentrations of other species in the biofilms. The model revealed that a simplified kinetic model with uniform biomass was able to simulate the DO concentration profiles in the biofilms. Additionally, in a low buffered medium where pH reduction was measured with microsensors, the model was able to simulate the pH shift and DO profiles simultaneously, using the same kinetic parameters as in the biofilms at constant pH. In the model, the substrate affinity for NH_3 was the same as in batch experiments, although the maximum rate constant had to be calibrated to simulate the DO profiles.

Based on the model results, no significant differences were found between the kinetics of cells in the biofilms and suspended cells of *N. europaea*. The differences between the two growth states lie in the environmental differences created by mass transport limitations in the biofilms, which create substrate limitations. The findings that gene expression and inhibition properties are similar in slow growing suspended cells and biofilms suggests that growth rate in the biofilm is more of a factor than attached growth properties.

The findings presented in this dissertation show that the physiology of *N. europaea* may be more influenced by rates of NH_3 oxidation than attached or suspended growth. In suspended cells of *N. europaea*, decreasing dilution rates,

which resulted in lower rates of NH_3 oxidation, were related to decreasing phenol inhibition and increasing up-regulation of genes from the biofilm microarray. The phenol tolerance increased with slower NH_3 oxidation rates of the cells in both biofilms and suspended cultures.

The findings of this research are significant for the understanding of processes occurring in biofilms, especially as they relate to nitrification. They will also apply to engineered systems such as wastewater treatment plants, where both suspended and attached biomass reactors are used in treatment processes. In the attached growth reactors, the substrate limitations inside the biofilms resulted in lower metabolism of the cells and thus less inhibition by phenol or toluene. The observed and modeled transport limitations in the biofilms were a significant factor affecting the metabolism of the cells and thus the inhibition of NH_3 oxidation. The biofilm model that was created in this work serves as a useful tool for investigating mass transport in biofilms, and the methodology used to examine the kinetics with a 2-D biofilm model and microsensors can be applied to other systems.

The research in this dissertation indicates that the phenol tolerance observed early on in the biofilm studies was actually a result of reduced metabolic activity in the biofilm cells, which also caused phenol tolerance in suspended cells. The correlation between suspended cell growth rates and up-regulation of biofilm-expressed genes also shows that the metabolic state was a factor in transcription. The DO profiles and the model indicate that NH_3 oxidation rates in the biofilms are limited due to mass transport limitation of substrates. These results suggest that the physiology, inhibition and gene expression of *N. europaea* in suspended and biofilm reactors may be mostly influenced by the rates of NH_3 oxidation and growth in the cells, which is dictated by mass transport of substrates in the reactors.

Recommendations for ongoing research of *N. europaea* biofilms include incorporation of an inhibition model into the existing biofilm model, which could describe the inhibition of O_2 uptake by the biofilms and the change in the DO concentration profile during phenol exposure. Additionally, similar experiments can

be undertaken with other inhibitory compounds, to determine if the relationship between growth rate and inhibition is present with other classes of inhibitors of NH_3 oxidation.

Bibliography

1. **Allison, S. M., and J. I. Prosser.** 1993. Ammonia oxidation at low pH by attached populations of nitrifying bacteria. Soil Biology & Biochemistry **25:**935-941.

2. **Amor, L., M. Eiroa, C. Kennes, and M. C. Veiga.** 2005. Phenol biodegradation and its effect on the nitrification process. Water Research **39:**2915-2920.

3. **Anderl, J. N., M. J. Franklin, and P. S. Stewart.** 2000. Role of antibiotic penetration limitation in *Klebsiella pneumoniae* biofilm resistance to ampicillin and ciprofloxacin. Antimicrobial Agents and Chemotherapy **44:**1818-1824.

4. **Arp, D. J., L. A. Sayavedra-Soto, and N. G. Hommes.** 2002. Molecular biology and biochemistry of ammonia oxidation by *Nitrosomonas europaea*. Archives of Microbiology **178:**250-255.

5. **Artiga, P., V. Oyanedel, J. M. Garrido, and R. Mendez.** 2003. A novel titrimetric method for monitoring toxicity on nitrifying biofilms. Water Science and Technology **47:**205-209.

6. **Batchelor, S. E., M. Cooper, S. R. Chhabra, L. A. Glover, G. S. A. B. Stewart, P. Williams, and J. I. Prosser.** 1997. Cell density-regulated recovery of starved biofilm populations of ammonia-oxidizing bacteria. Applied and Environmental Microbiology **63:**2281-2286.

7. **Bedient, P. B., H. S. Rifai, and C. J. Newell.** 1994. Ground Water Contamination: Transport and Remediation. PRT Prentice-Hall, Inc., New Jersey.

8. **Beenken, K. E., P. M. Dunman, F. McAleese, D. Macapagal, E. Murphy, S. J. Projan, J. S. Blevins, and M. S. Smeltzer.** 2004. Global gene expression in *Staphylococcus aureus* biofilms. Journal of Bacteriology **186:**4665-4684.

9. **Beloin, C., and J. M. Ghigo.** 2005. Finding gene-expression patterns in bacterial biofilms. Trends in Microbiology **13:**16-19.

10. **Beloin, C., J. Valle, P. Latour-Lambert, P. Faure, M. Kzreminski, D. Balestrino, J. A. J. Haagensen, S. Molin, G. Prensier, B. Arbeille, and J. M. Ghigo.** 2004. Global impact of mature biofilm lifestyle on *Escherichia coli* K-12 gene expression. Molecular Microbiology **51:**659-674.

11. **Bernet, N., O. Sanchez, D. Cesbron, J. P. Steyer, and J. P. Delgenes.** 2005. Modeling and control of nitrite accumulation in a nitrifying biofilm reactor. Biochemical Engineering Journal **24:**173-183.

12. **Bolstad, B. M., R. A. Irizarry, M. Astrand, and T. P. Speed.** 2003. A comparison of normalization methods for high density oligonucleotide array data based on variance and bias. Bioinformatics **19:**185-193.

13. **Borriello, G., E. Werner, F. Roe, A. M. Kim, G. D. Ehrlich, and P. S. Stewart.** 2004. Oxygen limitation contributes to antibiotic tolerance of Pseudomonas aeruginosa in biofilms. Antimicrobial Agents and Chemotherapy **48:**2659-2664.

14. **Buckingham-Meyer, K., D. M. Goeres, and M. A. Hamilton.** 2007. Comparative evaluation of biofilm disinfectant efficacy tests. Journal of Microbiological Methods **70:**236-244.

15. **Burton, E. O., H. W. Read, M. C. Pellitteri, and W. J. Hickey.** 2005. Identification of acyl-homoserine lactone signal molecules produced by *Nitrosomonas europaea* strain Schmidt. Applied and Environmental Microbiology **71:**4906-4909.

16. **Carrera, J., I. Jubany, L. Carvallo, R. Chamy, and J. Lafuente.** 2004. Kinetic models for nitrification inhibition by ammonium and nitrite in a suspended and an immobilised biomass systems. Process Biochemistry **39:**1159-1165.

17. **Chain, P., J. Lamerdin, F. Larimer, W. Regala, V. Lao, M. Land, L. Hauser, A. Hooper, M. Klotz, J. Norton, L. Sayavedra-Soto, D. Arciero, N. Hommes, M. Whittaker, and D. Arp.** 2003. Complete genome sequence of the ammonia-oxidizing bacterium and obligate chemolithoautotroph *Nitrosomonas europaea*. Journal of Bacteriology **185:**2759-2773.

18.   **Chandran, K., and N. G. Love.** 2008. Physiological state, growth mode, and oxidative stress play a role in Cd(II)-mediated inhibition of *Nitrosomonas europaea* 19718. Applied and Environmental Microbiology **74:**2447-2453.

19.   **Chang, S. W., M. R. Hyman, and K. J. Williamson.** 2002. Cooxidation of naphthalene and other polycyclic aromatic hydrocarbons by the nitrifying bacterium, *Nitrosomonas europaea*. Biodegradation **13:**373-381.

20.   **Chomczynski, P., and N. Sacchi.** 1987. Single-step method of RNA isolation by acid guanidinium thiocyanate phenol chloroform extraction. Analytical Biochemistry **162:**156-159.

21.   **Cornish-Bowden, A.** 2004. Fundamentals of Enzyme Kinetics, 3rd edition. Portland Press Ltd, London.

22.   **Costerton, J. W., P. S. Stewart, and E. P. Greenberg.** 1999. Bacterial biofilms: A common cause of persistent infections. Science **284:**1318-1322.

23.   **Cussler, E. L.** 1997. Diffusion: Mass transfer in fluid systems 2nd ed. Cambridge University Press, Cambridge.

24.   **Davies, D. G., M. R. Parsek, J. P. Pearson, B. H. Iglewski, J. W. Costerton, and E. P. Greenberg.** 1998. The involvement of cell-to-cell signals in the development of a bacterial biofilm. Science **280:**295-298.

25.   **Downing, L. S., and R. Nerenberg.** 2008. Effect of Oxygen Gradients on the Activity and Microbial Community Structure of a Nitrifying, Membrane-Aerated Biofilm. Biotechnology and Bioengineering **101:**1193-1204.

26.   **Eberl, H. J., and R. Sudarsan.** 2008. Exposure of biofilms to slow flow fields: The convective contribution to growth and disinfection. Journal of Theoretical Biology **253:**788-807.

27.   **Ely, R. L., K. J. Williamson, M. R. Hyman, and D. J. Arp.** 1997. Cometabolism of chlorinated solvents by nitrifying bacteria: kinetics, substrate interactions, toxicity effects, and bacterial response. Biotechnology and Bioengineering **54:**520-534.

28.   **EPA, U. S.** 2009. Nutrient Control Design Manual: State of Technology Review Report. EPA/600/R-09/012 EPA/600/R-09/012. U. S. Environmental Protection Agency.

29.   **EPA, U. S.** 1993. Process Design Manual: Nitrogen Control. 625/R-93/010. U. S. Environmental Protection Agency.

30.   **Evans, D. J., D. G. Allison, M. R. W. Brown, and P. Gilbert.** 1991. Susceptibility of Pseudomonas-Aeruginosa and Escherichia-Coli Biofilms Towards Ciprofloxacin - Effect of Specific Growth-Rate. Journal of Antimicrobial Chemotherapy **27:**177-184.

31.   **Fux, C. A., J. W. Costerton, P. S. Stewart, and P. Stoodley.** 2005. Survival strategies of infectious biofilms. Trends in Microbiology **13:**34-40.

32.   **Gernaey, K., L. Verschuere, L. Luyten, and W. Verstraete.** 1997. Fast and sensitive acute toxicity detection with an enrichment nitrifying culture. Water Environment Research **69:**1163-1169.

33.   **Gieseke, A., L. Bjerrum, M. Wagner, and R. Amann.** 2003. Structure and activity of multiple nitrifying bacterial populations co-existing in a biofilm. Environmental Microbiology **5:**355-369.

34.   **Gieseke, A., and D. deBeer.** 2004. Use of microelectrodes to measure in situ microbial activities in biofilms, sediments, and microbial mats. *In* G. A. Kowalchuk, F. de Bruijn, I. Head, A. Akkermans, and J. van Elsas (ed.), Molecular microbial ecology manual, 2nd ed. Springer, Heidelberg.

35.   **Gvakharia, B. O., P. J. Bottomley, D. J. Arp, and L. A. Sayavedra-Soto.** 2009. Construction of recombinant *Nitrosomonas europaea* expressing green fluorescent protein in response to co-oxidation of chloroform. Applied Microbiology and Biotechnology **82:**1179-1185.

36.   **Gvakharia, B. O., E. A. Permina, M. S. Gelfand, P. J. Bottomley, L. A. Sayavedra-Soto, and D. J. Arp.** 2007. Global transcriptional response of *Nitrosomonas europaea* to chloroform and chloromethane. Applied and Environmental Microbiology **73:**3440-3445.

37.   **Hageman, R. H., and D. P. Hucklesby.** 1971. Nitrate reductase from higher plants. Methods in Enzymology **23:**491-503.

38. **Hengge, R.** 2009. Principles of c-di-GMP signalling in bacteria. Nature Reviews Microbiology **7:**263-273.

39. **Hyman, M. R., and D. J. Arp.** 1995. Effects of ammonia on the *de novo* synthesis of polypeptides in cells of *Nitrosomonas europaea* denied ammonia as an energy source. Journal of Bacteriology **177:**4974-4979.

40. **Hyman, M. R., S. A. Russell, R. L. Ely, K. J. Williamson, and D. J. Arp.** 1995. Inhibition, inactivation, and recovery of ammonia-oxidizing activity in cometabolism of trichloroethylene by *Nitrosomonas europaea*. Applied and Environmental Microbiology **61:**1480-1487.

41. **Hyman, M. R., A. W. Sansome-Smith, J. H. Shears, and P. M. Wood.** 1985. A kinetic-study of benzene oxidation to phenol by whole cells of *Nitrosomonas europaea* and evidence for the further oxidation of phenol to hydroquinone. Archives of Microbiology **143:**302-306.

42. **Iizumi, T., M. Mizumoto, and K. Nakamura.** 1998. A bioluminescence assay using Nitrosomonas europaea for rapid and sensitive detection of nitrification inhibitors. Applied and Environmental Microbiology **64:**3656-3662.

43. **Irizarry, R. A., B. M. Bolstad, F. Collin, L. M. Cope, B. Hobbs, and T. P. Speed.** 2003. Summaries of affymetrix GeneChip probe level data. Nucleic Acids Research **31:**e15.

44. **Keener, W. K., and D. J. Arp.** 1993. Kinetic-studies of ammonia monooxygenase inhibition in *Nitrosomonas europaea* by hydrocarbons and halogenated hydrocarbons in an optimized whole-cell assay. Applied and Environmental Microbiology **59:**2501-2510.

45. **Keener, W. K., and D. J. Arp.** 1994. Transformations of aromatic compounds by *Nitrosomonas europaea*. Applied and Environmental Microbiology **60:**1914-1920.

46. **Konig, A., K. Riedel, and J. W. Metzger.** 1998. A microbial sensor for detecting inhibitors of nitrification in wastewater. Biosensors & Bioelectronics **13:**869-874.

47.   **Kreft, J. U., C. Picioreanu, J. W. T. Wimpenny, and M. C. M. van Loosdrecht.** 2001. Individual-based modelling of biofilms. Microbiology-Sgm **147:**2897-2912.

48.   **Laanbroek, H. J., P. L. E. Bodelier, and S. Gerards.** 1994. Oxygen-Consumption Kinetics of Nitrosomonas-Europaea and Nitrobacter-Hamburgensis Grown in Mixed Continuous Cultures at Different Oxygen Concentrations. Archives of Microbiology **161:**156-162.

49.   **Laanbroek, H. J., and S. Gerards.** 1993. Competition for Limiting Amounts of Oxygen between Nitrosomonas-Europaea and Nitrobacter-Winogradskyi Grown in Mixed Continuous Cultures. Archives of Microbiology **159:**453-459.

50.   **Lauchnor, E. G., T. S. Radniecki, and L. Semprini.** 2011. Inhibition and gene expression of *Nitrosomonas europaea* biofilms exposed to phenol and toluene. Biotechnology and Bioengineering **108:**750-757.

51.   **Lauchnor, E. G., T. S. Radniecki, and L. Semprini.** In press. Inhibition and gene expression of *Nitrosomonas europaea* biofilms exposed to phenol and toluene. Biotechnology and Bioengineering**:**DOI: 10.1002/bit.22999.

52.   **Lazazzera, B. A.** 2005. Lessons from DNA microarray analysis: the gene expression profile of biofilms. Current Opinion in Microbiology **8:**222-227.

53.   **Lenz, A. P., K. S. Williamson, B. Pitts, P. S. Stewart, and M. J. Franklin.** 2008. Localized gene expression in *Pseudomonas aeruginosa* biofilms. Applied and Environmental Microbiology **74:**4463-4471.

54.   **Li, J., and P. L. Bishop.** 2002. In situ identification of azo dye inhibition effects on nitrifying biofilms using microelectrodes. Water Science and Technology **46:**207-214.

55.   **Lide, D. R.** 2007. CRC Handbook of Chemistry and Physics, 88th ed. CRC Press, Boca Raton, FL.

56.   **Llorens, J. M. N., A. Tormo, and E. Martinez-Garcia.** 2010. Stationary phase in gram-negative bacteria. Fems Microbiology Reviews **34:**476-495.

57.   **Mah, T. F. C., and G. A. O'Toole.** 2001. Mechanisms of biofilm resistance to antimicrobial agents. Trends in Microbiology **9:**34-39.

58.   **Martens-Habbena, W., P. M. Berube, H. Urakawa, J. R. de la Torre, and D. A. Stahl.** 2009. Ammonia oxidation kinetics determine niche separation of nitrifying Archaea and Bacteria. Nature **461:**976-U234.

59.   **McCarty, P. L., and T. E. Meyer.** 2005. Numerical model for biological fluidized-bed reactor treatment of perchlorate-contaminated groundwater. Environmental Science & Technology **39:**850-858.

60.   **Morgenroth, E., H. J. Eberl, M. C. M. van Loosdrecht, D. R. Noguera, G. E. Pizarro, C. Picioreanu, B. E. Rittmann, A. O. Schwarz, and O. Wanner.** 2004. Comparing biofilm models for a single species biofilm system. Water Science and Technology **49:**145-154.

61.   **Morita, M., N. Kudo, H. Uemoto, A. Watanabe, and H. Shinozaki.** 2007. Protective effect of immobilized ammonia oxidizers and phenol-degrading bacteria on nitrification in ammonia- and phenol-containing wastewater. Engineering in Life Sciences **7:**587-592.

62.   **Nicolella, C., M. C. M. van Loosdrecht, and J. J. Heijnen.** 2000. Wastewater treatment with particulate biofilm reactors. Journal of Biotechnology **80:**1-33.

63.   **O'Toole, G. A., and R. Kolter.** 1998. Flagellar and twitching motility are necessary for *Pseudomonas aeruginosa* biofilm development. Molecular Microbiology **30:**295-304.

64.   **Okabe, S., H. Naitoh, H. Satoh, and Y. Watanabe.** 2002. Structure and function of nitrifying biofilms as determined by molecular techniques and the use of microelectrodes. Water Science and Technology **46:**233-241.

65.   **Okabe, S., H. Satoh, and Y. Watanabe.** 1999. In situ analysis of nitrifying biofilms as determined by in situ hybridization and the use of microelectrodes. Applied and Environmental Microbiology **65:**3182-3191.

66.   **Park, S., and W. Bae.** 2009. Modeling kinetics of ammonium oxidation and nitrite oxidation under simultaneous inhibition by free ammonia and free nitrous acid. Process Biochemistry **44:**631-640.

67.   **Park, S., W. Bae, and B. E. Rittmann.** 2010. Multi-Species Nitrifying Biofilm Model (MSNBM) Including Free Ammonia and Free Nitrous Acid

Inhibition and Oxygen Limitation. Biotechnology and Bioengineering **105:**1115-1130.

68. **Park, S., and R. L. Ely.** 2008. Candidate stress genes of *Nitrosomonas europaea* for monitoring inhibition of nitrification by heavy metals. Applied and Environmental Microbiology **74:**5475-5482.

69. **Park, S., and R. L. Ely.** 2008. Genome-wide transcriptional responses of *Nitrosomonas europaea* to zinc. Archives of Microbiology **189:**541-548.

70. **Peirson, S. N., J. N. Butler, and R. G. Foster.** 2003. Experimental validation of novel and conventional approaches to quantitative real-time PCR data analysis. Nucleic Acids Research **31:**e73.

71. **Peirson, S. N., J. N. Butler, and R. G. Foster.** 2003. Experimental validation of novel and conventional approaches to quantitative real-time PCR data analysis. Nucleic Acids Research **31:**-.

72. **Perez, J., E. Costa, and J. U. Kreft.** 2009. Conditions for Partial Nitrification in Biofilm Reactors and a Kinetic Explanation. Biotechnology and Bioengineering **103:**282-295.

73. **Perez, J., C. Picioreanu, and M. van Loosdrecht.** 2005. Modeling biofilm and floc diffusion processes based on analytical solution of reaction-diffusion equations. Water Research **39:**1311-1323.

74. **Picioreanu, C., M. C. M. van Loosdrecht, and J. J. Heijnen.** 1999. Discrete-differential modelling of biofilm structure. Water Science and Technology **39:**115-122.

75. **Picioreanu, C., M. C. M. van Loosdrecht, and J. J. Heijnen.** 2000. A theoretical study on the effect of surface roughness on mass transport and transformation in biofilms. Biotechnology and Bioengineering **68:**355-369.

76. **Powell, S. J., and J. I. Prosser.** 1986. Inhibition of ammonium oxidation by nitrapyrin in soil and liquid culture. Applied and Environmental Microbiology **52:**782-787.

77. **Powell, S. J., and J. I. Prosser.** 1992. Inhibition of biofilm populations of *Nitrosomonas europaea*. Microbial Ecology **24:**43-50.

78.   **Prosser, J. I.** 1989. Autotrophic nitrification in bacteria. Advances in Microbial Physiology **30:**125-181.

79.   **Radniecki, T. S., M. E. Dolan, and L. Semprini.** 2008. Physiological and transcriptional responses of *Nitrosomonas europaea* to toluene and benzene inhibition. Environmental Science & Technology **42:**4093-4098.

80.   **Radniecki, T. S., L. Semprini, and M. E. Dolan.** 2009. Expression of *merA*, *amoA* and *hao* in continuously cultured *Nitrosomonas europaea* cells exposed to zinc chloride additions. Biotechnology and Bioengineering **102:**546-553.

81.   **Rani, S. A., B. Pitts, H. Beyenal, R. A. Veluchamy, Z. Lewandowski, W. M. Davison, K. Buckingham-Meyer, and P. S. Stewart.** 2007. Spatial patterns of DNA replication, protein synthesis, and oxygen concentration within bacterial biofilms reveal diverse physiological states. Journal of Bacteriology **189:**4223-4233.

82.   **Rasche, M. E., R. E. Hicks, M. R. Hyman, and D. J. Arp.** 1990. Oxidation of monohalogenated ethanes and n-chlorinated alkanes by whole cells of *Nitrosomonas europaea*. Journal of Bacteriology **172:**5368-5373.

83.   **Rasche, M. E., M. R. Hyman, and D. J. Arp.** 1991. Factors limiting aliphatic chlorocarbon degradation by *Nitrosomonas europaea* - cometabolic inactivation of ammonia monooxygenase and substrate-specificity. Applied and Environmental Microbiology **57:**2986-2994.

84.   **Ren, D., L. A. Bedzyk, S. M. Thomas, R. W. Ye, and T. K. Wood.** 2004. Gene expression in *Escherichia coli* biofilms. Applied Microbiology and Biotechnology **64:**515-524.

85.   **Revsbech, N. P.** 1989. An Oxygen Microsensor with a Guard Cathode. Limnology and Oceanography **34:**474-478.

86.   **Revsbech, N. P., and B. B. Jorgensen.** 1986. Microelectrodes - Their Use in Microbial Ecology. Advances in Microbial Ecology **9:**293-352.

87.   **Riefler, R. G., and B. F. Smets.** 2003. Comparison of a type curve and a least-squared errors method to estimate biofilm kinetic parameters. Water Research **37:**3279-3285.

88. **Rittmann, B. E.** 1987. Water-Treatment Processes .6. Aerobic Biological Treatment. Environmental Science & Technology **21:**128-136.

89. **Rittmann, B. E., and P. L. McCarty.** 2001. Environmental Biotechnology: Principles and Applications. McGraw-Hill, New York.

90. **Rittmann, B. E., and P. L. Mccarty.** 1980. Model of Steady-State-Biofilm Kinetics. Biotechnology and Bioengineering **22:**2343-2357.

91. **Rittmann, B. E., A. Schwarz, and P. Saez.** 2000. Biofilms applied to hazardous waste treatment, p. 207-234. *In* J. D. Bryers (ed.), Biofilms II: Process Analysis and Applications. Wiley, New York.

92. **Robinson, R. A., and R. H. Stokes.** 1959. Electrolyte Solutions. Butterworths, London.

93. **Satoh, H., Y. Sasaki, Y. Nakamura, S. Okabe, and T. Suzuki.** 2005. Use of microelectrodes to investigate the effects of 2-chlorophenol on microbial activities in biofilms. Biotechnology and Bioengineering **91:**133-138.

94. **Satoh, H., T. Yamakawa, T. Kindaichi, T. Ito, and S. Okabe.** 2006. Community structures and activities of nitrifying and denitrifying bacteria in industrial wastewater-treating biofilms. Biotechnology and Bioengineering **94:**762-772.

95. **Schirmer, T., and U. Jenal.** 2009. Structural and mechanistic determinants of c-di-GMP signalling. Nature Reviews Microbiology **7:**724-735.

96. **Schmidt, I., P. J. M. Steenbakkers, H. J. M. op den Camp, K. Schmidt, and M. S. M. Jetten.** 2004. Physiologic and proteomic evidence for a role of nitric oxide in biofilm formation by *Nitrosomonas europaea* and other ammonia oxidizers. Journal of Bacteriology **186:**2781-2788.

97. **Schramm, A.** 2003. In situ analysis of structure and activity of the nitrifying community in biofilms, aggregates, and sediments. Geomicrobiology Journal **20:**313-333.

98. **Schramm, A., D. de Beer, J. C. van den Heuvel, S. Ottengraf, and R. Amann.** 1999. Microscale distribution of populations and activities of Nitrosospira and Nitrospira spp. along a macroscale gradient in a nitrifying

bioreactor: Quantification by in situ hybridization and the use of microsensors. Applied and Environmental Microbiology **65:**3690-3696.

99. **Spoering, A. L., and K. Lewis.** 2001. Biofilms and planktonic cells of Pseudomonas aeruginosa have similar resistance to killing by antimicrobials. Journal of Bacteriology **183:**6746-6751.

100. **Stein, L. Y., and D. J. Arp.** 1998. Loss of ammonia monooxygenase activity in Nitrosomonas europaea upon exposure to nitrite. Applied and Environmental Microbiology **64:**4098-4102.

101. **Stein, L. Y., D. J. Arp, and M. R. Hyman.** 1997. Regulation of the synthesis and activity of ammonia monooxygenase in Nitrosomonas europaea by altering pH to affect NH3 availability. Applied and Environmental Microbiology **63:**4588-4592.

102. **Suzuki, I., U. Dular, and S. C. Kwok.** 1974. Ammonia or Ammonium Ion as Substrate for Oxidation by Nitrosomonas-Europaea Cells and Extracts. Journal of Bacteriology **120:**556-558.

103. **Tarre, S., and M. Green.** 2004. High-rate nitrification at low pH in suspended- and attached-biomass reactors. Applied and Environmental Microbiology **70:**6481-6487.

104. **van Loosdrecht, M. C. M., J. J. Heijnen, H. Eberl, J. Kreft, and C. Picioreanu.** 2002. Mathematical modelling of biofilm structures. Antonie Van Leeuwenhoek International Journal of General and Molecular Microbiology **81:**245-256.

105. **Waite, R. D., A. Papakonstantinopoulou, E. Littler, and M. A. Curtis.** 2005. Transcriptome analysis of *Pseudomonas aeruginosa* growth: comparison of gene expression in planktonic cultures and developing and mature biofilms. Journal of Bacteriology **187:**6571-6576.

106. **Walters, M. C., F. Roe, A. Bugnicourt, M. J. Franklin, and P. S. Stewart.** 2003. Contributions of antibiotic penetration, oxygen limitation, and low metabolic activity to tolerance of Pseudomonas aeruginosa biofilms to ciprofloxacin and tobramycin. Antimicrobial Agents and Chemotherapy **47:**317-323.

107. **Wanner, O., and W. Gujer.** 1986. A Multispecies Biofilm Model. Biotechnology and Bioengineering **28:**314-328.

108. **Wei, X. M., N. Vajrala, L. Hauser, L. A. Sayavedra-Soto, and D. J. Arp.** 2006. Iron nutrition and physiological responses to iron stress in *Nitrosomonas europaea*. Archives of Microbiology **186:**107-118.

109. **Wei, X. M., T. F. Yan, N. G. Hommes, X. D. Liu, L. Y. Wu, C. McAlvin, M. G. Klotz, L. A. Sayavedra-Soto, J. Z. Zhou, and D. J. Arp.** 2006. Transcript profiles of *Nitrosomonas europaea* during growth and upon deprivation of ammonia and carbonate. FEMS Microbiology Letters **257:**76-83.

110. **Werner, E., F. Roe, A. Bugnicourt, M. J. Franklin, A. Heydorn, S. Molin, B. Pitts, and P. S. Stewart.** 2004. Stratified growth in *Pseudomonas aeruginosa* biofilms. Applied and Environmental Microbiology **70:**6188-6196.

111. **Whiteley, M., M. G. Bangera, R. E. Bumgarner, M. R. Parsek, G. M. Teitzel, S. Lory, and E. P. Greenberg.** 2001. Gene expression in *Pseudomonas aeruginosa* biofilms. Nature **413:**860-864.

112. **Wood, P. M.** 1986. Nitrification as a bacterial energy source, p. 39-62. *In* J. I. Prosser (ed.), Nitrification. Society for General Microbiology (IRL Press), Washington, D. C.

113. **Xu, K. D., G. A. McFeters, and P. S. Stewart.** 2000. Biofilm resistance to antimicrobial agents. Microbiology **146:**547-549.

114. **Xu, K. D., P. S. Stewart, F. Xia, C. T. Huang, and G. A. McFeters.** 1998. Spatial physiological heterogeneity in *Pseudomonas aeruginosa* biofilm is determined by oxygen availability. Applied and Environmental Microbiology **64:**4035-4039.

115. **Yu, R., and K. Chandran.** 2010. Strategies of *Nitrosomonas europaea* 19718 to counter low dissolved oxygen and high nitrite concentrations. BMC Microbiology **10:**1-11.

116. **Yurt, N., H. Beyenal, J. Sears, and Z. Lewandowski.** 2003. Quantifying selected growth parameters of Leptothrix discophora SP-6 in biofilms from oxygen concentration profiles. Chemical Engineering Science **58:**4557-4566.

117. **Zepeda, A., A. C. Texier, E. Razo-Flores, and J. Gomez.** 2006. Kinetic and metabolic study of benzene, toluene and m-xylene in nitrifying batch cultures. Water Research **40:**1643-1649.

118. **Zhou, X. H., H. C. Shi, Q. Cai, M. He, and Y. X. Wu.** 2008. Function of self-forming dynamic membrane and biokinetic parameters' determination by microelectrode. Water Research **42:**2369-2376.

APPENDICES

Appendix A. Supplemental microarray and RT-qPCR results

Table A1. *N. europaea* genes differentially expressed in microarrays of biofilm and suspended cells (exponential growth). *Ratio of biofilm to suspended cell expression, negative fold-change denotes down-regulation in biofilms.

Gene name	Locus tag	FUNCTION	*Fold change	p-value	e-value
Energy production and conversion					
SCO1	NE0509	SCO1/SenC	-4.47	0.0375	
pntAa	NE0859	Alanine dehydrogenase and pyridine nucleotide transhydrogenase	-2.47	0.0374	
	NE1046	Succinate dehydrogenase, cytochrome b subunit	-2.08	0.048	
	NE1274	Cytochrome c, class I	4.65	0.0429	
	NE1493	Cytochrome c, class IC:Cytochrome c, class I	-2.07	0.0371	
rnfB	NE2222	*3Fe-4S ferredoxin:4Fe-4S ferredoxin, iron-sulfur binding domain*	3.00	0.0362	1.0E-84
sdhB	NE2371	succinate dehydrogenase iron-sulfur subunit	-2.13	0.037	
ccmH	NE0770	putative cytochrome C-type biogenesis protein	-2.86	0.0408	
cycH	NE0771	*TPR repeat*	-2.90	0.0395	9.0E-140
bcp	NE0772	bacterioferritin comigratory protein	-6.37	0.0369	
Cell cycle control, mitosis and meiosis					
ccrB	NE1704	camphor resistance protein	2.07	0.0436	
minE	NE1829	cell division topological specificity factor	-3.12	0.0454	
mdrB	NE2066	Cell cycle proteins	2.93	0.0451	
gidA	NE2476	tRNA uridine 5-carboxymethylaminomethyl modification enzyme	-2.48	0.0419	
Amino acid transport and metabolism					
hisH	NE0645	imidazole glycerol phosphate synthase subunit	-2.83	0.0389	
hisB	NE0646	imidazoleglycerol-phosphate dehydratase	-2.20	0.0385	
leuD	NE0687	isopropylmalate isomerase small subunit	-2.36	0.0378	
trpB	NE0693	tryptophan synthase subunit beta	-2.15	0.0427	
	NE0831	phospho-2-dehydro-3-heoxyheptonate aldolase	-2.68	0.043	
leuA1	NE1320	2-isopropylmalate synthase	-3.18	0.0415	
dapD	NE2462	2,3,4,5-tetrahydropyridine-2-carboxylate N-succinyltransferase	-2.23	0.0419	
dapA	NE2403	dihydrodipicolinate synthase	-2.26	0.0369	
Nucleotide transport and metabolism					
ndk	NE0144	nucleoside diphosphate kinase	-4.38	0.039	
gmk	NE2254	Guanylate kinase	-2.13	0.0407	
purF	NE0699	amidophosphoribosyltransferase	-2.16	0.038	
	NE1167	Purine phosphorylase, family protein 1	-2.85	0.043	
	NE2221	dihydroorotate dehydrogenase 2	2.03	0.0438	
	NE1826	Phosphoribosyl transferase	-3.45	0.0427	
hitA	NE0640	HIT (Histidine triad) family	-2.91	0.0433	

Gene name	Locus tag	FUNCTION	*Fold change	p-value	e-value
Carbohydrate transport and metabolism					
	NE0622	*cupin 2 domain-containing protein*	-2.15	0.0375	3.00E-44
	NE0878	*Cupin 2 conserved barrel domain protein*	3.07	0.0492	2.00E-21
ppnK	NE1478	NAD(+)/NADH kinase family protein	2.58	0.0463	
cbbI	NE1743	ribose-5-phosphate isomerase A	-3.23	0.0429	
	NE1809	beta subunit of citrate lyase	-3.63	0.0387	
oenzyme transport and metabolism					
trpG	NE0014	panthranilate synthase component II (glutamine amido-transferase) protein	-3.93	0.0386	
nadA	NE0066	quinolinate synthetase	-2.54	0.044	
panB	NE0072	Ketopantoate hydroxymethyltransferase	2.11	0.0444	
phhB	NE0077	pterin-4-alpha-carbinolamine dehydratase	-4.30	0.0495	
thiG	NE0284	thiazole synthase	-2.94	0.0406	
thiS	NE0285	*thiamine biosynthesis protein*	-2.44	0.039	5.00E-07
	NE0598	*dephospho-CoA kinase*	2.10	0.0441	6.00E-69
metK	NE0659	S-adenosylmethionine synthetase	-2.81	0.038	
ahcY	NE0660	S-adenosyl-L-homocysteine hydrolase	-2.59	0.0484	
cobN	NE0757	cobaltochelatase	3.19	0.0396	
	NE1837	putative chorismate--pyruvate lyase	2.84	0.0361	
ubiG	NE2547	3-demethylubiquinone-9 3-methyltransferase	-3.13	0.0422	
	NE0334	D-isomer specific 2-hydroxyacid dehydrogenase	-2.68	0.0458	
Lipid transport and metabolism					
	NE0149	4-hydroxy-3-methylbut-2-en-1-yl diphosphate synthase	-3.33	0.0367	
accC1	NE0653	biotin carboxylase protein	-2.46	0.0444	
accD	NE0695	Acetyl-CoA carboxylase carboxyl transferase beta subunit	-2.89	0.0378	
	NE1168	Prenyltransferase and squalene oxidase repeats	-4.95	0.0381	
fabZ	NE1708	(3R)-hydroxymyristoyl-ACP dehydratase	-2.14	0.0349	
	NE1649	acyl carrier protein	-6.93	0.039	
fabF1	NE1650	Beta-ketoacyl synthase	-5.72	0.034	
Translation					
rph	NE0276	3' exoribonuclease family	2.27	0.0449	
	NE0190	ADP-glucose pyrophosphorylase	5.15	0.043	
	NE0427	Ribosomal protein L17	-4.14	0.0391	
	NE0762	Ribosome-binding factor A	-2.44	0.039	
rpmA	NE1292	50S ribosomal protein L27	-3.35	0.0387	
rpsB	NE1718	30S ribosomal protein S2	-4.34	0.0377	
rplY	NE1825	50S ribosomal protein L25/general stress protein Ctc	-3.77	0.0436	

Gene name	Locus tag	FUNCTION	*Fold change	p-value	e-value
Transcription					
	NE0554	Sigma factor, ECF subfamily	2.61	0.0436	
cbl	NE0572	transcriptional regulator CysB-like protein	2.27	0.0387	
	NE0896	Helix-turn-helix motif DNA-binding motif-containing protein	2.40	0.0376	
	NE1224	hypothetical protein	-2.85	0.0358	
nrdR	NE1432	Transcriptional regulator NrdR	-4.31	0.0409	
	NE1946	Bacterial regulatory proteins, TetR family	2.46	0.0485	
rpoC	NE2045	DNA-directed RNA polymerase subunit beta'	-2.56	0.0474	
	NE2153	*putative transcriptional regulator*	3.34	0.0408	4.0E-77
Replication, recombination and repair					
cas2	NE0112	*CRISPR-associated Cas2 family protein*	3.22	0.0393	2.00E-23
csm5	NE0119	*CRISPR-associated RAMP Csm5 family protein*	2.05	0.0428	9.00E-35
	NE0271	Transposase IS4 family	2.61	0.0388	
	NE0272	possible transposase	2.92	0.0403	
	NE0341	Transposase IS4 family	2.51	0.037	
	NE0342	possible transposase	2.59	0.0437	
	NE0519	Transposase IS4 family	2.01	0.0364	
	NE0715	possible transposase	2.48	0.0427	
	NE0716	Transposase IS4 family	2.37	0.0399	
	NE1132	transposase	2.35	0.0373	
	NE1223	putative transposase	-2.63	0.0377	
recN	NE1479	ABC transporter:DNA repair protein RecN	3.03	0.0383	
	NE1553	possible transposase	2.23	0.0406	
	NE1585	Transposase IS4 family	2.11	0.0365	
	NE1740	Transposase IS4 family	2.42	0.0401	
	NE1789	Transposase IS4 family	2.02	0.0427	
	NE1843	Integrase, catalytic core	4.89	0.0407	
	NE1990	possible transposase	2.62	0.0389	
intINeu	NE2189	Integron integrase	-2.82	0.0402	
	NE2223	*HhH-GPD:Iron-sulfur cluster loop (FCL)*	3.77	0.0371	4.0E-109
	NE2385	Staphylococcus nuclease (SNase) homologues	4.17	0.0472	
ssb	NE2453	Single-strand binding protein family	-2.57	0.0426	
Cell wall/membrane biogenesis					
cphA	NE0922	Cyanophycin synthetase	-6.04	0.037	
	NE0923	Cyanophycin synthetase	-10.8	0.0356	
	NE1025	Bacterial outer membrane protein	-3.15	0.0422	
lolC/E	NE1057	*lipoprotein releasing system,LolC/E family protein*	3.75	0.0371	2.0E-179
rkpI	NE1332	capsular polysaccharide biosynthesis/export transmembrane	2.16	0.0485	
rkpT1	NE1386	ABC 2 transport system integral membrane protein	2.12	0.0355	
	NE1682	*possible transmembrane protein*	2.44	0.0406	2.0E-140

Gene name	Locus tag	FUNCTION	*Fold change	p-value	e-value
	NE1709	*putative transmembrane protein*	-2.51	0.0473	6.00E-64
	NE2188	hypothetical protein	-2.08	0.0379	
	NE2269	Glycosyl transferase group 1	3.77	0.0392	
gidB	*NE2475*	*16S rRNA methyltransferase GidB*	-2.37	0.0378	2.00E-94

Cell motility

MotA	NE0046	flagellar motor protein MotA	3.36	0.0368	
pilD	NE0597	Prepilin cysteine protease (C20), type IV	3.38	0.0413	
pilC	NE0596	Bacterial type II secretion system protein	3.38	0.0439	
	NE0690	possible transmembrane protein	-3.01	0.0473	
pilW	NE1749	*type IV pilus assembly protein PilW*	4.05	0.0488	3.00E-67
pilV	NE1750	putative pre-pilin leader sequence	2.39	0.0366	
pilT	NE2113	*PilT protein domain protein*	2.14	0.0481	4.00E-39
	NE2159	TPR repeat	-2.99	0.0367	
	NE1609	Bacterial type II secretion system protein E	-2.11	0.0408	
fliT	NE1597	*flagellar protein FliT*	3.91	0.0401	3.00E-19

Posttranslational modification, protein turnover, chaperones

tig	NE0030	trigger factor	-3.04	0.0388	
ppiB	NE0041	Cyclophilin-type peptidyl-prolyl cis-trans isomerase	-4.29	0.0377	
	NE0431	Cytochrome oxidase assembly	2.03	0.0394	
sspA	NE0812	putative sspA; transcription modulator protein	-3.53	0.0387	
	NE0906	ftsH; cell division protein	-3.10	0.0372	
	NE1285	Band 7 protein	-2.12	0.049	
slyD	NE1706	FKBP-type peptidyl-prolyl cis-trans isomerase (PPIase)	-5.00	0.0382	
clpA	NE1733	ClpA, ATP dependent protease, chaperonin	-2.31	0.0379	
clpS	*NE1732*	*ATP-dependent Clp protease adaptor protein ClpS*	-3.03	0.0384	2.00E-47
	NE1911	Glutaredoxin-related protein	-3.81	0.0401	
osmC	NE1944	*OsmC family protein*	4.87	0.04	3.00E-77
	NE2467	Band 7 protein	2.71	0.0379	

Inorganic ion transport and metabolism

	NE0040	Rhodanese/cdc25 fold	-3.10	0.0367	
pcoB	NE0280	possible copper resistance protein B precursor	2.11	0.0407	
	NE0321	*OM ferric siderophore receptor*	2.47	0.0488	1.0E-170
	NE0354	possible TonB protein	2.53	0.0384	
fhuA	NE0556	*TonB-dependent ferrichrome receptor*	3.66	0.0471	2.0E-128
cysW	NE0577	cysW; sulfate transport ABC transporter protein	3.77	0.0445	
cysU	NE0578	*cysU; sulfate transport ABC transporter protein*	4.08	0.0405	3.0E-138
cah	NE0606	carbonic anhydrase	-3.25	0.0382	
fur1	NE0616	Leucine-rich repeat containing ferric uptake regulator	-2.81	0.0435	
	NE0758	*TonB-dependent receptor protein*	2.70	0.038	2.00E-32

Gene name	Locus tag	FUNCTION	*Fold change	p-value	e-value
	NE0977	putative nitrate transport system permease protein	2.93	0.037	
	NE1088	TonB-dependent receptor protein	3.64	0.0387	
	NE1721	TonB-dependent receptor	3.07	0.0428	
	NE1722	Ferric uptake regulator family	3.47	0.0481	
phoU	NE1744	*phosphate uptake regulator, PhoU*	-3.51	0.0389	1.00E-92
katA	NE1886	Catalase	-2.23	0.0436	
	NE1902	putative monovalent cation/H+ antiporter subunit C	2.05	0.0432	
	NE1904	putative monovalent cation/H+ antiporter subunit E	2.43	0.0356	
phaF	NE1905	putative monovalent cation/H+ antiporter subunit F	2.44	0.044	
	NE2140	TonB-dependent receptor protein	2.45	0.0391	
	NE2198	Integral membrane protein, DUF7	3.25	0.0428	
	NE2199	Flavin-containing monooxygenase (FMO)	4.50	0.037	
fecR/pupR	NE0817	*putative transmembrane sensor*	2.47	0.0371	6.00E-51

Secondary metabolites biosynthesis, transport and catabolism

Gene name	Locus tag	FUNCTION	*Fold change	p-value	e-value
	NE0565	hypothetical protein	3.93	0.0481	
	NE0832	*thioesterase superfamily protein*	-2.74	0.0386	2.00E-52
hss	NE1498	putative homospermidine synthase protein	4.08	0.0431	
	NE2304	Isochorismatase hydrolase family	-3.18	0.0479	

General function prediction only

Gene name	Locus tag	FUNCTION	*Fold change	p-value	e-value
	NE0067	*endonuclease/exonuclease/phosphatase*	-2.24	0.0365	2.0E-112
	NE0191	*aminoglycoside phosphotransferase*	5.27	0.044	4.0E-117
	NE0789	*peptidase C39, bacteriocin processing*	4.16	0.0438	1.00E-60
yjgPQ	NE0802	*permease YjgP/YjgQ family protein*	2.22	0.0373	5.0E-146
	NE0932	putative isomerase	-3.65	0.0401	6.00E-27
	NE1049	Ankyrin-repeat	-4.13	0.0404	
	NE1151	sec-independent protein translocase protein TatC	-2.29	0.0373	
hetN	NE1333	Short-chain dehydrogenase/reductase (SDR) superfamily	4.30	0.0385	
	NE1492	hypothetical protein	-2.77	0.0402	
	NE1515	Ankyrin-repeat	-2.29	0.0378	
	NE1897	Peptidase family M48	-4.00	0.0428	
	NE2095	hypothetical protein	-2.70	0.0395	
	NE2144	*Pirin-like*	-2.47	0.0369	8.0E-123
mviN	NE2405	Virulence factor MVIN-like	2.93	0.0375	
	NE2408	DNA internalization-related competence	2.88	0.0385	
	NE2464	Integral membrane protein, DUF6	4.12	0.0373	
	NE2569	*probable transmembrane protein*	2.51	0.0471	1.00E-38

Gene name	Locus tag	FUNCTION	*Fold change	p-value	e-value
Function unknown					
	NE0147	hypothetical protein	-2.26	0.0406	
	NE0151	hypothetical protein	-4.23	0.0401	
	NE0167	hypothetical protein	-3.03	0.0354	
	NE0210	hypothetical protein	-2.25	0.0394	
ybgF	NE0220	*TPR repeat*	-3.33	0.0376	5.00E-71
	NE0432	*putative transmembrane protein*	2.83	0.0471	7.00E-63
	NE0603	*possible transmembrane protein*	3.57	0.0412	3.00E-48
ecnAB	NE0686	*entericidin*	-2.75	0.0354	5.00E-11
rsmE	NE0779	*16S ribosomal RNA methyltransferase*	2.57	0.0459	6.00E-48
	NE0792	hypothetical protein	-3.28	0.0401	
	NE1145	hypothetical protein	-2.55	0.0436	
	NE1302	putative transposase	-2.45	0.047	
	NE1309	hypothetical protein	-2.42	0.0431	
	NE1352	hypothetical protein	5.05	0.0497	
	NE1410	hypothetical protein	-3.76	0.0481	
	NE1428	iron-sulfur cluster insertion protein ErpA	-2.68	0.0383	
	NE1885	DUF202	2.40	0.0472	
	NE2151	hypothetical protein	3.13	0.047	
	NE2471	hypothetical protein	-4.31	0.0426	
Signal transduction mechanisms					
EAL	NE0579	*Diguanylate cyclase/phosphodiesterase domain 2 (EAL)*	2.24	0.0498	2.00E-69
	NE0913	BolA-like protein	-3.46	0.0346	
	NE1124	atoC; response regulatory protein	-2.23	0.037	
	NE1296	cAMP-dependent protein kinase	-4.40	0.0429	
	NE1506	Universal stress protein (Usp)	-2.55	0.0405	
	NE1847	Guanylate cyclase	3.76	0.0386	
EAL	NE1909	Diguanylate cyclase/phosphodiesterase domain 2 (EAL)	3.65	0.0429	
EAL	NE2075	Diguanylate cyclase/phosphodiesterase domain 2 (EAL)	2.21	0.037	
Intracellular trafficking and secretion					
exbD1	NE0352	Biopolymer transport protein	-2.22	0.044	
tatA	NE0639	twin argininte translocase protein A	-2.16	0.0376	
exbB2	NE1171	MotA/TolQ/ExbB proton channel family	-2.24	0.0377	
Defense mechanisms					
mexB	NE0168	multidrug resistance protein	-2.06	0.038	
	NE0919	ABC transporter, fused permease and ATPase domains	-2.39	0.0362	
	NE1784	ABC transporter permease/ATP-binding protein	4.96	0.0427	
	NE1899	ATPase component ABC-type (unclassified) transport system	-2.24	0.0407	

| Gene name	Locus tag	FUNCTION	*Fold change	p-value	e-value
Not in COGs					
	NE0100	General substrate transporters	3.13	0.0363	
	NE0165	hypothetical protein	2.42	0.0401	
	NE0243	hypothetical protein	4.57	0.0422	
	NE0245	hypothetical protein	3.11	0.048	
	NE0289	Helix-turn-helix protein, CopG family	-2.83	0.0486	
mnxG	NE0315	multicopper oxidase	-2.47	0.0442	
	NE0319	hypothetical protein	2.45	0.0396	
	NE0363	hypothetical protein	-3.70	0.0441	
	NE0372	hypothetical protein	-2.41	0.0375	
	NE0508	hypothetical protein	-2.97	0.0367	
	NE0605	hypothetical protein	-3.94	0.047	
	NE0740	hypothetical protein	-2.23	0.0475	
	NE0784	hypothetical protein	-2.38	0.0381	
	NE0788	hypothetical protein	5.82	0.0406	
	NE0806	hypothetical protein	-2.46	0.038	
	NE1058	hypothetical protein	4.79	0.0471	
ccdB	NE1076	putative CcdB-like protein	2.50	0.0381	
	NE1232	hypothetical protein	-2.38	0.0376	
	NE1235	hypothetical protein	-2.40	0.037	
	NE1236	hypothetical protein	-2.04	0.044	
	NE1379	hypothetical protein	-3.78	0.0399	
	NE1442	hypothetical protein	2.70	0.0383	
	NE1504	hypothetical protein	-3.36	0.0431	
	NE1513	hypothetical protein	2.69	0.0402	
	NE1576	hypothetical protein	7.12	0.0428	
	NE1636	hypothetical protein	-4.37	0.0437	
	NE1637	hypothetical protein	-4.51	0.0409	
	NE1680	hypothetical protein	-3.26	0.042	
	NE1791	hypothetical protein	-2.58	0.0471	
	NE1841	hypothetical protein	-2.70	0.0367	
	NE2041	hypothetical protein	-2.07	0.0429	
	NE2099	hypothetical protein	3.20	0.043	
	NE2145	hypothetical protein	-3.19	0.0429	
	NE2179	hypothetical protein	-4.70	0.0408	
	NE2230	hypothetical protein	-4.76	0.0352	
	NE2243	hypothetical protein	4.48	0.0429	
	NE2427	pyrimidine dimer DNA glycosylase	3.19	0.0422	
	NE2441	hypothetical protein	-2.43	0.0389	

Table A2. qRT-PCR primer sequences of selected genes expressed in biofilm microarrays.

Primer	Sequence
NE16S For	5'-GGCTTCACACGTAATACAATGG-3'
NE16S Rev	5'-CCTCACCCCAGTCATGACC-3'
amoA For	5'-TGGCGACATACCTGTCACAT-3'
amoA Rev	5'-ACAATGCATCTTTGGCTTCC-3'
NE0597 For	5'-TGGCTGTTCAGATTGCTGAC-3'
NE0597 Rev	5'-GCCAAAGGGAAGTGTCATGT-3'
NE1749 For	5'-AAATGCACGTTACGCCTTTC-3'
NE1749 Rev	5'-TCACTTCAGATGGCAGAGCA-3'
NE0770 For	5'-CGTGTGCCAGAATGAATCAC-3'
NE0770 Rev	5'-CACCCAGAAACAAGGCAAAC-3'
NE1332 For	5'-CCATCACTGGCATCCTTTCT-3'
NE1332 Rev	5'-CCACTTTATCAGCGACAGCA-3'
NE1944 For	5'-CAATGGAATCAACATCAAGCA-3'
NE1944 Rev	5'-CAGAAGATCCTGCGGAGTG-3'
NE1909 For	5'-TGATGGCTCTGGTGTTTACG-3'
NE1909 Rev	5'-TGGCATCGGTACTCTTGTTG-3'
NE0923 For	5'-CGGATTCTGGGAGATGTGTT-3'
NE0923 Rev	5'-AGGCAAAGTTCACCTGCTTC-3'
NE2408 For	5'-TCTGGAGAAATCAGCGTGTG-3'
NE2408 Rev	5'-AAACAAACCGAGCGTAATCG-3'
NE0556 For	5'-GATACGCAACTGGATGTGGA-3'
NE0556 Rev	5'-GCTTGCCAATCGGAATTAAA-3'
NE1479 For	5'-TTACGCACGGTTGGTGAAT-3'
NE1479 Rev	5'-TTTTGTTCGCTGTGCTGTTC-3'

Table A3. Linear regression analysis of gene expression in fill-and-draw reactors. Relationships between NO_2^- production rate and HRT and gene expression were determined by linear regression. Values of R^2 and slope from linear regression results are shown for each comparison.

	NO_2^- production		HRT	
Gene	R^2	**slope**	R^2	**m**
NE0597	0.906	-26.23	0.758	0.38
NE1749	0.899	-42.97	0.924	0.68
NE1332	0.885	-19.34	0.708	0.27
NE1909	0.937	-40.69	0.838	0.60
NE0770	0.838	-3.12	0.344	0.03
NE0556	0.912	-73.39	0.854	1.11
NE0923	0.999	-5.94	0.720	0.08
NE1944	0.817	-47.67	0.883	0.78
NE1479	0.909	-30.51	0.823	0.46
NE2408	0.841	-7.63	0.875	0.12

Figure A1. Regression analysis of gene expression in chemostat and fill-and-draw reactor vs. expression of genes in batch cells. Points represent 10 genes used for qRT-PCR analysis. Solid line is linear regression best fit to data, dashed line represents identical gene expression in two reactors.
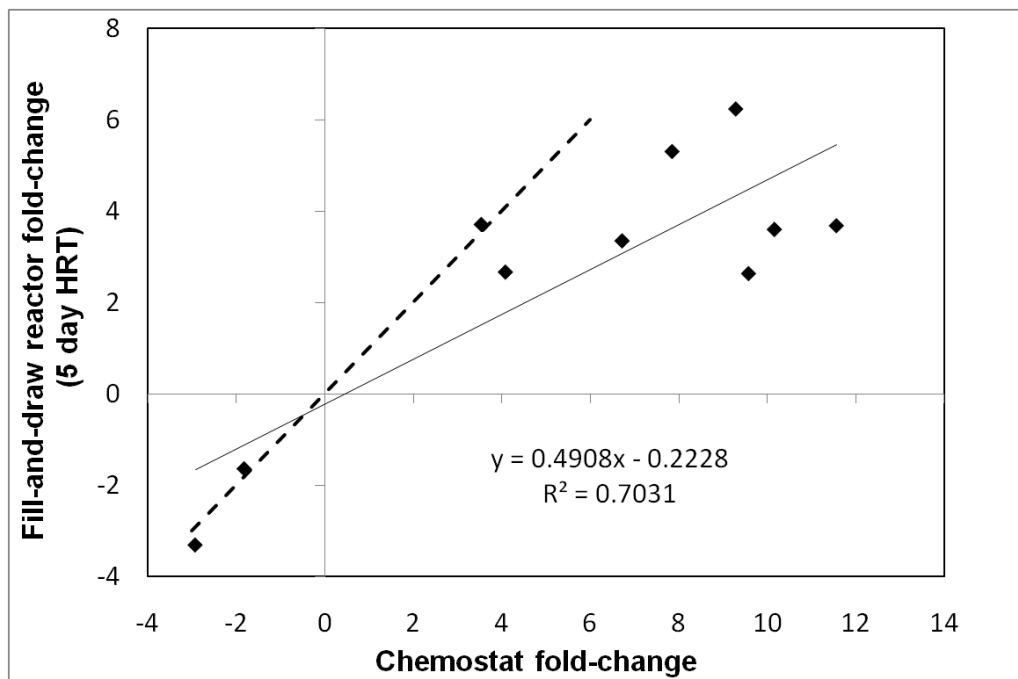
Appendix B. Supplemental information for biofilm model

Calculations for adjusted pH profiles from average measurements with pH microsensors.

The pH profiles were measured using sensors that obtained averaged pH readings over a depth of 150 μm above the tip. Therefore, the measurement at a specific tip location was actually the average pH from the tip to 150 μm above the tip. The following steps were taken to derive the actual pH values (pH_o) from the data of depth averaged pH (pH_{ave}).

The following assumptions were used to derive the actual pH:

1. The pH profile is monotonically decreasing, ie. the pH decreases as the depth increases in the biofilm.

2. The simplest form is assumed for the function of $pH_o(z)$, which was a third-order polynomial, based on the shape of the pH profile with depth z.

A third-order polynomial assumed for the function pH_o was integrated over the length of the sensor to obtain a relationship with the depth average pH_{ave}, as shown in the following equations:

$$pH_{ave}\big|_y = \frac{1}{L} \int_{z=y-L}^{z=y} pH_0(z)\,dz$$

$$pH_{ave}\big|_y = \frac{1}{L} \int_{z=y-L}^{z=y} \left[A + Bz + Cz^2 + Dz^3 \right] dz$$

$$pH_{ave}\big|_y = \frac{1}{L}\left[Ay + \frac{By^2}{2} + \frac{Cy^3}{3} + \frac{Dy^4}{4} \right] -$$

$$\frac{1}{L}\left[A(y-L) + \frac{B(y-L)^2}{2} + \frac{C(y-L)^3}{3} + \frac{D(y-L)^4}{4} \right]$$

Here, L is the sensor length of 150 µm, y is the location of the tip during the measurement, and z is the integration variable denoting the location along the sensor length. The coefficients A, B, C and D denote the constants for the polynomial fit of pH_o. The solution to the integrated equation for pH_{ave} is also a third-order polynomial where the coefficients a, b, c and d are related to the coefficients for pH_o by the following equations.

$$pH_{ave}(y) = a + by + cy^2 + dy^3$$

$$A = \frac{a}{L}$$

$$B = \frac{b}{L} + \frac{3}{2} AL$$

$$C = \frac{c}{L} - AL^2 + BL$$

$$D = \frac{d}{L} + \frac{A}{4} L^3 - \frac{B}{3} L^2 + C \frac{L}{2}$$

The coefficients A, B, C and D can be applied to the equation for pH_o and the actual value of pH was then derived from the measured profile of averaged pH.

In the calculations made here, the pH data taken from -200 µm above the biofilm surface into the biofilm was used in the polynomial fit, and -200 µm above the biofilm was adjusted to y=0, as shown in Table B1. The pH was assumed constant at 7.8 in the fluid above y=0 and was not used during the polynomial fitting. This data is shown in Table B1 below. Upon adjusting the depth, the data was input into Matlab where the function polyfit was used to apply a least squares fit of the data to a third-order polynomial and generate the coefficients which were related to the equation for pH_o.

Table B1. Raw data and depth adjusted values from pH profiles taken with microelectrodes.

Actual depth	Depth adjusted for polynomial fit (y)	Measured pH_{ave}	Calculated pH_0
μm	μm		
320	520	6.51	6.56
280	480	6.54	6.49
240	440	6.61	6.48
200	400	6.72	6.53
160	360	6.84	6.61
120	320	6.99	6.72
80	280	7.14	6.85
40	240	7.29	7.00
0	200	7.43	7.16
-100	100	7.69	7.52
-200	0	7.80	7.74
-300		7.80	7.80
-400		7.80	7.80
-500		7.80	7.80
-600		7.80	7.80
-700		7.80	7.80
-800		7.80	7.80
-900		7.80	7.80
-1000		7.80	7.80

Table B2. Kinetic and equilibrium rate expressions used in model.

Reaction	Expression
Ammonia oxidation	$K_{max} X \dfrac{NH_3}{K_{sn} + NH_3} \dfrac{O_2}{K_{so} + O_2}$
NH_3/NH_4^+ equilibrium	$k_2 \left[K_a NH_4^+ - NH_3 * H^+ \right]$
HEPES buffer equilibrium	$k_2 \left[K_{eq1}[HEPES_a] - [HEPES_b] * H^+ \right]$
Bicarbonate equilibrium	$k_2 \left[K_{aH} H_2CO_3 - HCO_3^- * H^+ \right]$
Endogenous respiration	bX

Table B3. Stoichiometric matrix of species in biofilm model.

	Ammonia oxidation	NH_3/NH_4^+ equilibrium	Hepes equilibrium	Endogenous respiration
NH_3	-1	1	—	—
NH_4^+	—	-1	—	—
NO_2^-	1	—	—	—
H^+	1	1	1	—
O_2	-1.5	—	—	-1
HEPES base	—	—	1	—
HEPES acid	—	—	-1	—

Figure B1. Sensitivity analysis of flow parameter D with 1mM NH$_4$-N simulation of DO profile, from solution of Study 1.
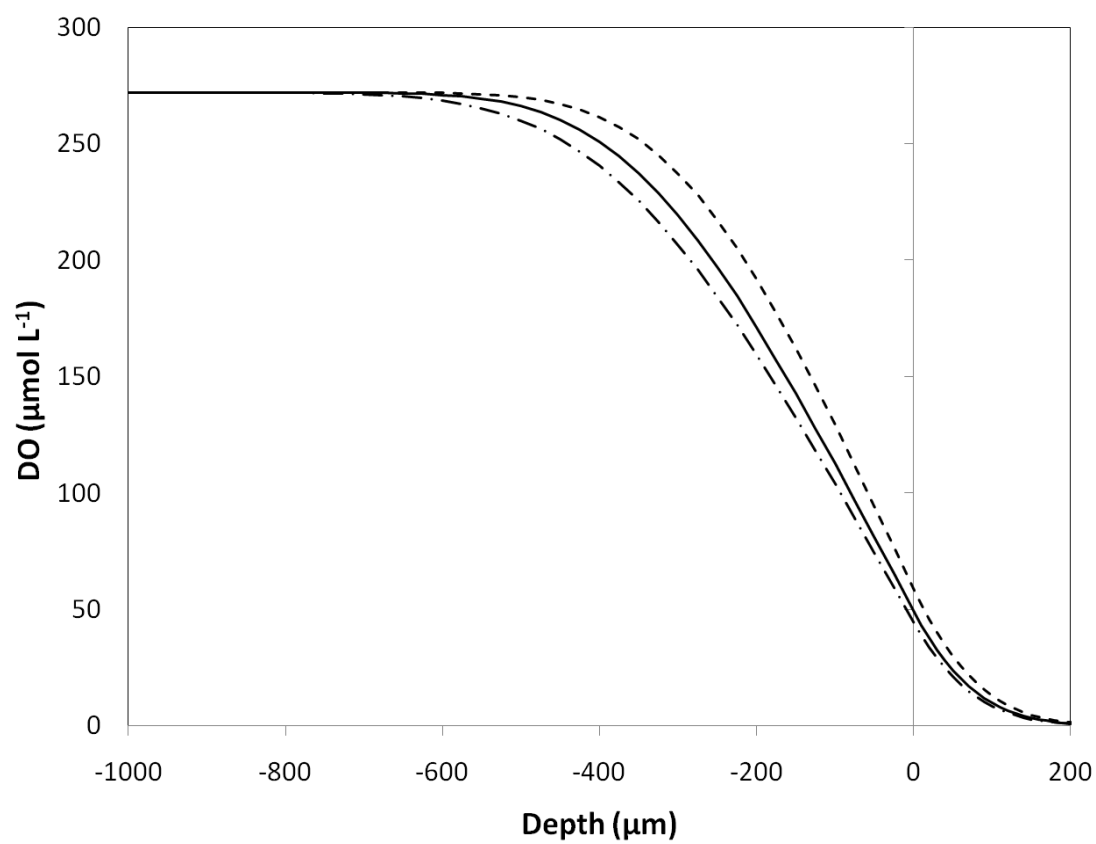
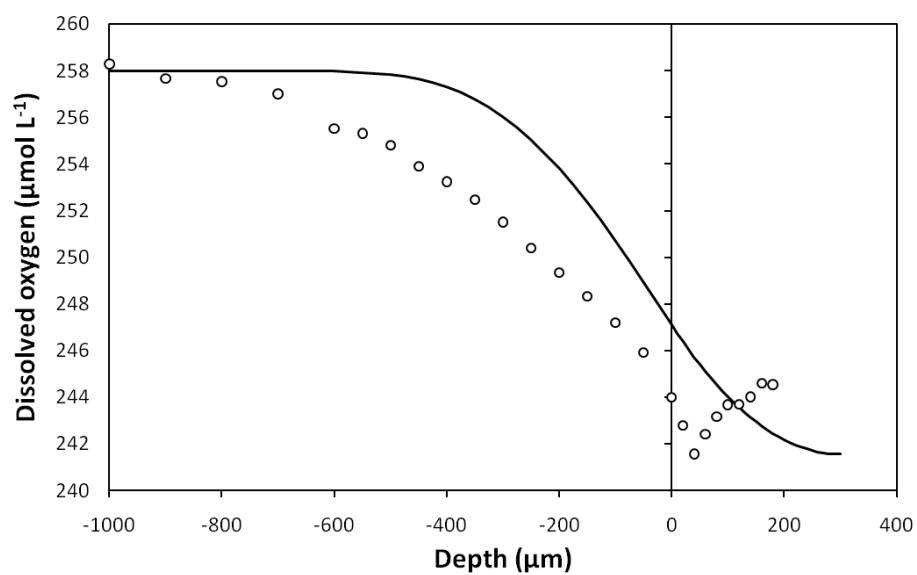**Figure B2.** Calibration of endogenous decay coefficient to DO profile with 0 mM NH$_3$.

Figure B3. Analytical solution vs. COMSOL model of 1-D diffusion with first-order reaction.
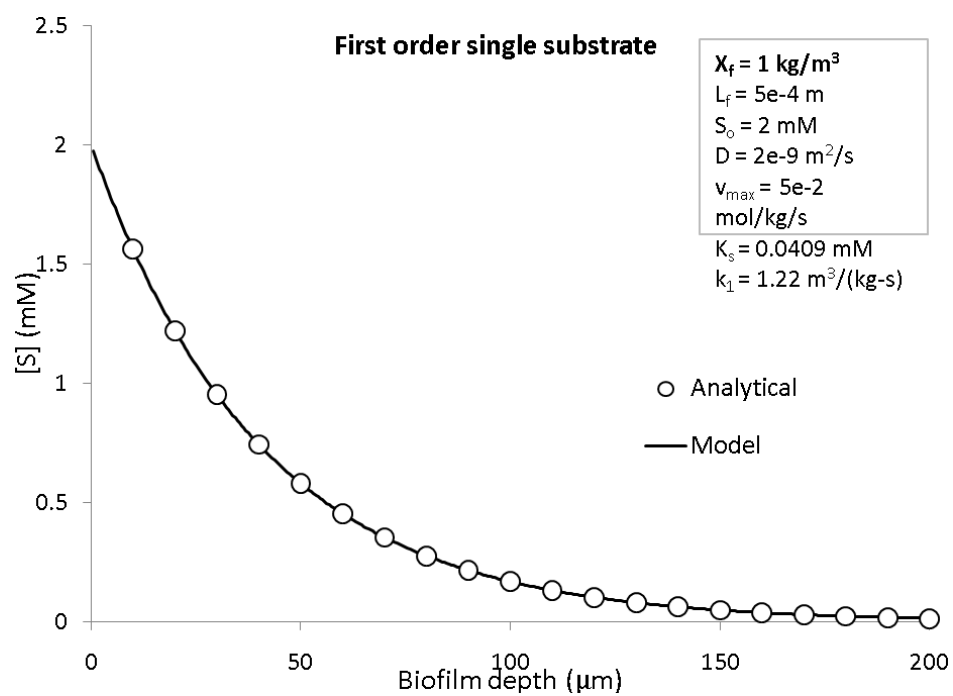

First order single substrate

$X_f = 1$ kg/m^3
$L_f = 5e-4$ m
$S_o = 2$ mM
$D = 2e-9$ m^2/s
$v_{max} = 5e-2$ mol/kg/s
$K_s = 0.0409$ mM
$k_1 = 1.22$ m^3/(kg-s)

○ Analytical
— Model

Figure B4. Sensitivity analysis of K_m with DO profiles. Profiles were taken at NH$_4$-N concentrations of 0.05 mmol L^{-1} (○) and 0.1 mmol L^{-1} (▲). Modeled results are with K_m of 1.5 μM (solid lines), 0.5 μM (dash dot) and 4 μM NH$_3$ (dashed).